



**HAL**  
open science

# Experimental investigation of mistuned bladed disks system vibration

Jia Li

► **To cite this version:**

Jia Li. Experimental investigation of mistuned bladed disks system vibration. Engineering Sciences [physics]. University of Michigan-Ann Arbor, 2007. English. NNT: . tel-00923790

**HAL Id: tel-00923790**

**<https://theses.hal.science/tel-00923790>**

Submitted on 4 Jan 2014

**HAL** is a multi-disciplinary open access archive for the deposit and dissemination of scientific research documents, whether they are published or not. The documents may come from teaching and research institutions in France or abroad, or from public or private research centers.

L'archive ouverte pluridisciplinaire **HAL**, est destinée au dépôt et à la diffusion de documents scientifiques de niveau recherche, publiés ou non, émanant des établissements d'enseignement et de recherche français ou étrangers, des laboratoires publics ou privés.

# **EXPERIMENTAL INVESTIGATION OF MISTUNED BLADED DISKS SYSTEM VIBRATION**

by

Jia Li

A dissertation submitted in partial fulfillment  
of the requirements for the degree of  
Doctor of Philosophy  
(Mechanical Engineering)  
in The University of Michigan  
2007

Doctoral Committee:

Professor Christophe Pierre, Co-Chair  
Professor Steven L. Ceccio, Co-Chair  
Professor Nickolas Vlahopoulos  
Associate Research Scientist Matthew P. Castanier



© Jia Li  
All Rights Reserved  
2007

*To my best friend and husband, Yun  
To my dearest Mom and Dad*

## ACKNOWLEDGEMENTS

It is much more difficult than I thought to even start this acknowledgement, which made the academic part slightly easier than it threatened to be. I never dreamed I would be overseas someday experiencing a five year adventure when I was only a kid, lying down on the hay stack near the country road with my childhood friends. We had nothing to do but staring at the stars, the same sparkling ones I had been relying on every time I caught a break outside the lab so many years later.

For an extremely special journey like this one, which is full of challenge, excitement as well as headache and frustration, there has to be countless people to whom I am so grateful. First of all, I wish to express my utmost gratitude to all my doctoral committee members for their consistent help. Without their supervision and support, I would never have been able to finish this work.

I am very fortunate to have Professor Christophe Pierre and Steven L. Ceccio as my advisors. They gave me nonstop inspiring and encouraging guidance during the past years. Despite their high expectations for me, they also tolerated my mistakes and immaturity at the beginning. They kept their patience, helping me grow from each failure or tiny progress. I will always remember that sweaty summer afternoon in the 1117 Auto Lab, Prof. Ceccio was working with me side by side on the speaker calibration. He said to me, “Jia, relax, every problem has a solution, I mean every problem.” Then he sang a song about a margarita to cheer me up. A month later, I finally had a solution and finished the first chapter in my thesis. Since then I really had the faith in myself that I could complete

this project even sometimes I was at the lowest downside. I owe many thanks to Dr. Matthew P. Castanier, he is a mentor as well as a great friend to me. I enjoyed the latest two years while we were working together on the GE project and my thesis.

I am also grateful to all my colleagues sharing the office with me for their warm friendship and genuine help. Every time I needed a installation crew, everyone was there supporting me. Once they helped me save all the equipments from a burst water pipe. All the moments we discussed, argued, comforted, laughed and celebrated together will be a precious memory for me. I would like to thank John Judge and Sang-Ho Lim specially, both worked with me closely everyday and always steered me into the right direction.

To all the people and friends I worked with in Auto Lab, especially Kent Pruss in the machine shop who put all my coarse design into final production, I can not say enough thanks for what you have brought into my life. I treasure the time we spent together, and your tremendous help and valuable advice, as well as your optimism and persistence.

Last but certainly not the least, I wish to thank my dearest Mom and Dad for their continuous loving support. They always believe in me and encourage me to finish what I start. My appreciation goes to my best friend and husband, Yun, for his patience, love and listening. He never hangs up on me even if I call him midnight because of the 12-hour time difference. And to my little brother, thank you for all you effort to be such a strong man and take care our parents all these years while I have been thousands of miles away from home.

No words will ever sound better than Wolverines, Tigers, Pistons, and Ann Arbor.

# TABLE OF CONTENTS

<b>DEDICATION</b> . . . . .	<b>ii</b>
<b>ACKNOWLEDGEMENTS</b> . . . . .	<b>iii</b>
<b>LIST OF FIGURES</b> . . . . .	<b>viii</b>
<b>LIST OF TABLES</b> . . . . .	<b>xv</b>
<b>LIST OF APPENDICES</b> . . . . .	<b>xvi</b>
<b>CHAPTER</b>	
<b>I. Introduction</b> . . . . .	<b>1</b>
1.1 Dissertation Objectives . . . . .	1
1.2 Background . . . . .	3
1.3 Dissertation Outline . . . . .	6
<b>II. Experimental Validation of A New Technique for Mistuning Identification and Model Updating</b> . . . . .	<b>8</b>
2.1 Introduction . . . . .	9
2.2 Theory . . . . .	12
2.2.1 Reduced Order Modeling Technique – Component Mode Mistuning . . . . .	12
2.2.2 Modeling Assumptions for Performing Mistuning Identification . . . . .	14
2.2.3 Mistuning Identification and Model Updating Based on CMM . . . . .	17
2.2.4 Equation Reformatting in Computational Process . . . . .	19
2.3 Experimental Apparatus . . . . .	21
2.3.1 Overview of Test Facilities . . . . .	21
2.3.2 Traveling Wave Excitation System . . . . .	22
2.4 Experimental Validation Results . . . . .	23
2.4.1 Validation Rotor . . . . .	23
2.4.2 NASA Bladed Disk . . . . .	28

2.5	Conclusions . . . . .	30
<b>III. Experimental Monte Carlo Mistuning Assessment of Bladed Disk Vibration Using Forcing Variations . . . . .</b>		
3.1	Introduction . . . . .	60
3.2	Theory . . . . .	62
3.2.1	Mistuning identification and model updating based on the CMM method . . . . .	62
3.2.2	Formulation for modified forces to mimic the effects of structural blade mistuning . . . . .	63
3.2.3	Estimation of the three-parameter Weibull distribution . . . . .	64
3.3	Experimental Specimen and Excitation System . . . . .	65
3.4	Computational Monte Carlo Simulation . . . . .	67
3.5	Experimental Monte Carlo Mistuning Assessment . . . . .	68
3.5.1	Experimental Trial 1 . . . . .	68
3.5.2	Experimental Trial 2 . . . . .	69
3.6	Conclusions . . . . .	70
<b>IV. Identification of Blade Excitation Parameters in Mistuned Blisk Vibration Tests . . . . .</b>		
4.1	Introduction . . . . .	88
4.2	External Forcing Identification . . . . .	90
4.2.1	Background—CMM Modeling for Mistuned Bladed Disks . . . . .	90
4.2.2	Simultaneous System and Forcing Identification . . . . .	93
4.2.3	Sequential System and Forcing Identification . . . . .	95
4.3	Numerical Validation . . . . .	96
4.3.1	Simultaneous Identification Method — Industrial Blisk . . . . .	96
4.3.2	Simultaneous Identification Method — NASA Blisk . . . . .	99
4.3.3	Comparison of Simultaneous and Sequential Identification Methods — Validation Blisk . . . . .	99
4.4	Experimental Validation . . . . .	101
4.4.1	Experimental Specimen and Excitation System . . . . .	101
4.4.2	Single-Blade Excitation . . . . .	102
4.4.3	Multi-Blade Excitation . . . . .	103
4.4.4	Perturbed Engine Order Excitation . . . . .	103
4.5	Conclusions . . . . .	104
<b>V. Conclusions . . . . .</b>		
5.1	Dissertation Contributions . . . . .	136
5.2	Future Research . . . . .	137
<b>APPENDICES . . . . .</b>		
		<b>140</b>

**BIBLIOGRAPHY . . . . . 171**

## LIST OF FIGURES

### Figure

2.1	Experimental set up of the non-contacting excitation and measurement system. . . . .	32
2.2	Non-contacting acoustic excitation system consisting of speakers. . . . .	33
2.3	Bladed disk set up with blisk system installed. . . . .	33
2.4	Picture of 24 blade validation rotor. . . . .	34
2.5	Finite element model of the validation bladed disk. . . . .	34
2.6	Natural frequencies versus the number of nodal diameters for the tuned rotor FEM simulation of validation bladed disk. . . . .	35
2.7	Measured natural frequencies of first flexible family for validation bladed disk compared to the FEM predictions. . . . .	35
2.8	Identified parameters for modal updating of validation rotor based on the experiment results. . . . .	36
2.9	Representation of mode shape of validation rotor at 2114.3 Hz, measured by the vibrometer and predicted by the updated CMM model. . . . .	37
2.10	Representation of mode shape of validation rotor at 2158.3 Hz, measured by the vibrometer and predicted by updated the CMM model. . . . .	38
2.11	Blade responses at 2114.3 Hz, from experiment and from the updated CMM models for different numbers of measured modes. . . . .	39
2.12	Identified parameters for modal updating of the validation rotor based on different sets of experiment results. . . . .	40
2.13	Comparison of frequency sweep responses, measured on the various blades while exciting the same one by single blade excitation. . . . .	41

2.14	Comparison of frequency sweep responses, measured on the various blades while exciting blade 1 in all cases. . . . .	42
2.15	Sensitivity of the cyclic modeling error to forced response, blade 4 by single blade excitation on blade 4. . . . .	43
2.16	Sensitivity of the cyclic modeling error to forced response, blade 19 by single blade excitation on blade 19. . . . .	43
2.17	Comparison of frequency sweep responses measured on various blades by different engine order excitation (EOE). . . . .	44
2.18	Comparison of the experimental results with various estimated responses, at 2150.6 Hz for validation rotor. . . . .	45
2.19	Comparison of frequency sweep responses without modal updating on various blades by engine order excitation (EOE) 11. . . . .	46
2.20	The NASA bladed disk mounted with speakers. . . . .	47
2.21	Finite element model of the NASA bladed disk. . . . .	48
2.22	Mode shape of the NASA bladed disk at nodal diameter 2. . . . .	48
2.23	The installation process of the NASA bladed disk. . . . .	49
2.24	Identified parameters for modal updating of the NASA blade disk based on the experiment results. . . . .	50
2.25	Natural frequencies versus the number of nodal diameters for the tuned rotor FEM of the NASA bladed disk. . . . .	51
2.26	Measured natural frequencies of first flexible family for the NASA bladed disk compared to the FEM predictions. . . . .	51
2.27	Mode shape of NASA bladed disk, predicted by updated CMM model and measured by SPLV (Single Point Laser Vibrometer). . . . .	52
2.28	Close-up of a blade of NASA bladed disk, showing the speaker behind the blade. . . . .	53
2.29	The mass (lead) added to tip of a blade of the NASA bladed disk. . . . .	53

2.30	Comparison of the intentional and the identified blade stiffness mistuning for the NASA bladed disk, without considering cyclic modeling errors.	54
3.1	Finite element model of the bladed disk.	71
3.2	Actual bladed disk used in the experiment, shown with the acoustic excitation system.	72
3.3	Monte Carlo simulation of originally mistuned system by engine order excitation (EOE) 6 – 7, 1000 random mistuning.	73
3.4	Monte Carlo simulation of originally mistuned system by engine order excitation (EOE) 8 – 9, 1000 random mistuning.	74
3.5	Monte Carlo simulation of originally mistuned system by engine order excitation (EOE) 10 – 11, 1000 random mistuning.	75
3.6	Monte Carlo simulation of originally mistuned system by engine order excitation (EOE) 12, 1000 random mistuning.	76
3.7	Histogram of the maximum blade response amplitude obtained by Monte Carlo simulation, based on 200 mistuning patterns generated from a uniform distribution with standard deviation = 0.1%.	77
3.8	Histogram of the frequencies at which the maximum response amplitudes occurred, based on 200 mistuning patterns generated from a uniform distribution with standard deviation = 0.1%.	78
3.9	Trial 1, 20 mistuning patterns generated from a uniform distribution with standard deviation = 0.1%. Comparison of the probability density function (PDF) and cumulative distribution function (CDF) between the experimental results and the predictions based on the updated CMM model.	79
3.10	Trial 1, 40 mistuning patterns generated from a uniform distribution with standard deviation = 0.1%. Comparison of the probability density function (PDF) and cumulative distribution function (CDF) between the experimental results and the predictions based on the updated CMM model.	80
3.11	Trial 1, 60 mistuning patterns generated from a uniform distribution with standard deviation = 0.1%. Comparison of the probability density function (PDF) and cumulative distribution function (CDF) between the experimental results and the predictions based on the updated CMM model.	81

3.12	Trial 1, 80 mistuning patterns generated from a uniform distribution with standard deviation = 0.1%. Comparison of the probability density function (PDF) and cumulative distribution function (CDF) between the experimental results and the predictions based on the updated CMM model.	82
3.13	Trial 2, 20 mistuning patterns generated from a uniform distribution with standard deviation = 0.1%. Comparison of the probability density function (PDF) and cumulative distribution function (CDF) between the experimental results and the predictions based on the updated CMM model.	83
3.14	Trial 2, 40 mistuning patterns generated from a uniform distribution with standard deviation = 0.1%. Comparison of the probability density function (PDF) and cumulative distribution function (CDF) between the experimental results and the predictions based on the updated CMM model.	84
3.15	Trial 2, 60 mistuning patterns generated from a uniform distribution with standard deviation = 0.1%. Comparison of the probability density function (PDF) and cumulative distribution function (CDF) between the experimental results and the predictions based on the updated CMM model.	85
3.16	Trial 2, 80 mistuning patterns generated from a uniform distribution with standard deviation = 0.1%. Comparison of the probability density function (PDF) and cumulative distribution function (CDF) between the experimental results and the predictions based on the updated CMM model.	86
4.1	Finite element model of the industrial blisk. . . . .	106
4.2	Natural frequencies versus the number of nodal diameters from the the tuned FEM of the industrial blisk. . . . .	107
4.3	Mistuning identification of the industrial blisk with forcing identification simultaneously (all forcing cases), 1F mode family. . . . .	108
4.4	Forcing identification results and errors for the SBE(3) case for the industrial blisk, 1F mode family. . . . .	109
4.5	Forcing identification for the MBE(3,17) case for the industrial blisk, 1F mode family. . . . .	110
4.6	Errors in forcing identification for the MBE(3,17) case for the industrial blisk, 1F mode family. . . . .	111
4.7	Forcing identification for the MBE(3,17,20) case for the industrial blisk, 1F mode family. . . . .	112

4.8	Errors in forcing identification for the MBE(3,17,20) case for the industrial blisk, 1F mode family. . . . .	113
4.9	Forcing identification results and errors for the SBE(3) case for the industrial blisk, 2T/2F mode family. . . . .	114
4.10	Finite element model of the NASA blisk. . . . .	115
4.11	Natural frequencies versus the number of nodal diameters for the tuned FEM of the NASA blisk. . . . .	116
4.12	Forcing identification results for the SBE(4) case for the NASA blisk. . . . .	117
4.13	Simultaneous mistuning and forcing identification results for the NASA blisk. . . . .	118
4.14	Finite element model of the validation blisk. . . . .	119
4.15	Natural frequencies versus the number of nodal diameters for the tuned FEM of the validation blisk. . . . .	120
4.16	Simultaneous forcing identification results for the MBE(2,9,17) case for the validation blisk. . . . .	121
4.17	Sequential forcing identification results for the MBE(2,9,17) case for the validation blisk. . . . .	122
4.18	Forcing identification errors for blade 2 of the validation blisk for the MBE(2,9,17) case. . . . .	123
4.19	Actual 24-blade validation blisk used in the experiment. . . . .	124
4.20	Validation blisk shown with the acoustic excitation system. . . . .	124
4.21	Detail of a blade with an attached mistuning mass. The selected measurement location is marked by a dot. . . . .	125
4.22	Comparison of intentional and identified blade stiffness mistuning values for the validation blisk, assuming consistent cyclic modeling errors before and after adding masses. . . . .	126
4.23	Forcing identification results and errors for the SBE(17) case for the validation blisk. . . . .	127

4.24	Forcing identification results and errors for the SBE(24) case for the validation blisk. . . . .	128
4.25	Forcing identification results for the MBE(17,24) case for the validation blisk. . . . .	129
4.26	Forcing identification errors for the MBE(17,24) case for the validation blisk. . . . .	130
4.27	Comparison of pure and perturbed engine order 8 excitation, both calculated based on the experimental responses of the validation blisk. . . . .	131
4.28	Comparison of frequency response results for blade 2 of the validation blisk subject to pure and perturbed engine order 8 excitation. . . . .	132
4.29	Comparison of frequency response results for blade 9 of the validation blisk subject to pure and perturbed engine order 8 excitation. . . . .	133
C.1	Finite element model of the validation bladed disk. . . . .	154
C.2	Modes Selection for CMM modeling of the validation rotor, blade-dominant mode is majority. . . . .	155
C.3	Modes Selection for CMM modeling of the validation rotor, disk-dominant mode is majority. . . . .	155
C.4	Identification results of blade stiffness mistuning based on a CMM model with 17 blade-dominant modes. . . . .	156
C.5	Identification results of blade stiffness mistuning based on a CMM model with 17 blade-dominant modes and 7 disk-dominant modes. . . . .	156
C.6	Wrong identification results of blade stiffness mistuning based on a CMM model with 17 blade-dominant modes, using 24 measured data at resonant frequencies. . . . .	157
C.7	Identification results of blade stiffness mistuning based on different CMM models. . . . .	158
C.8	Identification results of blade stiffness mistuning and cyclic modeling error based on a CMM model with 17 blade-dominant modes. . . . .	159

C.9	Identification results of blade stiffness mistuning and cyclic modeling error based on a CMM model with 17 blade-dominant modes and 7 disk-dominant modes. . . . .	160
D.1	Experimental set up of the non-contacting excitation and measurement system. . . . .	166
D.2	Front panel of a Labview code with 4 inputs, "Speaker Control.vi". . . .	167
D.3	PSV acquisition modes set up: step 1 General. . . . .	168
D.4	PSV acquisition modes set up: step 2 Channel. . . . .	168
D.5	PSV acquisition modes set up: step 3 Filters. . . . .	168
D.6	PSV acquisition modes set up: step 4 Frequency. . . . .	169
D.7	PSV acquisition modes set up: step 5 Window. . . . .	169
D.8	PSV acquisition modes set up: step 6 Triggers. . . . .	169
D.9	PSV acquisition modes set up: step 7 SE. . . . .	170
D.10	PSV acquisition modes set up: step 8 Vibrometer. . . . .	170

## LIST OF TABLES

### Table

2.1	Identified blade stiffness mistuning and cyclic modeling error from the experimental results based on the CMM model of the validation rotor. . . . .	55
2.2	Comparison of the measured natural frequencies of the validation rotor to various predictions based on the updated CMM model by using a different set of measured data. . . . .	56
2.3	Identified blade stiffness mistuning and cyclic modeling error from the experimental results based on the CMM model of the NASA bladed disk. . . . .	57
2.4	Mass of the leads added to the tip of blade of NASA blisk and corresponding intentional blade stiffness mistuning. . . . .	58
4.1	External forcing values for the single-blade and multi-blade excitation cases. . . . .	134
4.2	Mass of the leads added to the tip of blade of validation blisk and corresponding intentional blade stiffness mistuning. . . . .	135

# LIST OF APPENDICES

## Appendix

A.	Equation Reformatting in Computational Process for Mistuning Identification and Model Updating . . . . .	141
B.	Optimization of Identification – Least Squares Method . . . . .	147
C.	CMM Modeling Assumptions and Applying Limitations . . . . .	150
	C.1 Blade Stiffness Mistuning Identification Only . . . . .	151
	C.2 Mistuning identification and model updating . . . . .	152
D.	Automatic Vibration Test System . . . . .	161
	D.1 Scanning Laser Vibrometer . . . . .	161
	D.1.1 PSV–Software Environment for SLDV . . . . .	162
	D.1.2 PSV Acquisition Set Up . . . . .	162
	D.2 Excitation System . . . . .	163
	D.3 Data Process System . . . . .	164
	D.4 Automatic Test Control Code . . . . .	164

# CHAPTER I

## Introduction

### 1.1 Dissertation Objectives

Bladed disks are critical components in turbomachinery such as impeller pumps, compressors, jet engines, and turbine generators. The nominal design for a bladed disk is typically assumed to have cyclic symmetry, which means it is a cyclic assembly of identical substructures (or sectors) that are dynamically coupled in an identical manner. However, there are always small, random variations in the sector properties due to manufacturing tolerances, material defects, and operational wear and damage. Much research has focused on the investigation of the influence of blade-to-blade discrepancies, known as mistuning, which can have a dramatic effect on bladed disk vibration. In particular, mistuning can lead to concentrated vibration response in a small region of the bladed disk, a phenomenon known as localization. Furthermore, the forced response vibration amplitudes of particular blades can be significantly increased due to the spatial confinement of the vibration energy, leading to high stresses, high-cycle fatigue (HCF), and failure.

In recent decades, while comprehensive analytical and computational studies of mistuning have been performed, comparatively few experimental investigations have been conducted. Comprehensive experimental work is critically needed in order to corroborate physical phenomena due to mistuning, validate mistuning models and attendant reduced-

order models, and examine the factors that influence the dynamics of mistuned bladed disks in their jet-engine operational setting. Specifically, there are several phenomena of potentially great importance to the mistuned blade response that have yet to be modeled. For example, uncertainties in measurements, errors in finite element models (FEMs), and the influence of adjacent bladed disk stages could all introduce significant variability into the prediction of the mistuned forced response.

The primary objective of this research is to experimentally investigate the fundamental structural dynamics of mistuned bladed disks, and to achieve a further understanding of mistuning effects by including the influence of important phenomena that have been largely neglected in previous mistuning models, including variations in forcing levels delivered to the blades. In addition, blade mistuning identification methods that have recently been developed for single-piece bladed disks, or blisks, will be further developed and extended to include system identification of both structural and forcing parameters. The experiments carried out in this research work will serve to validate computational results from recently developed modeling methods, to help develop and validate new techniques for system identification and model updating, and to enrich mistuned bladed disk models.

In the short term, these higher-fidelity modeling, system identification, and testing methods will yield improved response predictions, more comprehensive and accurate assessments, and greater physical insight for actual bladed disk systems. In the long term, this research will help enable the design of more robust rotors that will be significantly less susceptible to HCF, and thus lead to safer and more cost-effective turbine engines.

The specific research objectives are summarized as follows:

- To further develop and validate an experimental approach for mistuning identification and reduced-order model updating of blisks

- To perform virtual mistuning experiments on blisks that mimic Monte Carlo simulations for assessing the effects of random mistuning on increases in forced response levels
- To develop new algorithms and testing methods for identifying external excitation parameters, which will serve to accelerate calibration procedures and improve the accuracy and capability of blisk vibration tests

## 1.2 Background

Mistuning phenomena have been studied by using analytical and numerical models since 1950s. Tobias and Arnold [1] showed that the resonant peak of a tuned system splits into “dual modes” because of inevitable mistuning. Whitehead [2] and Dye and Henry [3] used simple models to show that random mistuning could increase forced response levels dramatically compared to a tuned system.

Ewins [4] first evidenced mode localization in an experimental investigation of a detuned bladed disk assembly. He then carried out a series of investigations on vibration analysis of mistuned bladed disks [5–8], which were followed by experimental investigations by other researchers [9–12].

In general, finite element analysis is too computationally expensive for predicting mistuned bladed disk response for two main reasons. First, an industrial finite element model (FEM) of a bladed disk typically has hundreds of thousands or even millions of degrees of freedom (DOF). Second, blade mistuning is random, and therefore Monte Carlo simulations are used to predict the statistics of the forced response, requiring many numerical evaluations of mistuned bladed disks. Therefore, many research efforts have been devoted to developing various reduced-order models (ROMs) to reduce computational time and investigate the effects of mistuning on bladed disk vibration [13–18]. Castanier and

Pierre [19] recently provided a thorough review into the major developments in mistuning research over the decade.

Some physical insight into the localization phenomenon caused by mistuning may be gained by envisioning the vibration energy of the system as a circumferentially traveling wave. In a perfectly tuned system, the wave propagates through each blade in turn, causing equal vibration amplitude. If even very small levels of mistuning are present, however, the slight differences in properties between adjacent blades cause the traveling wave to be partially reflected as it encounters each blade. For certain mistuning patterns, this results in vibration energy becoming trapped in part of the bladed disk, and so certain blades vibrate with much greater amplitude than others. In this manner, the mode shapes and forced response shapes of a bladed disk with slightly mistuned blades can become qualitatively different from those of the perfectly tuned system. The problem is quite complex in that the blade or blades in which the energy becomes confined are not necessarily those with the greatest mistuning. Furthermore, one mistuning pattern could produce a highly localized mode at certain natural frequency but a nearly cyclic mode at a different natural frequency.

One prime application of ROMs is to identify mistuning in actual bladed disks [20, 21]. Mistuning identification is important as a means of monitoring the quality of the manufacturing process, and also in the maintenance checks of operational rotors. This is especially true for blisks, because the blades cannot be separated from the rotor for individual modal testing. Judge *et al.* [22, 23] presented and experimentally validated the very first method of a mistuning identification technique for blisks by combining a ROM and the measurements of system mode shapes and natural frequencies. The ROM employed in this case was based on the Craig-Bampton method[24] of component mode synthesis (CMS) enhanced with a second modal analysis (SMA) procedure [25, 26]. The mistuning was considered as the deviation of modal stiffness for a blade in a tested blisk from that of a blade

in a perfectly tuned system. Judge *et al* [27] also demonstrated experimentally the potential application of intentional mistuning[28] in preventing strong amplitude magnification due to random mistuning.

Another important use of a reduced-order modeling technique is to generate models that are sufficiently compact that Monte Carlo simulations can be performed to estimate the statistics of the forced response for a population of mistuned rotors. In such Monte Carlo simulations [13, 22, 29], mistuning patterns are assigned with a pseudo-random number generator, and a certain physical or modal property of each blade (e.g., Young's modulus or blade-alone natural frequency) is altered in the model according to its assigned mistuning value. However, it is much more difficult to assess the effects of random mistuning or validate numerical predictions using experimental methods. In particular, imposing specific mistuning patterns on a physical system is challenging. Although adding mistuning masses is an effective means of controlling mistuning in bench tests, it can be time-consuming and cumbersome to precisely manufacture and attach the individual mistuning masses. As a result, relatively few mistuning patterns can be tested using this approach [27, 30]. Other experimental statistical analyses were performed by Jones [31] and Rossi *et al* [32]. These investigators encountered the same practical difficulties in implementing the physical configuration changes that are required to carry out statistical mistuning studies in the laboratory. Therefore, developing an experimental analog of Monte Carlo simulation has remained an elusive goal in previous work.

In bladed disk vibration tests, by running only a few forced response tests for the full bladed disk, the individual blade mistuning values can be extracted, which are typically expressed as deviations of blade-alone natural frequencies from the nominal value for a specific mode. However, in general, the accuracy of bladed disk vibration tests depends on the careful mounting of the test specimen as well as the calibration of the external

excitation system. This is especially true for the case of engine order excitation. To generate true engine order excitation in a bench test environment, a sinusoidal forcing must be delivered with the same amplitude at each blade, and the blade-to-blade phase lag must also be consistent throughout the system by using speakers, horn drivers with vinyl tubing, electromagnets, or specifically designed “Flywheel” [22, 31, 33, 34]. Despite the meticulous calibrations required in order to gather sufficient information for precisely excitation control, the uncertainties in the forcing are inevitable during the vibration test. Therefore, accounting for these uncertainties may be crucial to improving the calibration as well as the accuracy of bladed disk vibration tests.

### **1.3 Dissertation Outline**

The remaining chapters of this dissertation are compiled from a collection of three manuscripts for technical papers that have been prepared for submission to scientific journals. Because of this, some of the background material is repeated in various chapters. The remaining chapters are summarized as follows.

In chapter II, the experimental approach to validate a new technique for mistuning identification and model updating of mistuned blisks is proposed. The technique is based on the component mistuning mode (CMM) ROM method, which was recently developed by Lim *et al* [18]. In the experiment, system responses are obtained by taking measurements at each blade and then combined with the resonant frequencies as the required information for blade mistuning identification. If needed, model updating parameters referred as “cyclic modeling error” can be identified simultaneously.

In chapter III, as an alternative approach for vibration testing of many mistuning patterns, it is proposed that varying the external forcing function provided to the blades can be used to mimic the influence of structural blade property mistuning on the vibration re-

sponse. Because it is much easier and more efficient to vary the external excitation than to physically alter the blades, this opens the possibility of running an experimental analog of a Monte Carlo simulation. The feasibility of this approach, referred to as an experimental Monte Carlo mistuning assessment, is explored. The modified forcing function required to mimic a given blade mistuning pattern is derived based on the CMM method. Then the probability density function (PDF) and cumulative distribution function (CDF) predicted by numerical Monte Carlo simulations are compared to those estimated from the new experimental approach.

In chapter IV, the identification of and impact of uncertainties on the external excitation are investigated in detail. The mistuning identification method described in chapter II is extended to also identify the amplitude and phase values of the forcing applied to the blades. It is shown that blade mistuning and forcing can be identified simultaneously or sequentially by carrying out a small set of prescribed forced response experiments. The accuracy and robustness of the forcing identification are examined both numerically and experimentally.

Finally, in chapter V, the contributions of this research are summarized, and ideas for future work are proposed.

## CHAPTER II

# Experimental Validation of A New Technique for Mistuning Identification and Model Updating

The primary objective of this research is to validate, by experimental testing of realistic bladed disk structures, a new method for the identification of blade mistuning, which is based on the recently developed component mode mistuning (CMM) reduced-order modeling technique for mistuned bladed disk vibration. The technique developed combines experimental measurements with CMM reduced-order models of finite element models of bladed disks. It produces not only the identification of blade mistuning parameters, but also the updating of the parameters of the CMM reduced-order model, thus enabling the accurate prediction of the vibratory response of industrial bladed disks. In this approach, forced response experimental data are used for the identification without requiring the knowledge of the applied forces, and a least-squares fit procedure is employed to reduce the effect of measurement errors. The method is also applicable to the free vibration mode shapes and natural frequencies. A sensitivity study is performed, which considers the errors in modeling parameters and measured data, and it is observed that the identification results are most sensitive to errors in the tuned system eigenvalues. In order to compensate for these errors, the “cyclic modeling error” is identified, which is the difference between the frequencies of the virtual tuned system of an actual mistuned bladed

disk and its tuned finite element model. Then, the CMM reduced-order model is updated using both the cyclic modeling error and the identified mistuning pattern, thus producing an accurate model of the tested bladed disk specimen. The method is validated experimentally for both a “validation rotor” with controlled mistuning and for an advanced NASA (National Aeronautics and Space Administration) compressor bladed disk.

## **2.1 Introduction**

Bladed disks are generally assumed to be an assembly of identical substructures (or sectors) that are dynamically coupled in an identical manner. However, there are always small, random variations in the sector properties due to manufacturing tolerances, material defects, and operational wear and damage. These blade-to-blade discrepancies, known as mistuning, can have a dramatic effect on bladed disk dynamics. In particular, mistuning can lead to vibration concentrated in small regions of the bladed disk, a phenomenon known as localization. Furthermore, the forced response amplitudes of particular blades can significantly increase due to the spatial confinement of the vibration energy. This may lead to large stresses, high-cycle fatigue, and failure.

A number of analytical and computational studies of mistuning in bladed disks have been performed since the late 1950s [1, 3]. Ewins [4] provided the first experimental evidence of localized vibration in a blade assembly with mistuning, and the phenomenon of mode localization was first elucidated by Wei and Pierre [35, 36]. Predicting the vibration response of industrial bladed disks requires the use of large-scale finite element models (FEMs) with several million degrees of freedom (DOF), and it carries a prohibitive computational cost. Therefore, much research has focused on the development of reduced-order models (ROMs) [13–18], which allow for parametric studies and statistical Monte Carlo simulations of bladed disk free and forced vibration at a reasonable cost. The ROMs

developed recently provide highly accurate estimates of forced response amplitudes for a size that is only on the order of the number of blades [15, 18].

While much analytical and computational research has been performed on mistuning, until recently there has been a lack of experimental investigations of mistuning. Kruse *et al* [37, 38] presented an experimental investigation of vibration localization on a pair of 12 bladed disk, one is tuned and the other is mistuned by varying the length of blades randomly. Mignolet *et al.* [39, 40] estimated the dynamic properties of the turbomachine blades from experimental results to provide more accurate prediction of forced response.

Judge *et al.* [23, 27, 41–43] were the first to carry out a series of systematic experiments to corroborate the physical phenomena that are caused by mistuning (*i.e.*, mode localization and forced response amplitude magnification), validate reduced-order models of mistuned bladed disks, and develop the very first technique for the identification of blade mistuning. Judge's identification method allows one to extract, from measurements of system modes of vibration or forced responses, the blade mistuning parameters for use in the attendant ROM. Note that this mistuning identification method is especially suited for integrally bladed disks, or blisks, in which the individual blades cannot be easily isolated from the rest of the structure.

Yang and Griffin [15] used the tuned-system normal modes of a bladed disk to develop a new ROM, called Subset of Nominal Modes (SNM). Their approach has the advantage of eliminating the error associated with the sub-structuring in component mode synthesis. Subsequently they applied the SNM technique to system identification within a higher modal density range [44]. Feiner and Griffin [16, 17, 45] developed a totally experimental, system-based method for the identification of sector mistuning (as opposed to blade mistuning) based on a Fundamental Mistuning Model (FMM), which does not require any FEM or ROM analysis. Recently, Lim *et al.* [18] reported a new ROM technique for

mistuned bladed disks, called Component Mode Mistuning (CMM). In this approach, the blade motion is described in terms of tuned-system normal modes, and the blade mistuning is projected onto these modes by using modal participation factors of cantilevered-blade modes. Key features of the CMM method are that it is able to handle non-proportional as well as large, “geometric” mistuning, and that it is applicable to closely-spaced groups of blade-dominated modes.

The primary contribution of this ROM method is that it provides a computational solution for an inverse problem, blade mistuning identification as Lim *et al.* [21] suggested. Moreover, a model updating parameter defined as “cyclic modeling error”, which can be used to compensate the difference between actual bladed disks and tuned FEM model, was presented by the author after conducting a sensitivity study. Numerous research of model updating [46–50] have been done in order to match the FEM model with its actual manufactured structure and Sinha [51] presented a survey on the development of model updating techniques. With this CMM method, only a few system responses taken at the resonant frequencies are sufficient to apply mistuning identification and model updating without knowing exactly what the external forcing is. It is extremely useful when the modal density is high and not every single mode can be isolated from others. Another major advantage of this algorithm is that no additional criteria is necessary to help selecting which are the proper measurements for an accurate identification. A least square method is adopted to optimize the results and strikes out the error automatically. Therefore this identification process is straightforward and efficient.

The chapter is organized as follows. In section 2.2, the CMM method is first introduced with small mistuning assumption. Then the ROM is further reduced by focusing on only one family modes where cantilever blade mode is dominant. And the identification algorithm is presented with details. The experiment facilities are described in section 2.3

as well as the test specimen used in validation. In section 2.4, the mistuning identification and modal updating approach is validated experimentally while using two different bladed disks. The conclusion is given in section 2.5.

## 2.2 Theory

### 2.2.1 Reduced Order Modeling Technique – Component Mode Mistuning

A component mode mistuning (CMM) method for reduced order model (ROM) was recently developed by Lim *et al.* [18, 52]. This technique can be applied to any mistuned system, no matter whether the mistuning is small or large, since there is no assumption made with respect to the mistuning. In the CMM approach, a mistuned bladed disk is treated as a combination of two components through a hybrid interface by employing component mode synthesis (CMS): one component is tuned, referring to the perfectly tuned blade disk system, and the other is a set of mistuned components representing blade mistuning.

#### Tuned Bladed Disk

For the tuned bladed disk system, the reduced mass and stiffness matrices in modal coordinates  $\boldsymbol{\mu}^S$  and  $\boldsymbol{\kappa}^S$ , can be written as in Eq. 2.1. In which,  $\mathbf{M}^S$  and  $\mathbf{K}^S$  are the corresponding reduced mass and stiffness matrices in physical coordinates;  $\boldsymbol{\Phi}^S$  is a *truncated* set of normal modes while  $\boldsymbol{\Psi}^S$  is a *complete* set of attachment modes;  $\boldsymbol{\Lambda}$  is a diagonal matrix of the eigenvalues of the remained normal modes. Both  $\mathbf{x}$  and  $\mathbf{p}$  are system response, *i.e.*, displacement, while the former one in physical coordinates and the latter one in modal coordinates. The superscript  $S$  denotes a tuned system, and the subscripts  $\Delta$  and  $\Gamma$  denote the DOF of the disk and the blades, respectively. Another pair of subscripts  $\Phi$  and  $\Psi$  distinguish the generalized coordinates for the remained normal modes from the interface modes.

$$\boldsymbol{\mu}^S = \begin{bmatrix} \mathbf{I} & \boldsymbol{\Phi}^{S^T} \mathbf{M}^S \boldsymbol{\Psi}^S \\ \boldsymbol{\Psi}^{S^T} \mathbf{M}^S \boldsymbol{\Phi}^S & \boldsymbol{\Psi}^{S^T} \mathbf{M}^S \boldsymbol{\Psi}^S \end{bmatrix} \quad (2.1a)$$

$$\boldsymbol{\kappa}^S = \begin{bmatrix} \boldsymbol{\Lambda}^S & \boldsymbol{\Phi}^{S^T} \mathbf{K}^S \boldsymbol{\Psi}^S \\ \boldsymbol{\Psi}^{S^T} \mathbf{K}^S \boldsymbol{\Phi}^S & \boldsymbol{\Psi}_\Gamma^S \end{bmatrix} \quad (2.1b)$$

$$\mathbf{x}^S = \begin{Bmatrix} \mathbf{x}_\Delta^S \\ \mathbf{x}_\Gamma^S \end{Bmatrix} = \begin{bmatrix} \boldsymbol{\Phi}_\Delta^S & \boldsymbol{\Psi}_\Delta^S \\ \boldsymbol{\Phi}_\Gamma^S & \boldsymbol{\Psi}_\Gamma^S \end{bmatrix} \begin{Bmatrix} \mathbf{p}_\phi^S \\ \mathbf{p}_\psi^S \end{Bmatrix} \quad (2.1c)$$

### Mistuning Component

For the mistuning component, *i.e.* blade mistuning, the mass and stiffness matrix in blade modal coordinates, referred as  $\boldsymbol{\mu}^\delta$  and  $\boldsymbol{\kappa}^\delta$ , are the same as those in blade physical coordinates, referred as  $\mathbf{M}^\delta$  and  $\mathbf{K}^\delta$ . Note that  $\delta$  denotes the mistuning component. The reason is that the constraint modes of the cantilevered blade alone are sufficient to describe the motion of the mistuning components in this situation without involving any normal modes. Therefore an identity matrix is the mode shape matrix because the constraint modes are obtained by exciting a unit displacement at each interface DOF.

$$\boldsymbol{\mu}^\delta = \mathbf{I}^T \mathbf{M}^\delta \mathbf{I} = \mathbf{M}^\delta \quad (2.2a)$$

$$\boldsymbol{\kappa}^\delta = \mathbf{I}^T \mathbf{K}^\delta \mathbf{I} = \mathbf{K}^\delta \quad (2.2b)$$

$$\mathbf{x}^\delta = \mathbf{I} \mathbf{p}_\psi^\delta = \mathbf{p}_\psi^\delta \quad (2.2c)$$

## Mistuned Bladed Disk Synthesis

Note that the DOF of the mistuning components and those of hybrid interface are identical. By satisfying displacement compatibility at the component interface,  $\mathbf{x}_\Gamma^S = \mathbf{x}^\delta$ , the synthesized representation of a mistuned system is :

$$[-\omega^2 \boldsymbol{\mu}^{syn} + (1 + j\gamma) \boldsymbol{\kappa}^{syn}] \mathbf{p}^{syn} = [\Phi^S \quad \Psi^S] \mathbf{f} \quad (2.3a)$$

$$\boldsymbol{\mu}^{syn} = \boldsymbol{\mu}^S + \begin{bmatrix} \Phi_\Gamma^{S^T} \mathbf{M}^\delta \Phi_\Gamma^S & \Phi_\Gamma^{S^T} \mathbf{M}^\delta \Psi_\Gamma^S \\ \Psi_\Gamma^{S^T} \mathbf{M}^\delta \Phi_\Gamma^S & \Psi_\Gamma^{S^T} \mathbf{M}^\delta \Psi_\Gamma^S \end{bmatrix} \quad (2.3b)$$

$$\boldsymbol{\kappa}^{syn} = \boldsymbol{\kappa}^S + \begin{bmatrix} \Phi_\Gamma^{S^T} \mathbf{K}^\delta \Phi_\Gamma^S & \Phi_\Gamma^{S^T} \mathbf{K}^\delta \Psi_\Gamma^S \\ \Psi_\Gamma^{S^T} \mathbf{K}^\delta \Phi_\Gamma^S & \Psi_\Gamma^{S^T} \mathbf{K}^\delta \Psi_\Gamma^S \end{bmatrix} \quad (2.3c)$$

$$\mathbf{p}^{syn} = \begin{Bmatrix} \mathbf{p}_\phi^S \\ \mathbf{p}_\psi^S \end{Bmatrix} \quad (2.3d)$$

where  $\omega$  is the resonant frequency of the mistuned system,  $\gamma$  is the structural damping factor,  $\boldsymbol{\mu}^{syn}$  and  $\boldsymbol{\kappa}^{syn}$  are the reduced mass and stiffness matrices of the mistuned system, and  $\mathbf{p}^{syn}$  is a vector of displacement in modal coordinates.

### 2.2.2 Modeling Assumptions for Performing Mistuning Identification

While there is no assumption made for creating a reduced-order model based on CMM technique to represent a mistuned bladed disk system, several assumptions are considered in the this section in order to perform the inverse process, mistuning identification.

#### Blade Stiffness Mistuning Only

Generally the mistuning component, includes the mass and stiffness variations from the tuned system. However, through this thesis only the stiffness variations are considered

while the mass matrix is assumed as an invariant.

$$\boldsymbol{\mu}^{syn} = \boldsymbol{\mu}^S \quad (2.4a)$$

$$\boldsymbol{\kappa}^{syn} = \boldsymbol{\kappa}^S + \begin{bmatrix} \boldsymbol{\Phi}_\Gamma^{S^T} \mathbf{K}^\delta \boldsymbol{\Phi}_\Gamma^S & \boldsymbol{\Phi}_\Gamma^{S^T} \mathbf{K}^\delta \boldsymbol{\Psi}_\Gamma^S \\ \boldsymbol{\Psi}_\Gamma^{S^T} \mathbf{K}^\delta \boldsymbol{\Phi}_\Gamma^S & \boldsymbol{\Psi}_\Gamma^{S^T} \mathbf{K}^\delta \boldsymbol{\Psi}_\Gamma^S \end{bmatrix} \quad (2.4b)$$

### Small Mistuning

As for small mistuning cases, the main idea presented by Lim *et al.* [18, 52] for their method is that, the mistuned normal modes can be expressed as a linear combination of tuned normal modes since a slightly mistuned bladed disk features closely spaced modes as a tuned bladed disk does in the same frequency range. This means that  $\boldsymbol{\Psi}^S$  and the corresponding displacement in modal coordinates,  $\mathbf{p}_\psi^S$ , can be ignored in Eq. 2.3, then the synthesized representation becomes :

$$\boldsymbol{\mu}^{syn} = \mathbf{I} \quad (2.5a)$$

$$\boldsymbol{\kappa}^{syn} = \left[ \boldsymbol{\Lambda}^S + \boldsymbol{\Phi}_\Gamma^{S^T} \mathbf{K}^\delta \boldsymbol{\Phi}_\Gamma^S \right] \quad (2.5b)$$

$$\mathbf{p}^{syn} = \{ \mathbf{p}_\phi^S \} \quad (2.5c)$$

### Blade Mistuning Projection

Bladh *et al.* [14] suggested a method in CMS approach for mistuning projection, where the stiffness mistuning matrices in physical coordinates are projected to the normal modes of a tuned cantilevered blade. This method yields a diagonal matrix of modal stiffness deviations and it holds the assumption that the tuned and mistuned blade-alone mode shapes

are the same. Lim *et al.* [18, 52] inherited this approach with system mode basis instead of sub-structuring the bladed disk system into blade and disk parts. And a new concept, modal participation factors of a tuned cantilevered blade  $\mathbf{Q}$ , was introduced in order to represent the blade portion of the tuned system normal modes  $\Phi_r^S$ .

Furthermore, it is presumed that the displacements at the blade structural boundaries in the tuned-system normal modes are so small that the contribution of the boundary modes to the mistuning projection can be neglected. This assumption is especially true for unshrouded rotors used in this research. Then, the dominant cantilevered-blade normal modes are sufficient to project mistuning without losing accuracy which leads to a simplification as:

$$\Phi_r^{ST} \mathbf{K}^\delta \Phi_r^S \approx \mathbf{Q}^T \boldsymbol{\kappa}^\delta \mathbf{Q} \quad (2.6)$$

Therefore, Eq. 2.5 can be rewritten as follows:

$$[-\omega^2 \mathbf{I} + (1 + j\gamma)(\boldsymbol{\Lambda}^S + \mathbf{Q}^T \boldsymbol{\kappa}^\delta \mathbf{Q})] \mathbf{p}^S = \mathbf{f}^S \quad (2.7)$$

where  $\omega$  is an excitation frequency,  $\boldsymbol{\Lambda}^S$ ,  $\mathbf{p}^S$ , and  $\mathbf{f}^S$  are the modal stiffnesses, displacements, and forces, respectively. Note that these parameters are tailored corresponding to a truncated set of tuned-system normal modes, which might not cover all the frequency range of the mistuned bladed disk.  $\boldsymbol{\kappa}^\delta$  is a mistuning projection matrix, which contains the projection of blade stiffness mistuning to a truncated set of cantilevered-blade modes.  $\mathbf{Q}$  is the matrix of participation factors of the cantilevered-blade modes for the blade motion in the tuned-system modes.  $\gamma$  is a structural damping factor.

## Blade Dominant Modes

As Lim *et al.* [18, 52] proposed, blade mistuning is usually represented by the variations of cantilevered-blade eigenvalues, *i.e.* natural frequencies, from the nominal values. These variations are obtained by projecting the blade stiffness mistuning to the cantilevered-blade modes. In case of supposing very small displacements at the blade root, the mistuning projection to cantilevered-blade *constraint* modes is neglected. Thus  $\mathbf{Q}$  is replaced by  $\mathbf{Q}^{CB}$  which contains only the factors corresponding to the cantilevered-blade *normal* modes. In addition, the off-diagonal coupling term of the mistuning projection matrix,  $\boldsymbol{\kappa}^\delta$ , can be ignored while assuming the motion of a blade in a bladed disk is dominated by a single cantilevered-blade normal mode. Consequently,  $\boldsymbol{\kappa}^\delta$  is approximated by  $\boldsymbol{\Lambda}^{CB}$ , which is a diagonal matrix of the eigenvalue deviations of the remained cantilevered-bladed normal modes.

Based on the four assumptions discussed above, the equation of steady-state forced response can be expressed in tuned system modal coordinates as:

$$\left[ -\omega^2 \mathbf{I} + (1 + j\gamma) \left( \boldsymbol{\Lambda}^S + \mathbf{Q}^{CBT} \delta \boldsymbol{\Lambda}^{CB} \mathbf{Q}^{CB} \right) \right] \mathbf{p} = \mathbf{f}^S \quad (2.8)$$

where  $\mathbf{p}$  is introduced to the equation instead of  $\mathbf{p}^S$  since  $\mathbf{p}$  itself denotes the modal coordinates.

### 2.2.3 Mistuning Identification and Model Updating Based on CMM

The advent of one-piece bladed disks, or blisks, in the turbine engine industry means that mistuning in an industrial rotor cannot always be measured simply by removing and testing individual blades. This has led to the development of several techniques for identifying mistuning experimentally based on the vibration response of the full blisk [16–18, 22, 44]. By running only a few forced response tests for the full blisk, the individual

blade mistuning values can be extracted, which are typically expressed as deviations of blade-alone natural frequencies or eigenvalues from the nominal (tuned) value for a specific blade mode of interest.

In addition, the CMM method has recently been extended by the authors [18,53] to perform both mistuning identification and reduced-order model updating. This was motivated by a sensitivity study that was performed to consider the influence of errors in modeling parameters and measured data on the mistuning identification results [18]. 100 group of random perturbation with a uniform distribution, were added to each parameters appeared in Eq. 2.8 such as tuned-system mode shape, tuned-system eigenvalues, modal participation factors, measured data, etc. It was observed that the identification results are most sensitive to errors in the tuned system eigenvalues. In order to compensate for these errors, the ‘‘cyclic modeling error’’ terms,  $\delta\Lambda^S$ , were defined as the difference between the tuned system eigenvalues of an actual bladed disk, which are deduced from the test data assuming the mistuning has a mean value of zero, and the eigenvalues predicted from the tuned finite element model (Lim *et al.* [21]). Incorporating these model updating terms leads to the following equations of motion:

$$\left[ -\omega^2 \mathbf{I} + (1 + j\gamma) \left( \Lambda^S + \delta\Lambda^S + \mathbf{Q}^{CBT} \delta\Lambda^{CB} \mathbf{Q}^{CB} \right) \right] \mathbf{p} = \mathbf{f}^S \quad (2.9a)$$

$$\mathbf{x} = \Phi_{CB}^S \mathbf{p} \quad (2.9b)$$

$$\mathbf{f}^S = \Phi_{CB}^{ST} \mathbf{f}^{CB} \quad (2.9c)$$

where  $\omega$  is the excitation frequency,  $\gamma$  is the structural damping factor,  $\mathbf{p}$  and  $\mathbf{x}$  are the modal and physical displacements vector respectively, and  $\mathbf{f}^S$  and  $\mathbf{f}^{CB}$  are the modal and physical force vector. In addition,  $\Lambda^S$  is the diagonal matrix of eigenvalues for the selected

set of system modes used as a modeling basis and  $\Phi_{CB}^S$  is a full matrix of the blade portion of tuned system mode shape. Individual blade mistuning is presented by a diagonal matrix  $\delta\Lambda^{CB}$  containing the mistuning values for all of the blades in cantilevered blade modal coordinates. In particular, a matrix of modal participation factors corresponding to cantilevered-blade normal mode only,  $\mathbf{Q}^{CB}$ , is generated, which defines the transformation of blade mistuning from cantilevered-blade modal coordinates to the generalized coordinates of the reduced-order model.

While identifying the unknown blade mistuning and cyclic modeling error, the forcing is eliminated by subtracting the equations at two different resonant frequencies,  $\omega_i$  and  $\omega_j$ , assuming the same external forcing at each excitation frequency. Applying this approach to Eq. 2.9 leads to the following expression:

$$-(\omega_i^2 \mathbf{p}_i - \omega_j^2 \mathbf{p}_j) + (1 + j\gamma) \left[ \Lambda^S + \delta\Lambda^S + \mathbf{Q}^{CBT} \delta\Lambda^{CB} \mathbf{Q}^{CB} \right] (\mathbf{p}_i - \mathbf{p}_j) = \mathbf{0} \quad (2.10)$$

Otherwise, if the structural damping is small and individual system modes can be excited near their natural frequencies, the forcing in Eq. 2.9 can be ignored by assuming a free response case:

$$\left[ -\omega^2 \mathbf{I} + (1 + j\gamma) \left( \Lambda^S + \delta\Lambda^S + \mathbf{Q}^{CBT} \delta\Lambda^{CB} \mathbf{Q}^{CB} \right) \right] \mathbf{p} = \mathbf{0} \quad (2.11)$$

#### 2.2.4 Equation Reformatting in Computational Process

Although  $\delta\Lambda^S$  and  $\delta\Lambda^{CB}$  are the unknowns introduced in the Eq. 2.8, the actual variables identified from the algorithm,  $\mathbf{D}^S$  and  $\mathbf{D}^{CB}$ , are slightly different yet related to them based on the following expressions:

$$\delta\Lambda^S = \Lambda^S \cdot \mathbf{D}^S \quad (2.12a)$$

$$\delta\Lambda^{CB} = \lambda^{CB} \cdot \mathbf{D}^{CB} \quad (2.12b)$$

where  $\lambda^{CB}$  is the tuned cantilevered blade eigenvalue for this investigated family,  $\mathbf{D}^S$  and  $\mathbf{D}^{CB}$  are both diagonal matrix respectively in the same format as  $\delta\Lambda^S$  and  $\delta\Lambda^{CB}$ . Thus Eq. 2.11 can be re-written as follows:

$$\left[ -\omega^2 \mathbf{I} + (1 + j\gamma) \left( \Lambda^S (\mathbf{I} + \mathbf{D}^S) + \mathbf{Q}^{CBT} (\lambda^{CB} \cdot \mathbf{D}^{CB}) \mathbf{Q}^{CB} \right) \right] \mathbf{p} = \mathbf{0} \quad (2.13)$$

Since the unknowns in this case is only the diagonal terms of  $\mathbf{D}^S$  and  $\mathbf{D}^{CB}$  which can be represented respectively by two vectors notated as  $\mathbf{d}^S$  and  $\mathbf{d}^{CB}$ , the algorithm for mistuning identification and model updating can be reformatted and abbreviated as:

$$\begin{bmatrix} \mathbf{A}_S & \mathbf{A}_{CB} \end{bmatrix} \begin{Bmatrix} \mathbf{d}^S \\ \mathbf{d}^{CB} \end{Bmatrix} = \mathbf{B} \quad (2.14)$$

where  $\mathbf{A}_S$  and  $\mathbf{A}_{CB}$  are the reframed coefficient matrices in order to arrange unknowns from  $\delta\Lambda^S$  and  $\delta\Lambda^{CB}$  into  $\mathbf{d}^S$  and  $\mathbf{d}^{CB}$ .

$$\mathbf{d}^S = \begin{Bmatrix} d_1^S \\ d_2^S \\ \dots \\ d_M^S \end{Bmatrix}, \quad \mathbf{d}^{CB} = \begin{Bmatrix} d_1^{CB} \\ d_2^{CB} \\ \dots \\ d_N^{CB} \end{Bmatrix} \quad (2.15)$$

All of them are fully known once the blade responses  $\mathbf{p}$  are obtained at desired excitation frequencies  $\omega$ . Generally there are more than one measurement required to identify the

blade stiffness mistuning and cyclic modeling error, for example,  $\mathbf{p} = [\mathbf{p}_1 \quad \mathbf{p}_2 \quad \cdots \quad \mathbf{p}_L]$  is a group of measurements in modal coordinates taken at a series of system resonant frequencies, where  $L$  is the number of measurements. More detailed explanation of the mistuning identification and model updating process in abbreviated matrix format are introduced in the Appendix A. Note that As  $L$  increasing, there are more than necessary rows added to the coefficient matrices  $\mathbf{A}_S$  and  $\mathbf{A}_{CB}$ . In other word, there are more equations than unknowns so that least squares method is adopted by applying pseudo inverse (Matlab function “pinv”) on the entire coefficient matrix in the purpose of minimizing the fitting errors.

$$\begin{Bmatrix} \mathbf{d}^S \\ \mathbf{d}^{CB} \end{Bmatrix} = \text{pinv} \left( \begin{bmatrix} \mathbf{A}_S & \mathbf{A}_{CB} \end{bmatrix} \right) \cdot \mathbf{B} \quad (2.16)$$

## 2.3 Experimental Apparatus

### 2.3.1 Overview of Test Facilities

The experimental facility used to examine the effect of mistuning in a controlled environment, shown in Figure 2.1, includes a non-contacting, traveling-wave excitation system, as well as a non-contacting measurement system featuring a Scanning Laser Doppler Vibrometer (SLDV). The SPLV used for quantitative vibration measurements consists of a Polytec OFV 2602 Vibrometer Controller and a Polytec OFV 353 Sensor Head. The laser head is mounted on a two-dimensional linear traverse, which allows it to be moved in a plane parallel to the surface of the specimen so that vibration can be measured at various locations. The SLDV used for full-field measurement of vibration consists of a Polytec OFV 3001S Vibrometer Controller and a Polytec OFV056 Scanning Head. Instead of being moved mechanically on the traverse, the scanning head changes its laser

beam position optically by moving two inside mirrors in both  $x$  and  $y$  directions. The measurement results obtained by SLDV can be either exported numerically or visualized as 2-D or 3-D images. Both the excitation system and the measurement system are automatically controlled by a PC workstation through LabView. The experiment takes place on a vibration-isolated workstation, which isolates the test specimen and measurement system from vibration transmitted through the floor of the room.

### **2.3.2 Traveling Wave Excitation System**

Figure 2.2 and 2.3 shows a close-up of the traveling-wave excitation system. Behind each blade, there is a round speaker mounted in a parallel position with the surface of the blade in order to apply an acoustic force. These speakers are driven by a series of Hewlett-Packard 8904 Multifunction Synthesizers, each with two independent but phase-synchronized channels. Before reaching to each speaker, the output signals from HP8904 were conditioned by being passed through variable gain amplifiers [30].

Moreover, the speakers are carefully calibrated using white noise excitation first. Then, the speakers are mounted on the plastic fixtures, and a sinusoidal signal is sent to each speaker, one at a time. A calibrated microphone is used to record the sound pressure level at a fixed distance from the speaker, similar to the distance to the individual blade when it is mounted on the fixture. The amplitude and phase of the excitation signal are adjusted in order to achieve a flat frequency response of the sound pressure level produced by the speaker. This process is digitally controlled and it is repeated, in turn, for each speaker on the fixture. Both Single Blade Excitation (SBE) and Engine Order Excitation (EOE) can be imposed on the bladed disk. For SBE, only a single speaker is active at a time. In case of EOE, all the speakers are active simultaneously, delivering forces of same amplitude, but with a certain phase lag corresponding to the selected EOE, between adjacent speakers.

For example, the excitation of a particular blade can be written as:

$$f_n = f_0 \cos(\omega t + (n - 1) \phi) \quad (2.17a)$$

$$\phi = \frac{2\pi C}{N} \quad (2.17b)$$

where  $f_0$  is the force amplitude,  $\omega$  the frequency of excitation,  $N$  the blade number,  $\phi$  the phase difference between adjacent blades,  $n$  the engine order of the excitation. Thus any EOE can be obtained by simply changing the phase lag. The traveling-wave excitation not only simulates the realistic operating system in which the rotating bladed disk passes through a stationary excitation source, but also ensures the feasibility of the observation system (Judge *et al.* [23]). To achieve engine order excitation, all the speakers are driven simultaneously to deliver forces of the same amplitude, but with a certain phase lag between adjacent speakers.

## 2.4 Experimental Validation Results

### 2.4.1 Validation Rotor

Figure 2.4 shows a validation rotor with 24 blades of rectangular cross section and Fig. 2.5 shows its finite element model. This rotor is used to experimentally validate the new ROM approach and model updating method discussed above. It is designed and manufactured to an extremely tight tolerance so as to minimize residual blade mistuning. The first flexural blade mode family (2110.0 — 2170.0 *Hz*, nodal diameters 6 — 12) is investigated, which involves 13 system modes and for which the blade mode is dominant.

## Resonant Frequencies of Mistuned Rotor

Figure 2.8(a) and 2.8(b) present the identification results of blade stiffness mistuning and cyclic modeling error combined the measurements and the tuned CMM model of the validation rotor, where the blade stiffness mistuning is assumed to possess a zero mean. The specific value of those identified parameters is shown in Table 2.1.

Figure 2.7 compares the experimentally determined natural frequencies of the validation rotor and those obtained from the CMM model updated using the identified blade stiffness mistuning and the cyclic modeling error. As observed by other researchers [9, 54, 55] in their previous work, the phenomena of peak slitting was demonstrated in table 2.2. Various sets of modal measurements are selected to calculate the model updating parameters. Observe that when 13 measured modes are used, the experimental and estimated frequencies agree nearly perfectly, but that the use of six modes, or even only of two modes, yields errors that are quite acceptable. Thus an important advantage of the technique is that an incomplete set of measurements can produce an accurate updated CMM model. This feature is especially useful for systems with high modal densities, such as bladed disks with large numbers of blades or weak inter-blade coupling.

## Mode Shapes of Mistuned Rotor

Figure 2.9(a) and 2.10(a) shows the excellent match between the experimental and updated CMM model results, for the first and last vibration mode of the validation rotor at 2114.3  $Hz$  and 2158.3  $Hz$ , respectively. The 3-D images of the same mode shapes are depicted in Figure 2.9(b) and 2.10(b), which were obtained with the SLDV. (Note that the variation in amplitude at the tip of each blade is not physical but results from optical scattering at the edge of the vibrating blade). While mode 1 (Figure 2.9) is extended throughout the rotor, other modes were found to be localized to a few blades. For example,

strong localization occurs for mode 13 as shown in Figure 2.10, such that vibration energy is confined to blades 1 — 3 and 22 — 24, while blades 9 — 14 feature minute motion. Therefore, the mistuning problem is complicated by the fact that mistuning may produce a highly localized mode at certain natural frequency yet an extended mode at a different frequency. Also, the blade or blades with the greatest deviation in geometry or properties are not necessarily those in which the energy becomes confined.

It is advantageous that an incomplete set of measurements can yield an accurately updated CMM model, especially for a system with high modal density. Figure 2.18 shows the accuracy of two updated CMM models, where either all 13 or only 3 measured modes are used for the model updating. At 2114.3  $Hz$ , the measured forced response due to EOE 6 is compared to various forced responses and mode shapes predicted by the updated CMM models. Due to the relatively small structural damping (0.00015) for the validation rotor, both EOE and SBE primarily excite the mode shape at the corresponding natural frequency. Thus the predicted mode shape and the SBE and EOE responses are similar. Note that all the predicted mode shape, SBE, and EOE responses agree with experimental measurements within an acceptable level. However, as the number of involved modes decreases from 13 to 3, this agreement deteriorates somewhat. In the case of single blade excitation, SBE 4 is selected because the even-numbered blades feature a stronger response for this mode shape, ensuring its successful observation. This advantage can be further understood by considering the comparison of identified blade stiffness mistuning and cyclic modeling error. As can be seen in the Fig. 2.12, apparent errors occur only when only 2 measured data are used to apply the identification algorithm.

## Forced Responses and Sensitivity Study

The new mistuning identification and model updating techniques have also been validated for the forced response of mistuned rotors. Figure 2.13 shows the good agreement between the measured frequency response and the estimated response of the updated CMM model, for a case of harmonic single blade excitation (SBE). In this case, the blade on which the measurement is performed is the blade being excited. For example, fig. 2.13(a) shows the frequency sweep response of blade 2 while only speaker 2 was driven. Figure 2.14 is for another case of SBE, where blade 1 is excited and the responses of blade 4,5,19 and 24 are measured. Again, good agreement is observed, particularly for the resonant frequencies, but there are some discrepancies in the relative amplitudes of the measured and estimated peak amplitudes.

Next, 1000 sets of random perturbations were artificially added to the cyclic modeling error in order to assess the sensitivity of the forced response to uncertainties in the cyclic modeling error. Perturbations ranging from -4% to +4% of the identified cyclic modeling error were considered. Figure 2.15 and 2.16 shows the envelopes of the maximum and minimum responses for these 1000 random patterns (the amplitudes of blade 4 and 19 are depicted for a SBE of that blade). Considerable variations in the resonant peak amplitudes are observed, indicating that the forced response of the bladed disk is highly sensitive to the cyclic modeling error. In particular, the discrepancies observed in Figure 2.13(b) are well within the minimum and maximum envelopes of Figure 2.15; for example, consider the lowest-frequency resonant peak of blade 4 for the experiment in Fig. 2.13(b), of amplitude 0.5, which is higher than the corresponding minimum value in Fig. 2.15.

Finally, the new identification and updating method is validated for various cases of engine order excitation (EOE). Figure 2.17 shows good agreement between the measured and estimated frequency responses of blade 9 for EOE 8 in Fig. 2.17(a), blade 3 for EOE 12

in Fig. 2.17(b), and a comparative set of blade 2 and blade 4 for EOE 11 in Fig. 2.17(c) and 2.17(d). For a tuned bladed disk under EOE, only the free vibration mode with the same interblade phase angle as the excitation is excited, producing a single resonance peak. For a mistuned system all modes are excited. The results shown in Figure 2.17 indicate that several modes in this frequency range, 2113.0 — 2165.0  $Hz$ , are excited simultaneously for all EOE considered. Since the identified mistuning of the validation rotor is quite small (0.29%), one would expect the pair of mistuned modes that is a perturbation of the tuned mode with the same number of nodal diameters as the excitation to feature the strongest response, and this is seen in Fig. 2.17(a). However, the responses for EOE 11 and 12 are different compared with those for EOE 8, where the pair of modes 8 is dominant. As can be seen in Fig. 2.17(b), EOE 12 not only excites mode 12 strongly but also mode 11. Moreover the response of blade 3 by EOE 12 reveals an even stronger response at the adjacent mode 11. The modal density of this frequency range (2150.0 — 2165.0  $Hz$ ) is especially high, with 7 modes grouped within 10  $Hz$ . Fig. 2.17(c) and 2.17(d) compare the responses of different blades excited by the same EOE, which are not necessarily similar. For example for blade 2, modes 10, 11 and 12 all respond strongly, while for blade 4, mode 12 is relatively quiet. Note that the discrepancies between predicted and observed responses are caused by the sensitivity of the forced response to uncertainties in the cyclic modeling error.

### **Advantage of Model Updating**

The most innovative aspect of the new method is the introduction of the cyclic modeling error into the CMM model, along with the traditional blade mistuning terms. The updated model thus reflects errors or uncertainties present in the eigenvalues of not only the cantilevered blades but also the tuned bladed disk. Figure 2.18 compares, at 2150.6

$Hz$ , the measured EOE 10 response with various forced responses and mode shapes predicted by CMM models with and without updated cyclic modeling error. Observe that updated CMM responses agree very well with the measured response in all cases. The CMM model without updating does well at predicting the mode shape, but both SBE and EOE responses are incorrectly estimated.

This observation is corroborated in Figure 2.5, where the measurements for blades 2 and 4 are as in Fig. 2.17(c) and 2.17(d). However, for these cases no model updating is done, and only the blade mistuning is included into the CMM. The predicted frequency responses of blade 2 and 4 at EOE 11 do not match with the experimental observations. Both these results suggest that the cyclic modeling error plays a critical role in model updating and that it cannot be neglected.

#### **2.4.2 NASA Bladed Disk**

As a further validation, the new identification and updating method is applied to an advanced NASA bladed disk prototype with 26 blades, shown in Figure 2.20. A special fixture was designed and manufactured to mount both the NASA bladed disk and speakers on the vibration-isolated table. The proper installation steps (fig. 2.23) are described as follows.

1. Install the NASA bladed disk to the flange and then attach the flange to the L-shape fixture in the workshop(fig. 2.23(a)).
2. Bolt the plastic wedges as speaker's holding fixture to the outside ring in the workshop(fig. 2.23(b)).
3. Move and mount the whole piece on the vibration-isolated table by crane and then insert speakers with cable connected to the signal generators(fig. 2.23(c)).

4. Cover the NASA bladed disk with white powder for a better reflection especially for the holographic interferometry(fig. 2.23(d)).

### **Measured Resonant Frequencies and Mode Shapes**

The finite element model (FEM) of the NASA bladed disk is depicted in Figure 2.21 and a computational mode shape at nodal diameter 2 is displayed as Figure 2.22. Compared to the validation rotor, the designed configuration of NASA bladed disk is much more complicated, especially at the blade part. The blades are twisted and the thickness of the blade varies along the axis pointing from the root to the tip. Apparently the degree of freedom (DOF) of the NASA bladed disk increases significantly to millions per sector, which is only 265 for the validation rotor. Therefore the expensive computational time for a mode shape shown in Figure 2.22 is expectable. And the CMM technique can be applied to create a reduced order model on the order of blade number, *i.e.* 26, for the NASA bladed disk.

This compressor stage features a high modal density, and the 26 modes of the first-bending blade-dominated family are grouped within a range of 13  $Hz$ . Figure 2.24(a) and 2.24(b) present the identification results of blade stiffness mistuning and cyclic modeling error combined the measurements and the tuned CMM model of the NASA bladed disk. The specific value of those identified parameters is shown in Table 2.3. Figure 2.26 compares the free vibration natural frequencies obtained from measurements with those predicted by the updated CMM model. An incomplete set of natural frequencies (22 out of 26) was found from testing, probably due to the high modal density and insufficient frequency resolution (0.1  $Hz$ ).

However, since the identification and updating method only needs partial measurements, the complete mistuning pattern and the cyclic modeling error can be extracted

from just a few of the 22 measured shapes. Note in Figure 2.26 the very good match for the 22 natural frequencies. Also, Figure 2.27(a) shows good agreement between the predicted and measured mode shapes at 738.9  $Hz$ , while Figure 2.27(b) shows a nearly perfect match at 764.1  $Hz$ . Figure 2.27(b) shows the severe localization of the mode shape to blades 18 and 19, indicating the high sensitivity to residual mistuning in the specimen tested. Note how well the updated CMM model is able to capture this localized behavior.

### **Identification of Intentional Mistuning**

Mistuning was added to the NASA bladed disk by gluing small pieces of lead with different weights to the blade tips, as shown in Figure 2.29. Five blades were mistuned in this way: blades 11, 18, 19, 22 and 26. Since the masses of the lead shims were known, this intentional mistuning was calculated (details in table 2.4) by expressing the relationship between the mass change and the blade stiffness change. Judge [30] and Lim [52] suggested that the mass change can be presented by introducing mistuning into stiffness matrix only without disturbing the mass matrix instead. An experiment was then performed to identify the added mistuning and update the CMM model. The excellent agreement between the expected and the identified mistuning is shown in Figure 2.30.

## **2.5 Conclusions**

A new component mode mistuning reduced-order modeling method has been validated. The approach permits both mistuning identification and updating of the reduced-order model. The experimental validation has been carried out for both a validation rotor and an industrial bladed disk. For the latter, the method has been further validated by identifying mistuning that was intentionally added to several blades. The critical effects of mistuning have been demonstrated experimentally, including the localization of mode shapes, the increase in forced response amplitudes, and the increase in the range of nat-

ural frequencies. One important feature of the method developed is that an incomplete set of measured responses can be used to yield an accurate updated reduced-order model and accurate mistuning parameters; this is especially important for bladed disks with high modal densities, for which it is difficult to experimentally observe all modes. The cyclic modeling error is a critical and unique feature of the new method, and it allows the updated CMM model to predict force responses as well as natural modes of vibration that match very well with the experimental measurements. However, one limitation of the present method is that it can only be applied to a frequency range of blade-dominated modes, and not to modes that are disk-dominated.

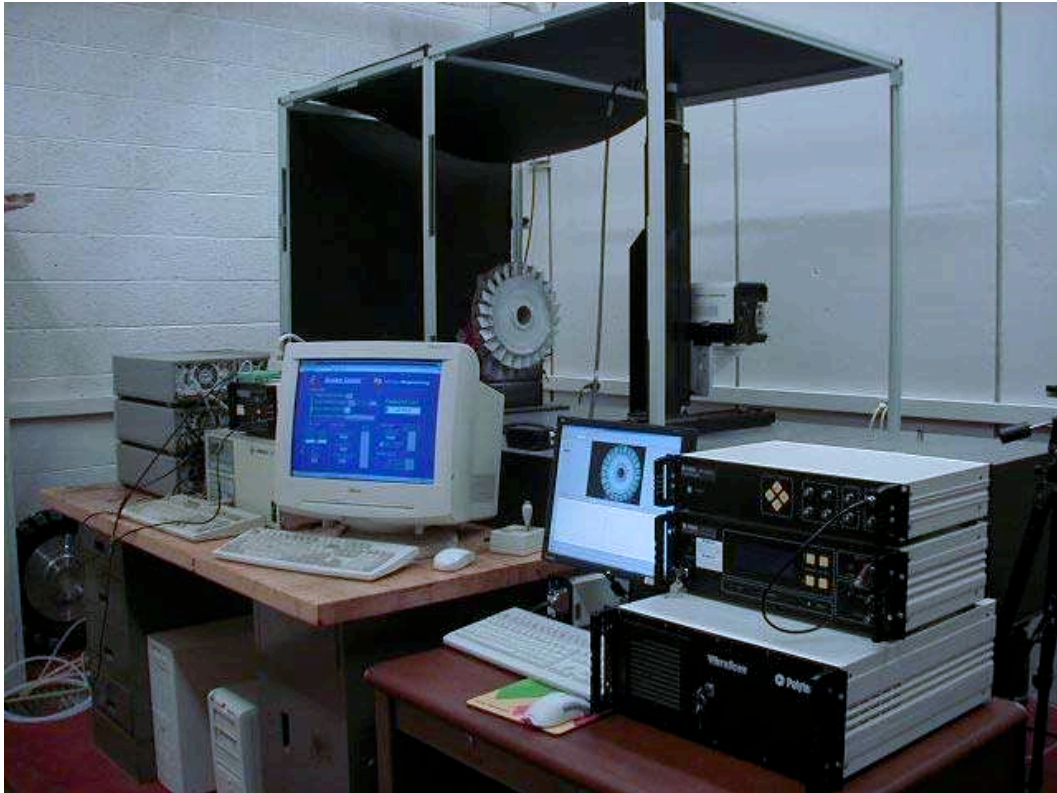


Figure 2.1: Experimental set up of the non-contacting excitation and measurement system.

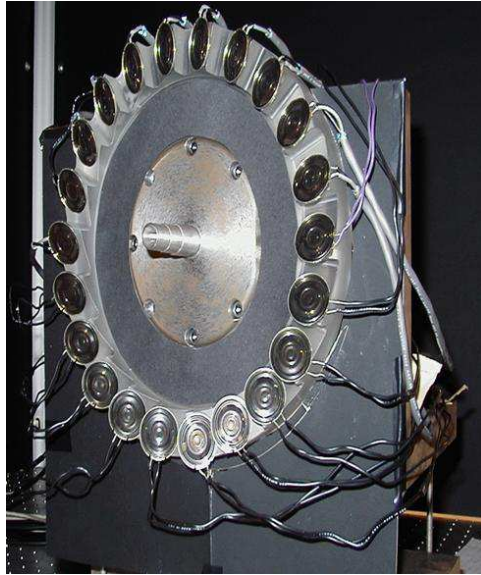


Figure 2.2: Non-contacting acoustic excitation system consisting of speakers.



Figure 2.3: Bladed disk set up with blisk system installed.



Figure 2.4: Picture of 24 blade validation rotor.

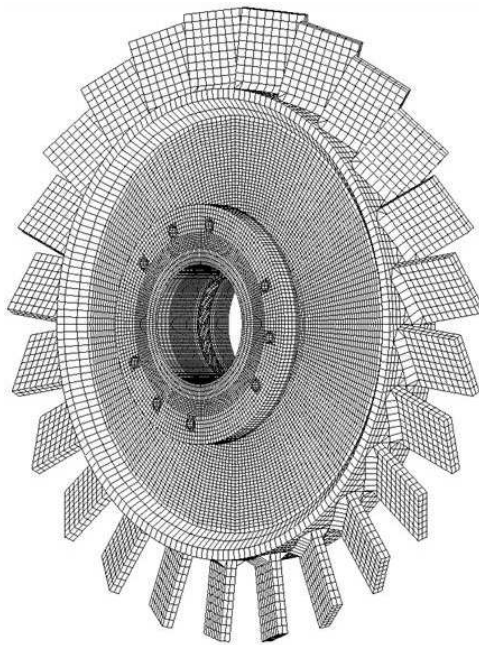


Figure 2.5: Finite element model of the validation bladed disk.

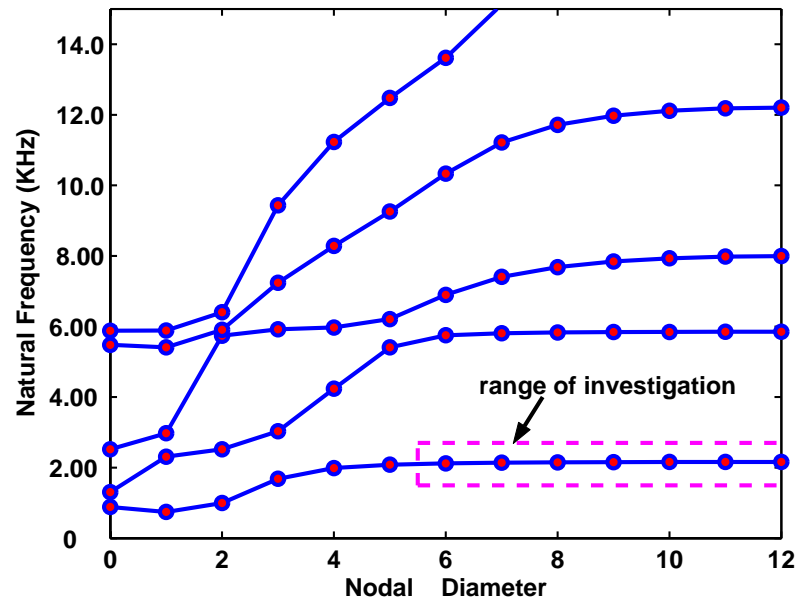


Figure 2.6: Natural frequencies versus the number of nodal diameters for the tuned rotor FEM simulation of validation bladed disk.

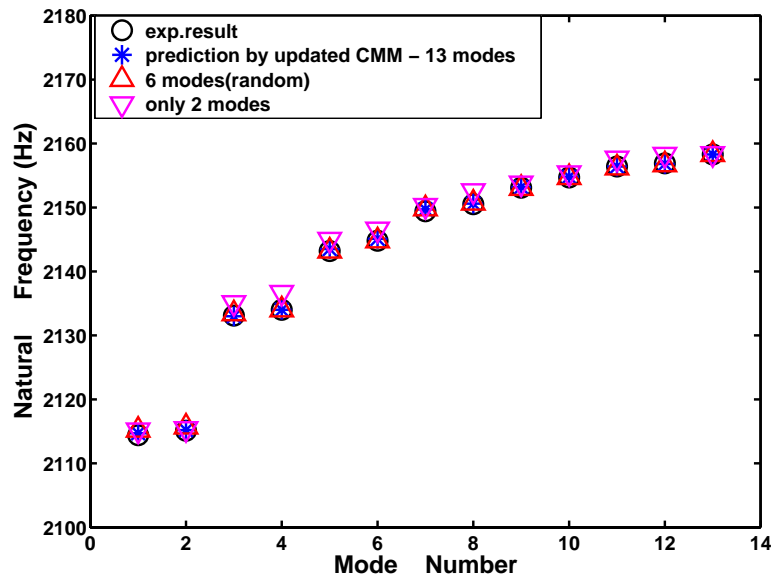
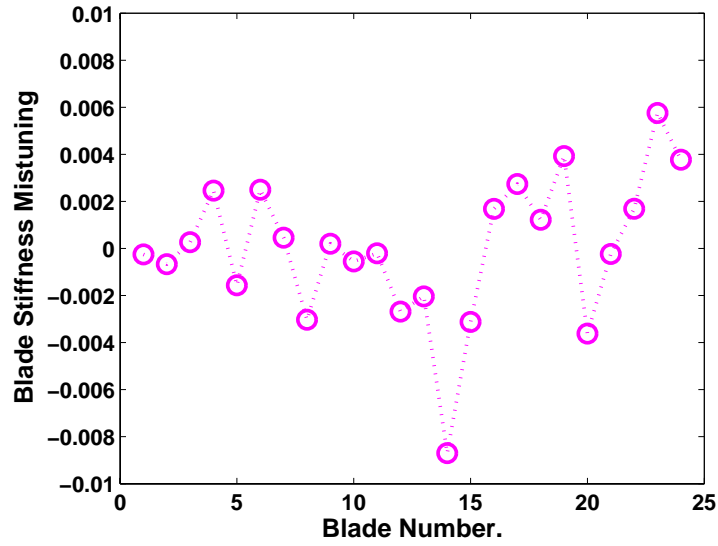
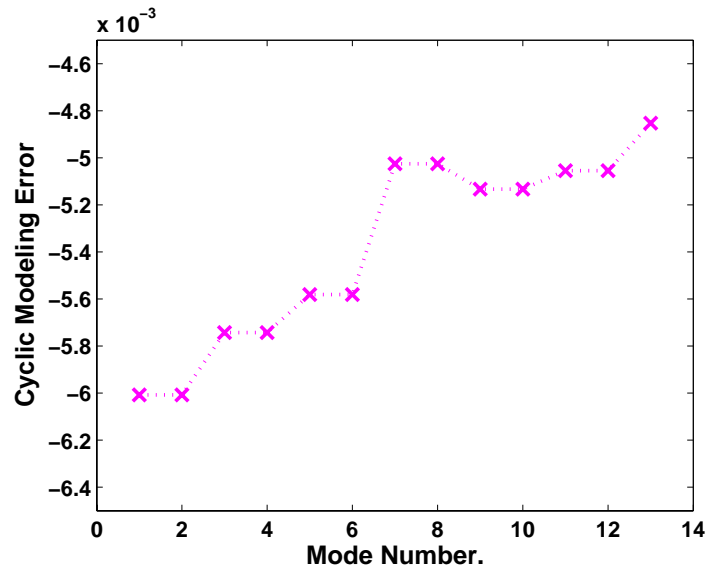


Figure 2.7: Measured natural frequencies of first flexible family for validation bladed disk compared to the FEM predictions.

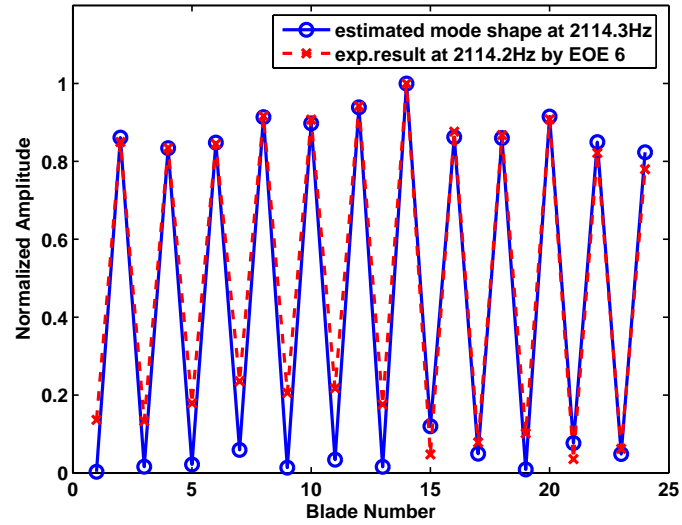


(a) Identified blade stiffness mistuning

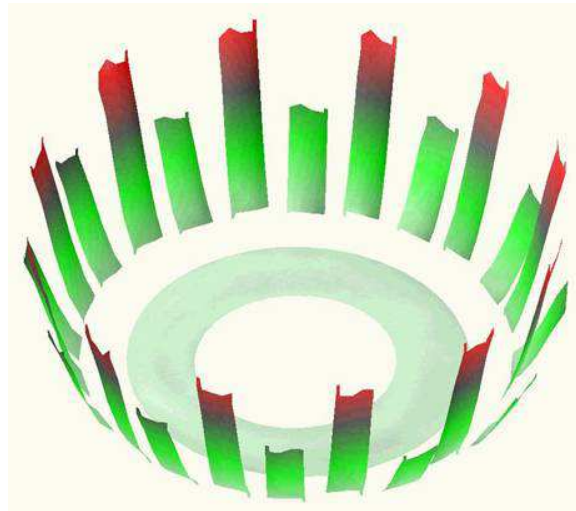


(b) Identified cyclic modeling error

Figure 2.8: Identified parameters for modal updating of validation rotor based on the experiment results.

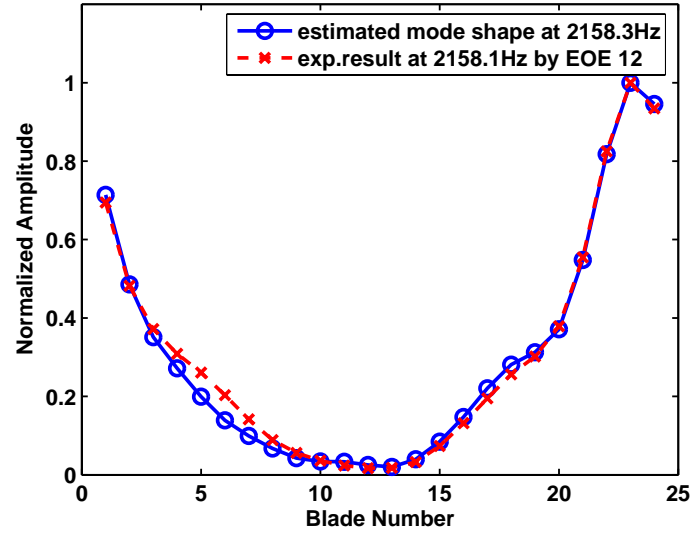


(a) Measured mode shape acquired with the Single Point Laser Vibrometer

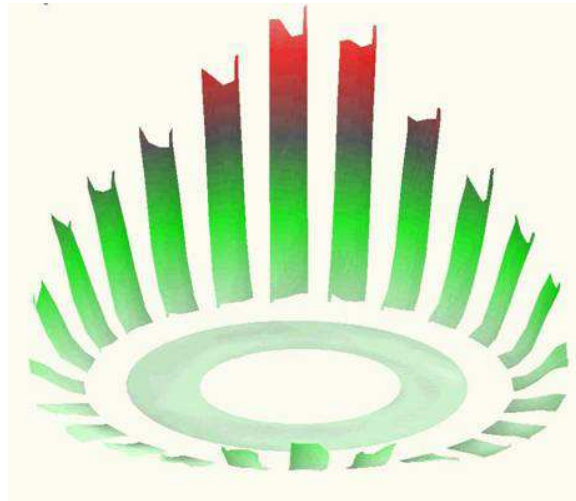


(b) Measured mode shape acquired with the Scanning Vibrometer

Figure 2.9: Representation of mode shape of validation rotor at 2114.3  $Hz$ , measured by the vibrometer and predicted by the updated CMM model.

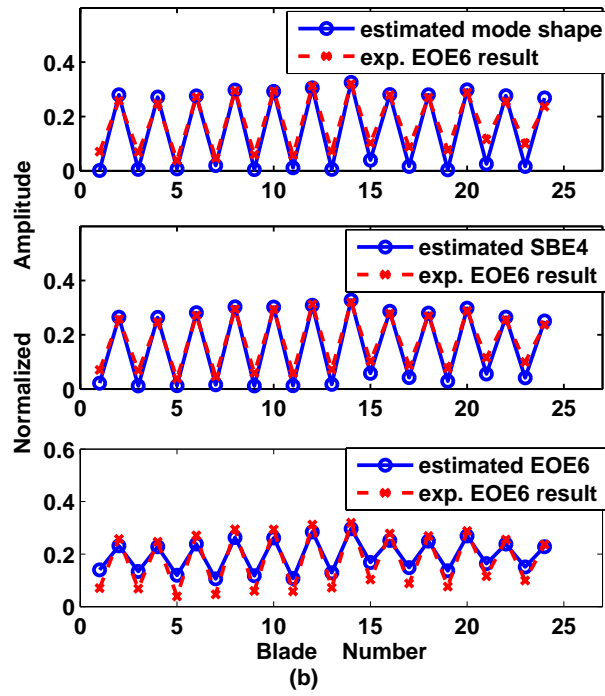


(a) Measured mode shape acquired with the Single Point Laser Vibrometer

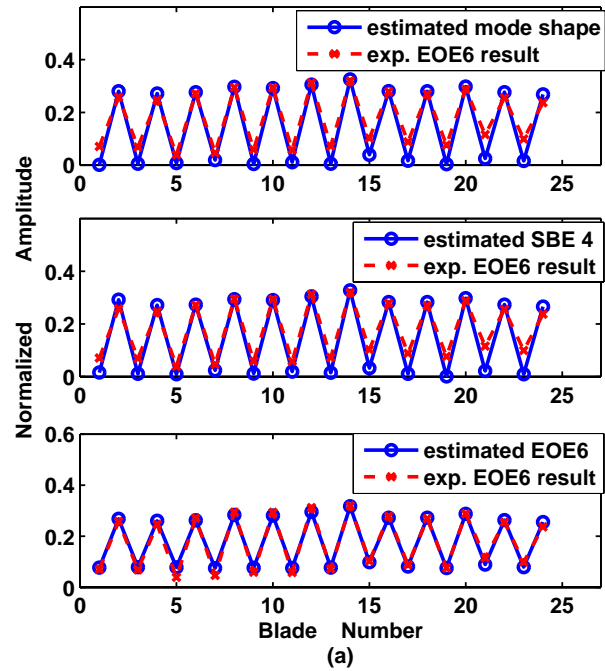


(b) Measured mode shape acquired with the Scanning Vibrometer

Figure 2.10: Representation of mode shape of validation rotor at 2158.3  $Hz$ , measured by the vibrometer and predicted by updated the CMM model.

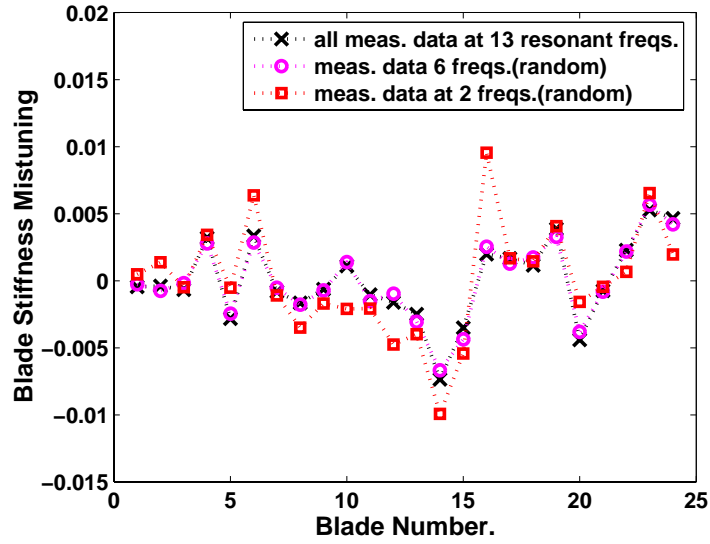


(a) With 3 modes

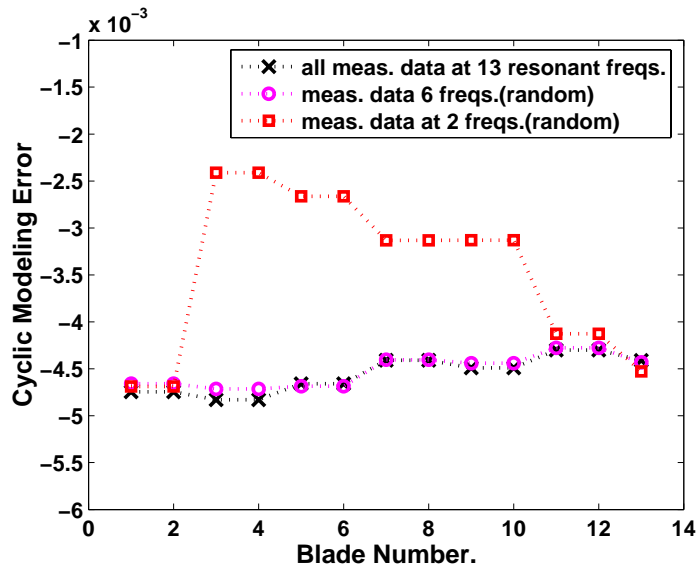


(b) With 13 modes

Figure 2.11: Blade responses at 2114.3 Hz, from experiment and from the updated CMM models for different numbers of measured modes.

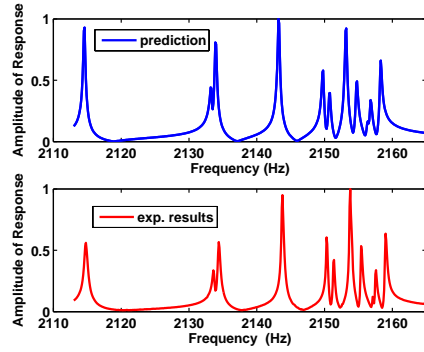


(a) Identified blade stiffness mistuning

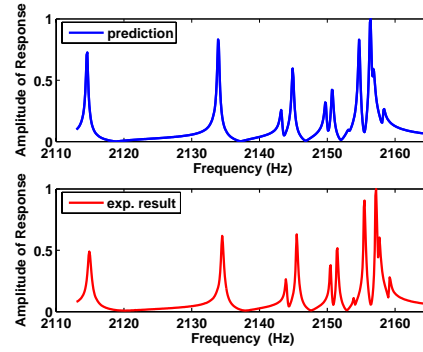


(b) Identified cyclic modeling error

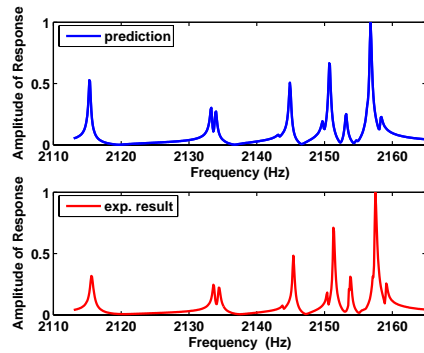
Figure 2.12: Identified parameters for modal updating of the validation rotor based on different sets of experiment results.



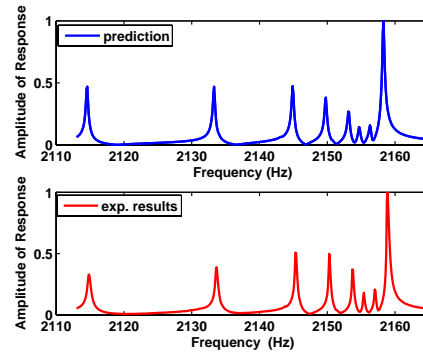
(a) Response of blade 2 by SBE 2



(b) Response of blade 4 by SBE 4

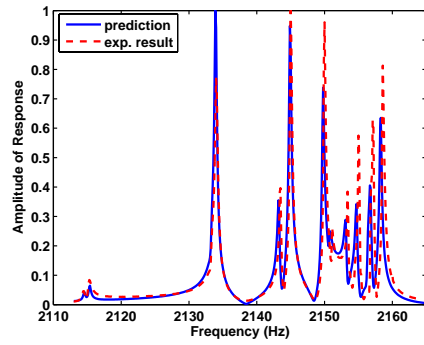


(c) Response of blade 19 by SBE 19

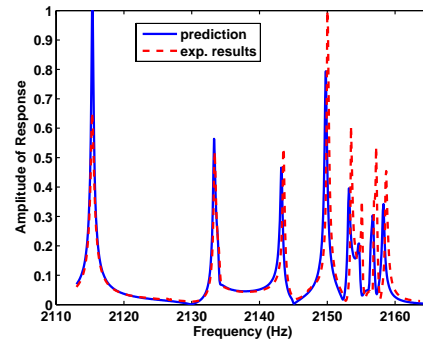


(d) Response of blade 22 by SBE 22

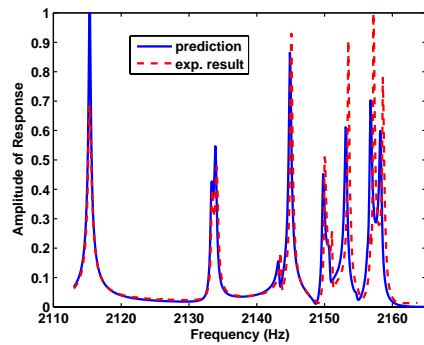
Figure 2.13: Comparison of frequency sweep responses, measured on the various blades while exciting the same one by single blade excitation.



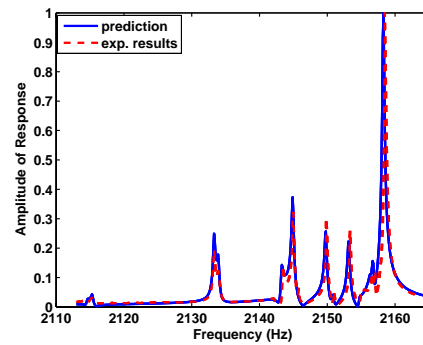
(a) Response of blade 4



(b) Response of blade 5



(c) Response of blade 19



(d) Response of blade 24

Figure 2.14: Comparison of frequency sweep responses, measured on the various blades while exciting blade 1 in all cases.

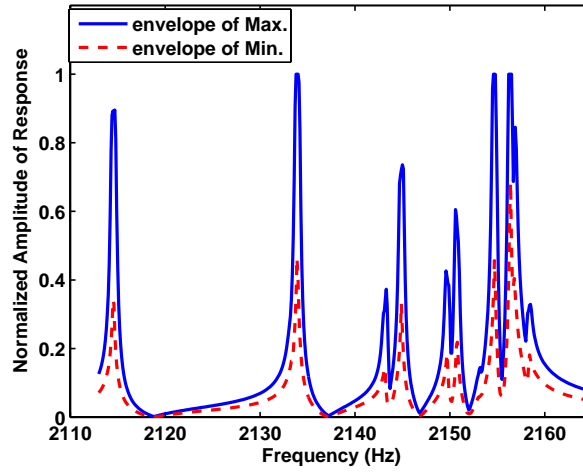


Figure 2.15: Sensitivity of the cyclic modeling error to forced response, blade 4 by single blade excitation on blade 4.

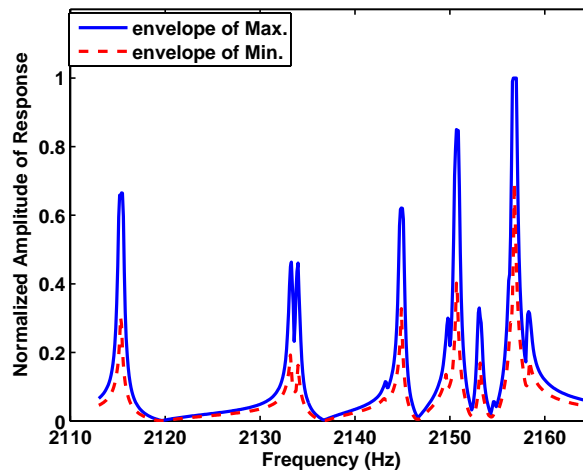
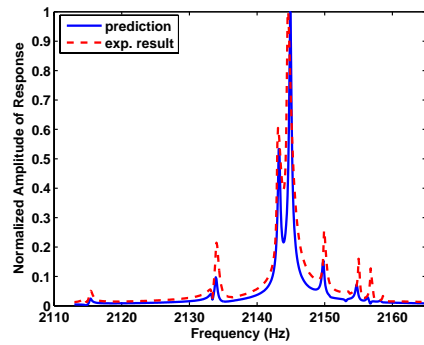
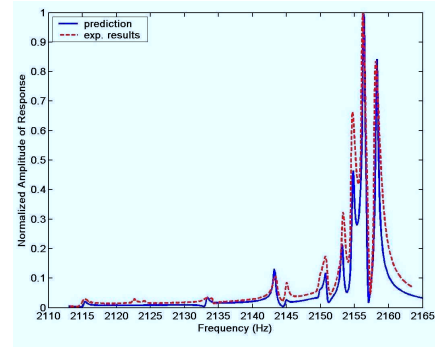


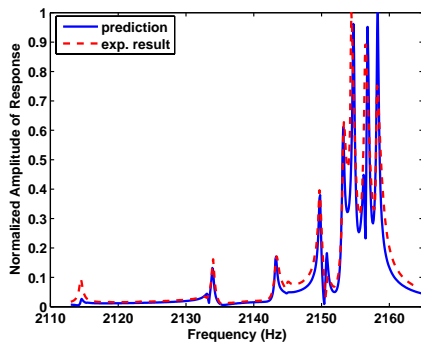
Figure 2.16: Sensitivity of the cyclic modeling error to forced response, blade 19 by single blade excitation on blade 19.



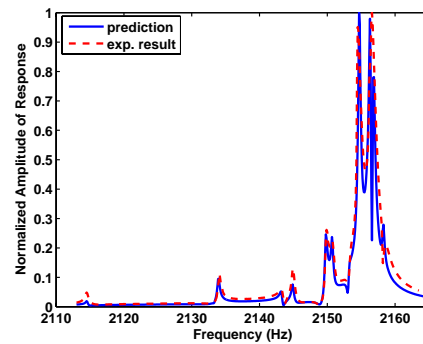
(a) Response of blade 9 by EOE 8



(b) Response of blade 3 by EOE 12

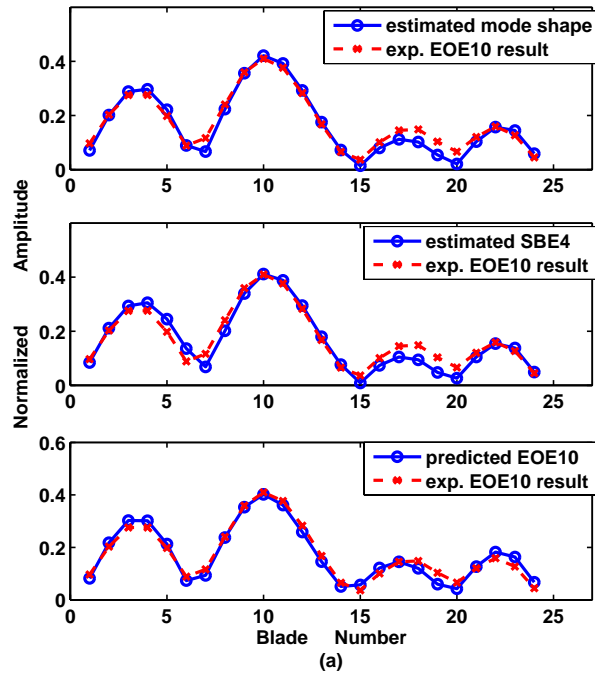


(c) Response of blade 2 by EOE 11

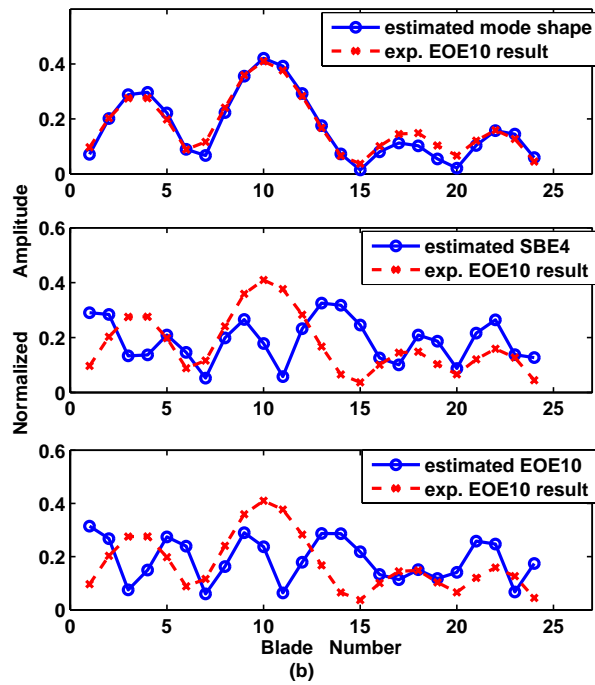


(d) Response of blade 4 by EOE 11

Figure 2.17: Comparison of frequency sweep responses measured on various blades by different engine order excitation (EOE).

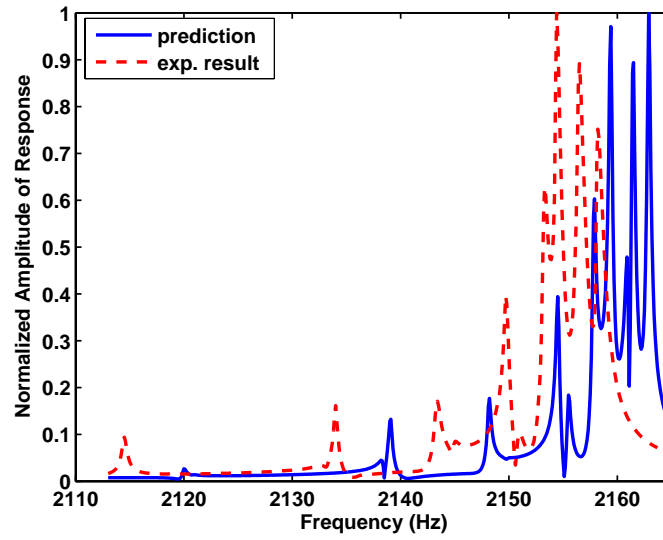


(a) Prediction by the CMM model with modal updating

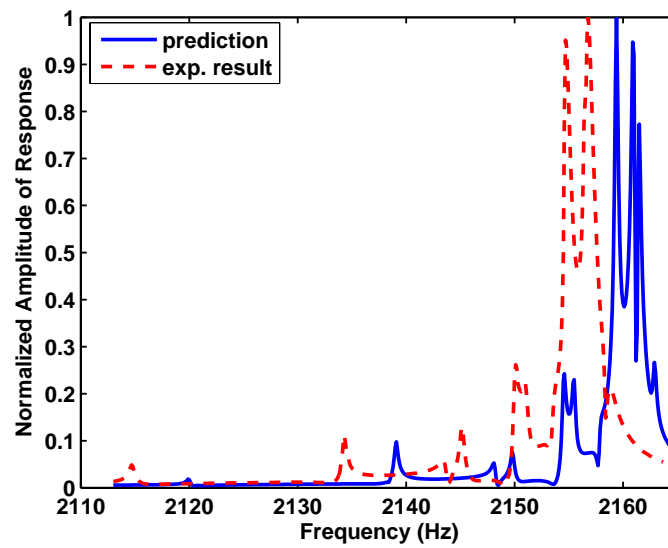


(b) Predicted by the CMM model without modal updating

Figure 2.18: Comparison of the experimental results with various estimated responses, at 2150.6 Hz for validation rotor.



(a) Response of blade 2 by EOE 11



(b) Response of blade 4 by EOE 11

Figure 2.19: Comparison of frequency sweep responses without modal updating on various blades by engine order excitation (EOE) 11.



Figure 2.20: The NASA bladed disk mounted with speakers.



Figure 2.21: Finite element model of the NASA bladed disk.

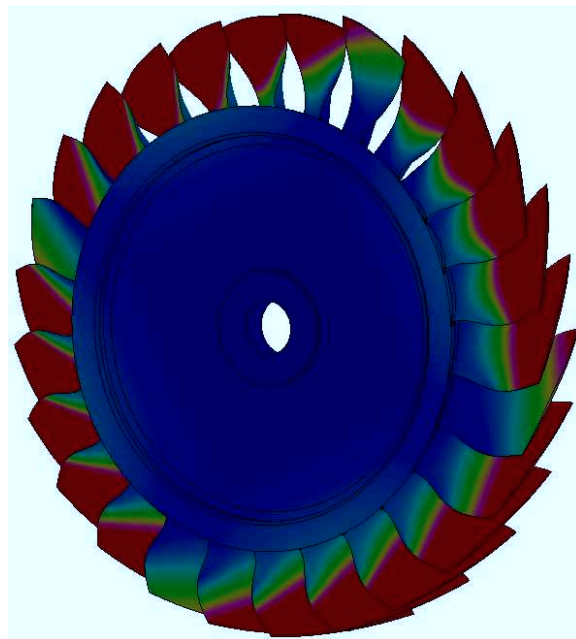


Figure 2.22: Mode shape of the NASA bladed disk at nodal diameter 2.



(a) Attach NASA bladed disk to fixture flange in the workshop



(b) Install the holding fixture for speakers in the workshop

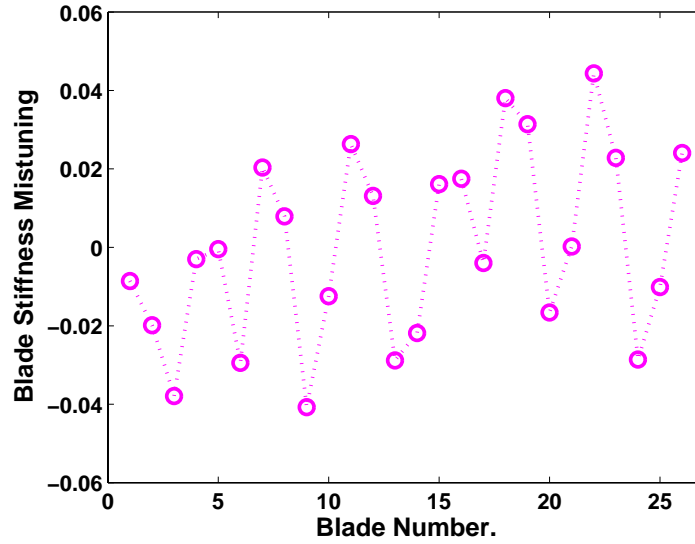


(c) Mount speaker behind each blade on the anti-vibration table, connected to signal generator

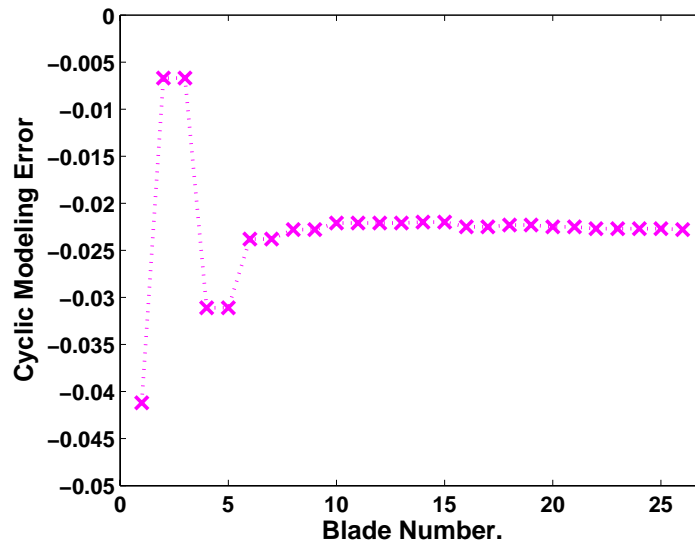


(d) Set up single point laser vibrometer and interferometry

Figure 2.23: The installation process of the NASA bladed disk.



(a) Identified blade stiffness mistuning of the NASA blisk



(b) Identified cyclic modeling error of the NASA blisk

Figure 2.24: Identified parameters for modal updating of the NASA blade disk based on the experiment results.

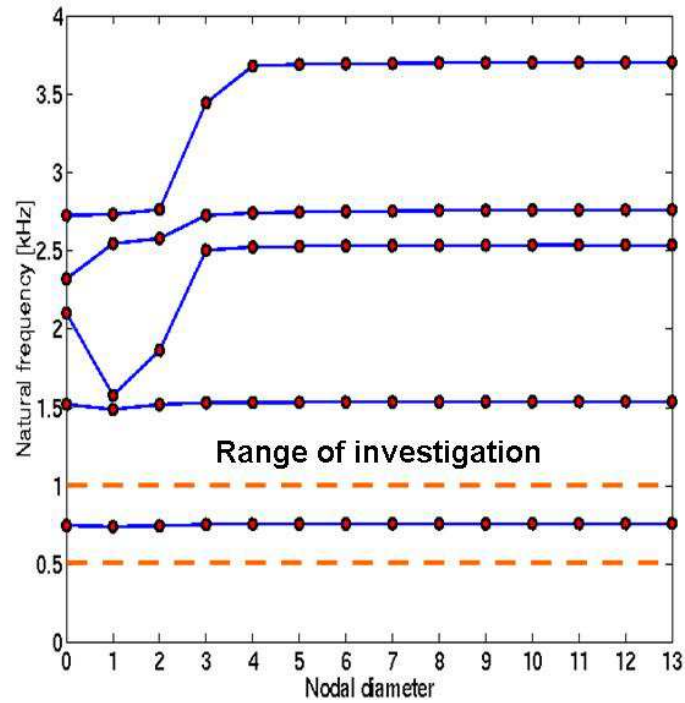


Figure 2.25: Natural frequencies versus the number of nodal diameters for the tuned rotor FEM of the NASA bladed disk.

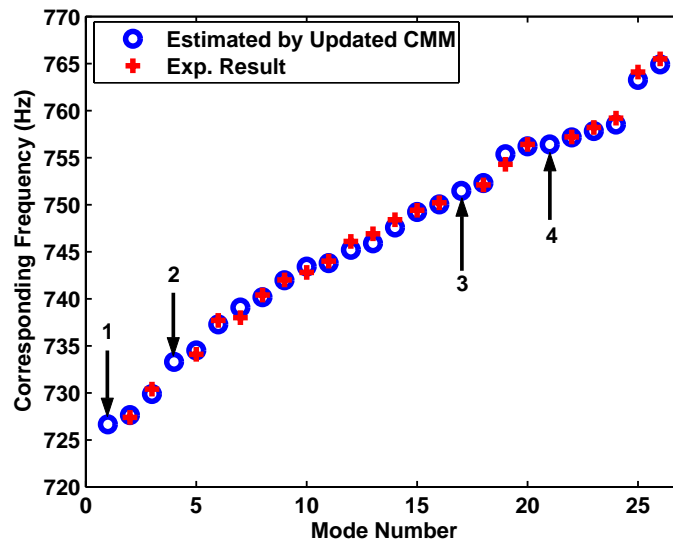
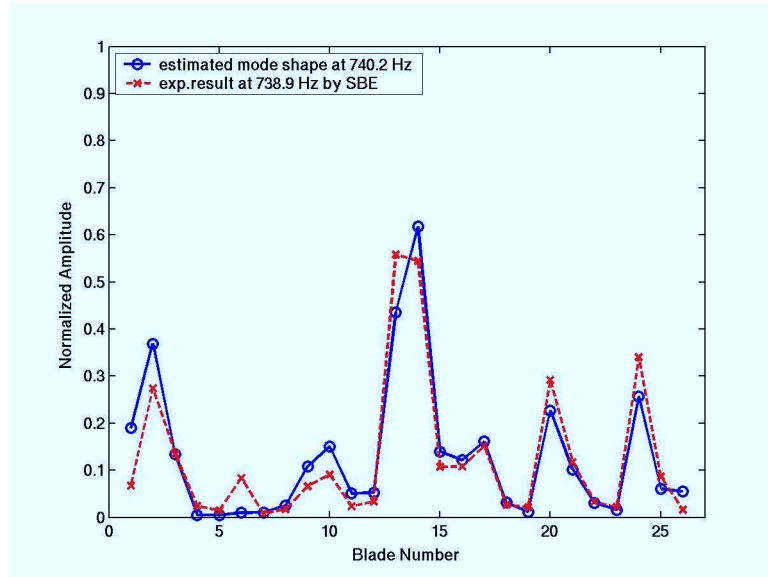
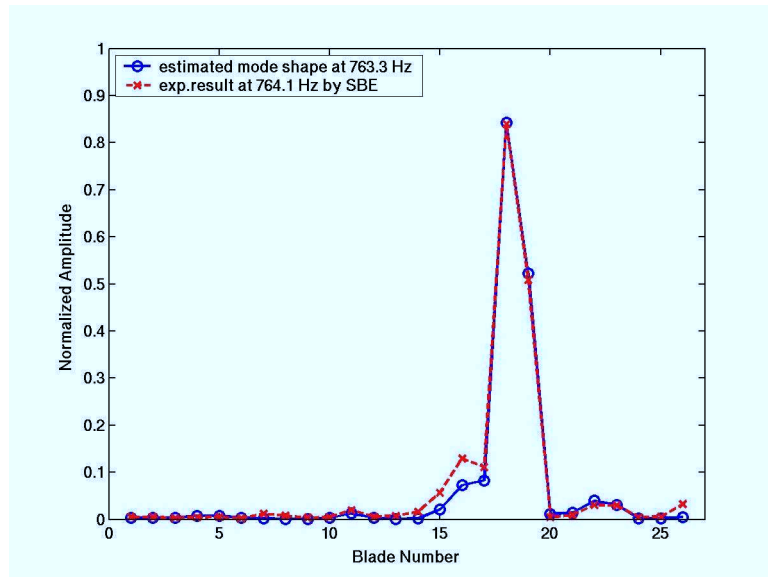


Figure 2.26: Measured natural frequencies of first flexible family for the NASA bladed disk compared to the FEM predictions.



(a) 740.2 Hz



(b) 763.3 Hz

Figure 2.27: Mode shape of NASA bladed disk, predicted by updated CMM model and measured by SPLV (Single Point Laser Vibrometer).

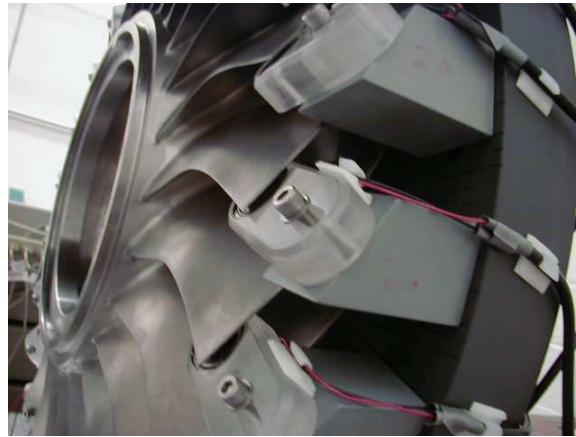


Figure 2.28: Close-up of a blade of NASA bladed disk, showing the speaker behind the blade.



Figure 2.29: The mass (lead) added to tip of a blade of the NASA bladed disk.

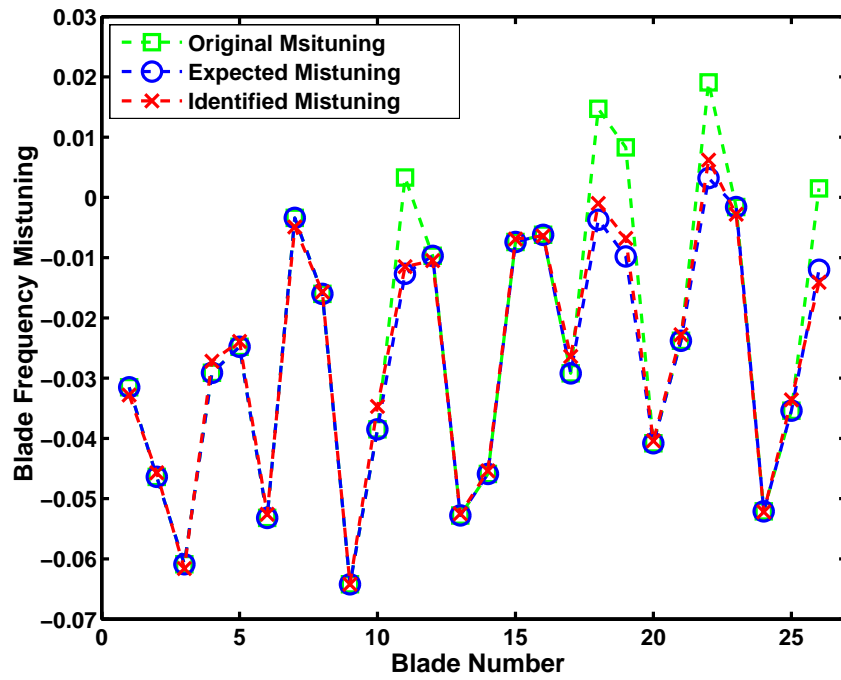


Figure 2.30: Comparison of the intentional and the identified blade stiffness mistuning for the NASA bladed disk, without considering cyclic modeling errors.

Table 2.1: Identified blade stiffness mistuning and cyclic modeling error from the experimental results based on the CMM model of the validation rotor.

Blade stiffness mistuning vs. Blade number					
1	-0.0003	9	0.0002	17	0.0027
2	-0.0007	10	-0.0006	18	0.0012
3	0.0003	11	-0.0002	19	0.0039
4	0.0025	12	-0.0027	20	-0.0036
5	-0.0016	13	-0.0020	21	-0.0002
6	0.0025	14	-0.0087	22	0.0017
7	0.0005	15	-0.0031	23	0.0058
8	-0.0030	16	0.0017	24	0.0038

Cyclic Modeling Error vs. Mode number					
1	-0.0060	6	-0.0056	11	-0.0051
2	-0.0060	7	-0.0050	12	-0.0051
3	-0.0057	8	-0.0050	13	-0.0049
4	-0.0057	9	-0.0051		
5	-0.0056	10	-0.0051		

Table 2.2: Comparison of the measured natural frequencies of the validation rotor to various predictions based on the updated CMM model by using a different set of measured data.

Estimated Frequencies by Updated CMM Using Different Number of Set of Experiment Results ( $Hz$ )					Experiment Results ( $Hz$ )	Maximum Error (%)
13 modes	7 modes	4 modes	3 modes	2 modes		
2114.6	2114.4	2114.3	2114.3	2112.2	2114.3	0.099
2115.3	2115.7	2115.5	2114.6	2114.3	2115.3	0.047
2133.3	2133.2	2132.0	2135.4	2132.3	2133.2	0.103
2133.9	2133.5	2132.3	2137.4	2136.6	2134.0	0.159
2143.2	2143.2	2143.2	2143.6	2140.7	2143.2	0.117
2144.9	2145.1	2144.8	2144.6	2143.8	2144.9	0.042
2149.8	2149.9	2149.0	2150.1	2147.0	2150.1	0.144
2150.7	2150.7	2150.2	2151.5	2152.0	2150.6	0.065
2153.2	2153.2	2153.2	2153.7	2154.3	2153.2	0.051
2154.7	2154.8	2154.4	2156.1	2158.0	2154.7	0.153
2156.4	2156.3	2156.3	2157.1	2158.3	2156.3	0.093
2156.8	2156.8	2156.8	2158.3	2158.3	2156.9	0.065
2158.3	2158.3	2158.3	2158.5	2176.2	2158.3	0.824

Table 2.3: Identified blade stiffness mistuning and cyclic modeling error from the experimental results based on the CMM model of the NASA bladed disk.

Blade stiffness mistuning vs. Blade number							
1	-0.0085	9	-0.0416	17	-0.0040	25	-0.0101
2	-0.0198	10	-0.0129	18	0.0385	26	0.0245
3	-0.0384	11	0.0268	19	0.0316		
4	-0.0029	12	0.0133	20	-0.0172		
5	-0.0003	13	-0.0292	21	0.0003		
6	-0.0302	14	-0.0220	22	0.0457		
7	0.0207	15	0.0163	23	0.0230		
8	0.0081	16	0.0177	24	-0.0292		

Cyclic Modeling Error vs. Mode number							
1	-0.0412	9	-0.0228	17	-0.0225	25	-0.0227
2	-0.0067	10	-0.0221	18	-0.0223	26	-0.0228
3	-0.0067	11	-0.0221	19	-0.0223		
4	-0.0311	12	-0.0221	20	-0.0225		
5	-0.0311	13	-0.0221	21	-0.0225		
6	0.0238	14	-0.0220	22	-0.0227		
7	0.0238	15	-0.0220	23	-0.0227		
8	-0.0228	16	-0.0225	24	-0.0227		

Table 2.4: Mass of the leads added to the tip of blade of NASA blisk and corresponding intentional blade stiffness mistuning.

blade number	lead mass (with estimated glue weight 0.005g)	intentional mistuning
11	0.418	-0.0160
18	0.475	-0.0184
19	0.467	-0.0181
22	0.415	-0.0159
26	0.315	-0.0135

## CHAPTER III

# Experimental Monte Carlo Mistuning Assessment of Bladed Disk Vibration Using Forcing Variations

Vibration responses of bladed disks in turbine engine rotors has been proved, both analytically and experimentally, to be extremely sensitive to small, random blade-to-blade variations, or mistuning. Because blade mistuning is random, probabilistic analysis, such as Monte Carlo simulation, plays a crucial role in forced responses prediction in order to assess the reliability and safety of the bladed disk performance. However, it is cumbersome to assess the effects of random mistuning or validate numerical predictions for a population of mistuned bladed disks using experimental methods. In this work, as an alternative approach for performing vibration testing of many physical mistuning patterns, it is proposed that varying the external forcing function provided to the blades can be used to mimic the influence of structural blade property mistuning on the vibration response. Because it is much easier and more efficient to vary the external excitation than to physically alter the blades, this opens the possibility of running an experimental analog of a Monte Carlo simulation. This approach, referred to as an experimental Monte Carlo mistuning assessment, is explored and validated maby comparing simulations and test data for a 24-bladed disk. The experimental Monte Carlo results are found to have excellent agreement with numerical Monte Carlo simulation results for a case of small standard deviation of

mistuning.

### 3.1 Introduction

It is well known that the vibration response of bladed disks found in turbine engine rotors can be extremely sensitive to small, random blade-to-blade variations, or mistuning. In particular, mistuning can lead to the vibration energy becoming localized in a few blades, causing significant increases in maximum blade vibration amplitudes and stress levels [2–4, 56–58]. Sinha [59, 60] and Mignolet [61–63] proposed various methods to perform statistical analysis of the mistuned forced response using lumped-parameter model. In order to predict the mistuned forced response in a computationally efficient manner, several reduced-order modeling techniques have been developed [13, 15, 18, 64, 65]. These methods can be used to generate reduced-order models that are sufficiently compact that Monte Carlo simulations, a conventional sample-based approach, can be performed to estimate the statistics of the forced response for a population of mistuned rotors. In these Monte Carlo simulations [22, 29, 66, 67], mistuning patterns are assigned with a pseudo-random number generator, and a certain physical or modal property of each blade (*e.g.*, Young's modulus or blade-alone natural frequency) is altered in the model according to its assigned mistuning value.

However, it is much more difficult to assess the effects of random mistuning or validate numerical predictions for a decent population using experimental methods. In particular, imposing specific mistuning patterns on a physical system is challenging. Adding mass is a usual approach in experimental investigation to apply intentional mistuning, for example, Jones [31] attached aluminum bar stock with accelerometer wax to the blade tip in order to implement a truncated infinite linear mistuning pattern, which reduced the maximum forced response level of a mistuned bladed disk. Judge [30] glued precisely cut and

measured lead piece to the blade for experimental investigation on the effect of random mistuning to forced responses. Although it is an effective means of controlling mistuning in bench tests, it can be time-consuming and cumbersome to precisely manufacture and attach the individual mistuning masses. As a result, relatively few mistuning patterns can be tested using this approach [27, 68]. In an experimental validation of probabilistic analysis employing FMM model, Rossi *et al.* [32] generated a fleet of 10 mistuned bladed disk by attaching mass to blade and obtained test data to compare with the predictions.

In this work, as an alternative approach for vibration testing of many mistuning patterns, it is proposed that varying the external forcing function provided to the blades can be used to mimic the influence of structural blade property mistuning on the vibration response. Because it is much easier and more efficient to vary the external excitation than to physically alter the blades, this opens the possibility of running an experimental analog of a Monte Carlo simulation. In the following sections, the feasibility of this approach, referred to as an experimental Monte Carlo mistuning assessment, is explored.

The chapter is organized as follows. In section 3.2, CMM method is once again used to generate the equation of motion for a mistuned blade disk system. Then, the modified forcing function is derived to meet the requirement of mimic a given blade mistuning pattern followed by statistic analysis using Weibull distribution. The excitation system used in experiment for the forcing supply is specified in section 3.3. In section 3.4, computational Monte Carlo simulation is performed to narrow down the investigation range of experiment. The probability density function (PDF) and cumulative distribution function (CDF) predicted by numerical Monte Carlo simulations are compared to those estimated from the new experimental approach in section 3.5. Finally the conclusion is given in section 3.6.

## 3.2 Theory

### 3.2.1 Mistuning identification and model updating based on the CMM method

In the CMM method [18], a selected set of system modes of the tuned bladed disk is used as a modeling basis [15]. The diagonal matrix of eigenvalues for this set of tuned system modes is  $\Lambda^S$ . Individual blade mistuning is modeled as the deviation of mistuned cantilevered-blade modal stiffness values from the tuned values. The diagonal matrix containing the mistuning values for all of the blades in cantilevered-blade modal coordinates is  $\delta\Lambda^{CB}$ . This individual blade mistuning is then projected to the reduced-order model of the system by relating the cantilevered-blade (component) mode shapes to the blade part of the system mode shapes. In particular, a matrix of modal participation factors,  $\mathbf{Q}^{CB}$ , is generated, which defines the transformation of blade mistuning from cantilevered-blade modal coordinates to the generalized coordinates of the reduced-order model.

In addition, the CMM method has recently been extended by the authors to perform both mistuning identification and reduced-order model updating [21, 52, 53]. A sensitivity study was performed to consider the influence of errors in modeling parameters and measured data on the mistuning identification results. It was observed that the identification results are most sensitive to errors in the tuned system eigenvalues. In order to compensate for these errors, it was proposed that the ‘‘cyclic modeling error’’ could be identified from the test data assuming the mistuning in the actual system has a mean value of zero [21, 52]. The cyclic modeling error,  $\delta\Lambda^S$ , is defined as the difference between the tuned system eigenvalues predicted from the finite element model and those identified for the actual bladed disk. Thus, after identifying the blade mistuning and the cyclic modeling error, the modal stiffness matrix of the updated model is:

$$\mathbf{K}^U = \Lambda^S + \delta\Lambda^S + \mathbf{Q}^{CBT} \delta\Lambda^{CB} \mathbf{Q}^{CB} \quad (3.1)$$

Then, the equations of motion can be expressed in tuned system modal coordinates as:

$$\left[-\omega^2 \mathbf{I} + (1 + j\gamma) \mathbf{K}^U\right] \mathbf{p} = \mathbf{f} \quad (3.2)$$

where  $\omega$  is the excitation frequency,  $j = \sqrt{-1}$ ,  $\gamma$  is the structural damping factor,  $\mathbf{p}$  is the response vector, and  $\mathbf{f}$  is the forcing vector. Note that the size of the reduced-order model is equal to the number of selected tuned system modes.

### 3.2.2 Formulation for modified forces to mimic the effects of structural blade mistuning

In order to perform an experimental Monte Carlo mistuning assessment, the required forcing variations are determined as follows. Suppose that a given mistuning pattern,  $\delta \mathbf{\Lambda}_{int}^{CB}$ , is intentionally imposed on a test specimen and a certain engine order excitation vector,  $\mathbf{f}_E$ , is applied as the forcing function. The equations of motion are then:

$$\left[-\omega^2 \mathbf{I} + (1 + j\gamma) \left(\mathbf{K}^U + \mathbf{Q}^{CBT} \delta \mathbf{\Lambda}_{int}^{CB} \mathbf{Q}^{CB}\right)\right] \mathbf{p}_m = \mathbf{f}_E \quad (3.3)$$

where  $\mathbf{p}_m$  is the mistuned vibration response for the given engine order excitation. Now, assume that the same response could be achieved by mistuning the forcing vector instead of the structural system. The corresponding equations of motion are:

$$\left[-\omega^2 \mathbf{I} + (1 + j\gamma) \mathbf{K}^U\right] \mathbf{p}_m = \mathbf{f}_m \quad (3.4)$$

where  $\mathbf{f}_m$  is the modified (or mistuned) forcing vector. From Eq. 3.3, the mistuned response can be expressed in terms of the given mistuning pattern and engine order excitation:

$$\mathbf{p}_m = \left[-\omega^2 \mathbf{I} + (1 + j\gamma) \left(\mathbf{K}^U + \mathbf{Q}^{CBT} \delta \mathbf{\Lambda}_{int}^{CB} \mathbf{Q}^{CB}\right)\right]^{-1} \mathbf{f}_E \quad (3.5)$$

Substituting Eq. 3.5 into Eq. 3.4, the mistuned forcing vector is solved as:

$$\mathbf{f}_m = \left[ -\omega^2 \mathbf{I} + (1 + j\gamma) \mathbf{K}^U \right] \left[ -\omega^2 \mathbf{I} + (1 + j\gamma) \left( \mathbf{K}^U + \mathbf{Q}^{CBT} \delta \mathbf{\Lambda}_{int}^{CB} \mathbf{Q}^{CB} \right) \right]^{-1} \mathbf{f}_E \quad (3.6)$$

Note that the mistuned forcing is frequency-dependent.

### 3.2.3 Estimation of the three-parameter Weibull distribution

For mistuned bladed disk vibration, the variable of interest is the maximum blade response for any blade in the system. Therefore, the theory of the statistics of extremes [69, 70] can be used to accelerate the Monte Carlo simulations. In particular, the distribution of the maximum blade response will tend toward a Weibull distribution. The PDF of a three-parameter Weibull distribution for maximum values is:

$$PDF = \frac{\beta}{\delta} \left( \frac{\lambda - x}{\delta} \right)^{\beta-1} e^{-\left( \frac{\lambda - x}{\delta} \right)^\beta} \quad (3.7)$$

where  $\delta$ ,  $\beta$  and  $\lambda$  are the scale, shape, and location parameters, respectively, and  $x$  is the variable of interest (*i.e.*, the maximum blade response amplitude or magnification factor). The location parameter represents the upper limit of the value  $x$ . In this paper, it is taken to be the approximate maximum response magnification factor calculated by Whitehead [58], which is

$$\lambda = \frac{1}{2} \left( 1 + \sqrt{N} \right) \quad (3.8)$$

where  $N$  is the number of blades in the bladed disk. In a numerical simulation, by using this approximate value for the upper limit, the other two parameters of the Weibull distribution can be estimated using data obtained from relatively few Monte Carlo realizations [29, 67]. In the case of an experimental Monte Carlo assessment, this corresponds to running relatively few tests with mistuned excitation fields as specified in Eq. 3.6.

### 3.3 Experimental Specimen and Excitation System

The experimental facility used to perform experimental Monte Carlo assessment in a precisely controlled environment, shown in Figure 2.1, includes a non-contacting, traveling-wave excitation system, as well as a non-contacting measurement system featuring a Scanning Laser Doppler Vibrometer (SLDV). A 24-bladed disk was examined for this study, and it is shown in Figs. 3.6 and 3.6. Figure 3.6 shows the finite element model and Fig. 3.6 shows the actual bladed disk, which was manufactured to extremely tight tolerances [30]. This bladed disk, which is referred to as the validation rotor, has been used to experimentally validate the CMM approach and the reduced-order model updating method discussed above [53]. In this study, the frequency range 2110.0 — 2170.0  $Hz$  was considered, which excites the first flexural bending family of blade-dominated system modes.

Acoustic excitation was provided to the blades by an array of speakers [22, 23, 41], as seen in Fig. 3.6. Behind each blade, there is a round speaker mounted in a parallel position with the surface of the blade in order to apply an acoustic force. These speakers are driven by a series of Hewlett-Packard 8904 Multifunction Synthesizers, each with two independent but phase-synchronized channels. The speakers were carefully calibrated using white noise excitation first. Then, the speakers were mounted on the plastic fixtures, and a sinusoidal signal was sent to each speaker, one at a time. A calibrated microphone was used to record the sound pressure level at a fixed distance from the speaker, similar to the distance to the individual blade when it is mounted on the fixture. The amplitude and phase of the excitation signal were adjusted in order to achieve a flat frequency response of the sound pressure level produced by the speaker. This process was digitally controlled and it was repeated, in turn, for each speaker on the fixture.

To achieve engine order excitation, all the speakers are driven simultaneously to deliver

forces of the same amplitude, but with a proscribed phase lag between adjacent speakers:

$$\phi = \frac{2\pi C}{N} \quad (3.9)$$

where  $C$  is the engine order of the excitation. Thus, the force for blade number  $n$  can be written as:

$$f_n = f_0 \cos(\omega t + (n - 1) \phi) \quad (3.10)$$

where  $f_0$  is the force amplitude. Thus any engine order excitation can be obtained by simply changing the phase lag. The traveling-wave excitation system not only simulates the forcing experienced by a rotating bladed disk in an engine, but it also provides non-contacting excitation [23, 30].

For the experimental system used in this investigation, the amplitude of the excitation was controlled independently for each speaker. However, only 12 channels were available for independent phase control. For the validation rotor with 24 blades, this was sufficient to deliver engine order excitation. This is because, for any engine order, the phase of speaker  $n + 12$  is either 0 or 180 degrees behind the phase of speaker  $n$ . Therefore, specific phase values were delivered to blades 1 to 12, and the same or inverted signals were delivered to blades 13 to 24, respectively. However, when the “mistuned” excitation of Eq. 3.6 is used, this phase relationship no longer holds, and individual phase control would be needed to deliver the mistuned excitation field precisely. The lack of independent phase control for all speakers thus introduced some experimental error. Shelley *et al.* [71] demonstrated that a feedback control technique known as eigenvector scaling to modify the entire set of system mode shape, however, it is extremely difficult to match every single pattern with desired excitation even if feedback control is adopted in case of lacking independent access to amplitude and phase respectively.

### 3.4 Computational Monte Carlo Simulation

In order to perform computational Monte Carlo simulations, mistuning identification and model updating techniques were first applied to the validation rotor experimentally to obtain the updated CMM model for the first flexural bending family of blade-dominated system modes. The standard deviation of identified blade stiffness mistuning was 0.29%. Then, for a given value of standard deviation of mistuning, 1000 random mistuning patterns generated from a uniform distribution were added to the updated CMM model. For each simulated mistuned system, a frequency sweep was performed, and the highest peak response value of any blade in the mistuned system was determined. This value was divided by the peak response value of the tuned system to yield a magnification factor. Then the Weibull distribution of the magnification factor was estimated from the data. This process was performed for engine orders 6 to 12.

The Monte Carlo simulation results for engine orders 6 to 12 are depicted in Figs. 3.6 and 3.6. It is seen that the magnification factor can be very sensitive to the mistuning level for small values of standard deviation. However, the case of engine order 8 excitation shows smoother slope than engine order 12 for small mistuning levels. This was also found to be true while comparing to engine orders 6, 7, and 9 to 11. Therefore, engine order 8 excitation was chosen for conducting the experimental Monte Carlo assessments.

As mentioned above, the experimental setup had entirely independent control over the amplitudes of external forces but not the phases. Therefore, it was desired to keep the mistuned part of the force used in the experiment sufficiently small so that no dramatic effect on the phase relative to engine order 8 excitation was required. For this reason, a mistuning standard deviation of 0.1% was chosen.

Focusing on a mistuning level of 0.1%, 200 random mistuning patterns were added to

the updated CMM model, and the maximum blade response amplitudes were calculated for engine order 8 in the range 2145–2160  $Hz$ . The histogram of maximum mistuned blade response amplitudes is shown in Fig. 3.6, and the resonant frequency distribution is depicted in Fig. 3.6. Based on these results, the investigated frequency range was selected as 2147.2 — 2152.5  $Hz$  for the experimental work, in order to reduce the required testing time.

### **3.5 Experimental Monte Carlo Mistuning Assessment**

In all of the following experiments, the tuned force needed on the right-hand side of Eq. 3.6 was chosen as engine order 8 excitation, and the investigated frequency range was 2147.2 — 2152.5  $Hz$  with a step size of 0.1  $Hz$ . The raw measured results obtained with a Scanning Laser Doppler Vibrometer were the displacements at the tips of the blades excited by mistuned forces, and the maximum blade response amplitude was found for each mistuning pattern. These values were later divided by the maximum blade response of the rotor subject to engine order 8 excitation (the “tuned” case) to obtain the magnification factors as the input data for the Weibull distribution. Using the three-parameter Weibull distribution given in equation 3.7, the PDF and CDF were calculated from the experimental data. The test results were then compared to numerical predictions by applying the same group of mistuning patterns to the updated CMM model.

#### **3.5.1 Experimental Trial 1**

The first experimental trial was run for a set of 80 mistuning patterns. Figure 3.6 shows the PDF and CDF results for the first 20 mistuning patterns tested, which match fairly well with the predictions. For example, the CDF from the Monte Carlo simulation indicates that 99.9% of the magnification factors are expected to be lower than 1.6, which is corroborated by the experimental results. The capability of forecasting such a high-

percentile response is especially useful in assessing the durability and reliability of bladed disks. Figure 3.6 shows the PDF and CDF results for the first 40 mistuning patterns tested. There is excellent agreement between the numerical and experimental results.

However, as the number of mistuning patterns was increased to 60 and then to 80, the experimental Monte Carlo results started to deviate from the numerical simulation results, as seen in Figs. 3.6 and 3.6. It is believed that this was due to a breakdown of the temperature control in the experimental laboratory, which led to inconsistent room temperatures for the last 40 patterns of this first trial. The room temperature should be kept consistent, since the blade displacements being measured are on the micron level. Nevertheless, note that there is still good agreement for the high-percentile values (e.g., 99.9th percentile) of the magnification factors. This indicates that the experimental Monte Carlo assessment shows great promise in terms of providing a robust prediction of the worst-case mistuning effects.

### **3.5.2 Experimental Trial 2**

For a second experimental trial, another 80 random mistuning patterns were analyzed for the validation rotor. This time, the experimental environment was kept consistent throughout the testing. The PDF and CDF results from trial 2 are depicted in Figs. 3.6–3.6. It can be seen that both the PDF and CDF results match well with the predictions, especially when all 80 mistuning patterns are considered. Regarding the discrepancies seen in Figs. 3.6 and 3.6, the main source of error is most likely the lack of precise phase control for all speakers. However, unlike the results of trial 1, these results seem to indicate that the experimental and computational results are starting to converge after 80 mistuning patterns, and it is expected that the agreement would improve with more patterns.

### 3.6 Conclusions

An innovative method for experimental Monte Carlo assessment of mistuned bladed disks has been established. The blade mistuning was recast in the equations of motion as modified external forces. This implies that various mistuning patterns can be imposed in a test environment by varying the external excitation rather than making structural changes. This approach was then validated with a series of tests performed on a 24-blade validation rotor. For a case with 0.1% standard deviation of the implemented mistuning, the experimental results matched the numerical predictions quite well. The match was especially good for high-percentile response values, which indicates that this approach might be useful for assessing the safety and reliability of a bladed disk.

The main limitation for the application of the technique in this initial study was the lack of individual phase control over each speaker that provides external excitation to each blade. As a result, only mistuning patterns generated from a distribution with a small standard deviation could be investigated in this work. However, if one had independent phase and amplitude control for each speaker in the acoustic excitation system, this restriction to small mistuning levels would be alleviated. Moreover, compared to previous experimental mistuning methods such as attaching masses to the blades, this new approach is more flexible and efficient.

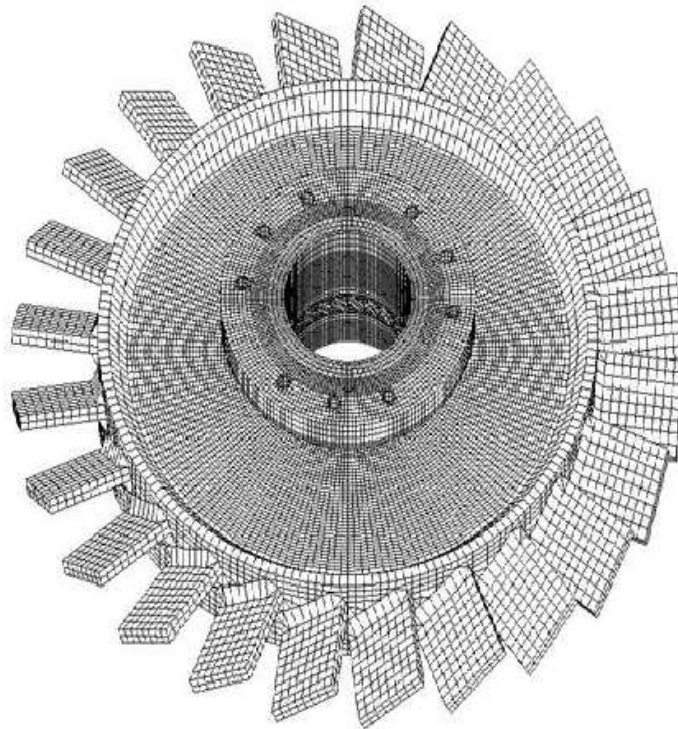
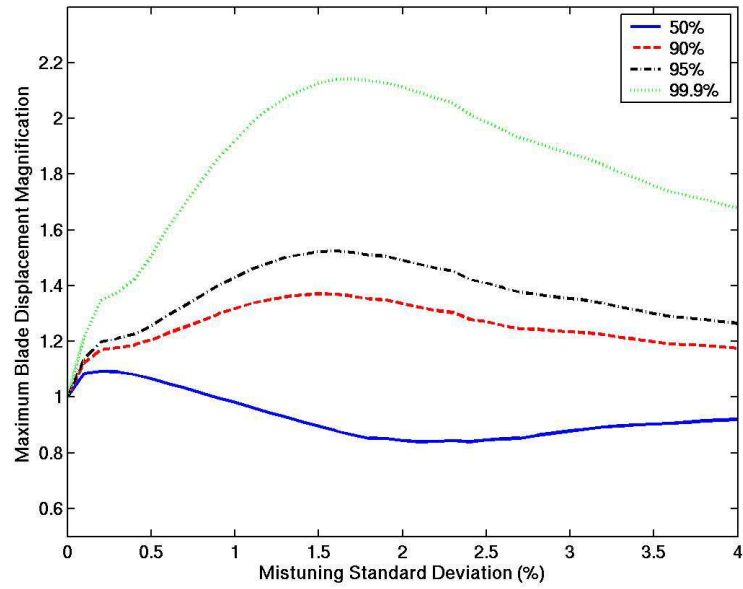


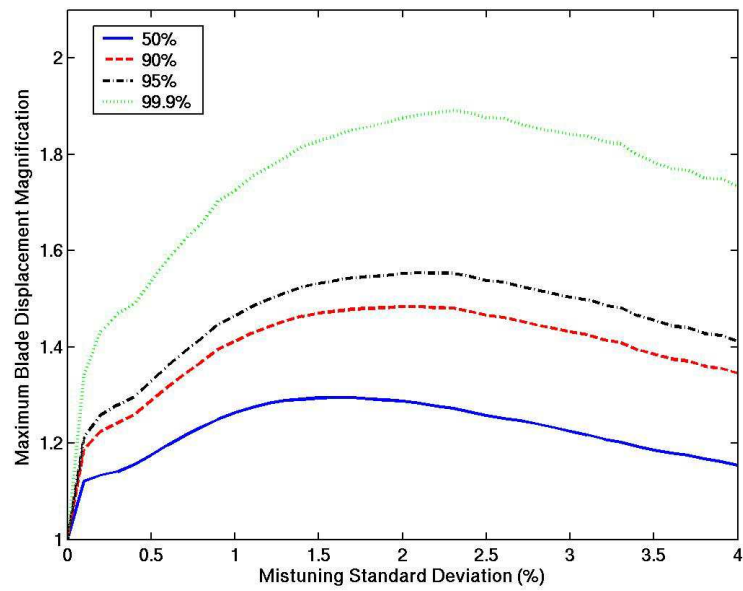
Figure 3.1: Finite element model of the bladed disk.



Figure 3.2: Actual bladed disk used in the experiment, shown with the acoustic excitation system.

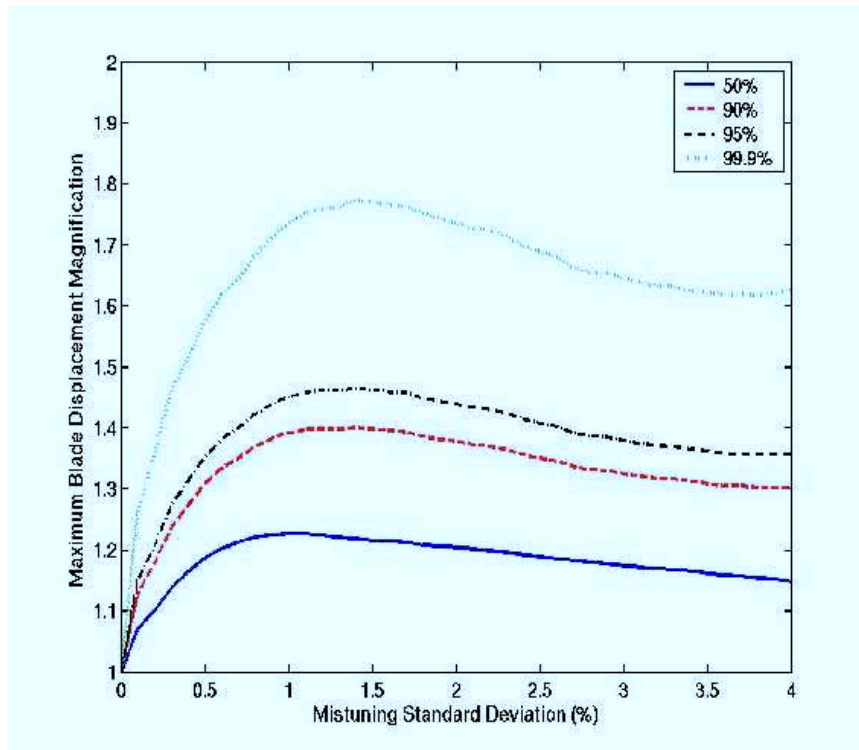


(a) EOE 6

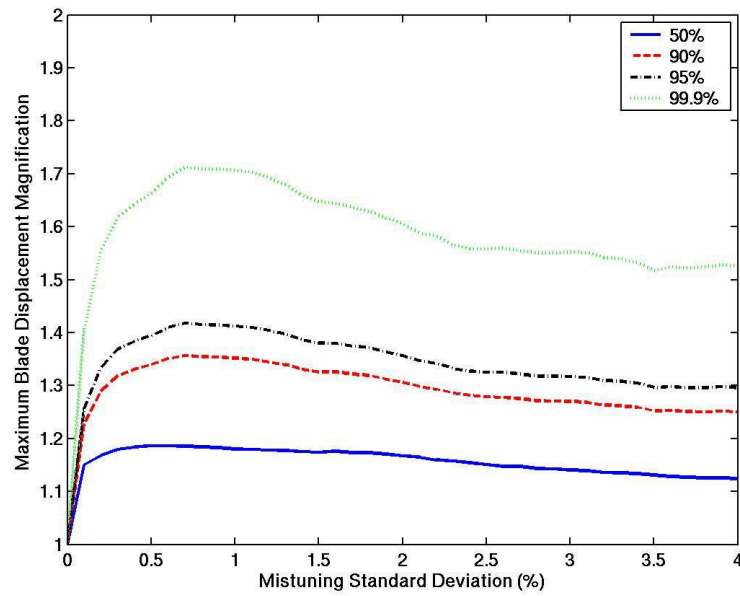


(b) EOE 7

Figure 3.3: Monte Carlo simulation of originally mistuned system by engine order excitation (EOE) 6 – 7, 1000 random mistuning.

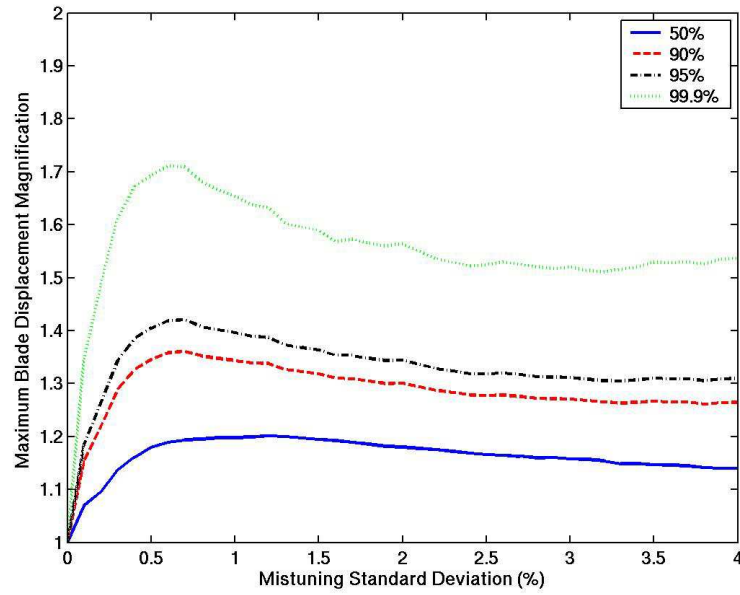


(a) EOE 8

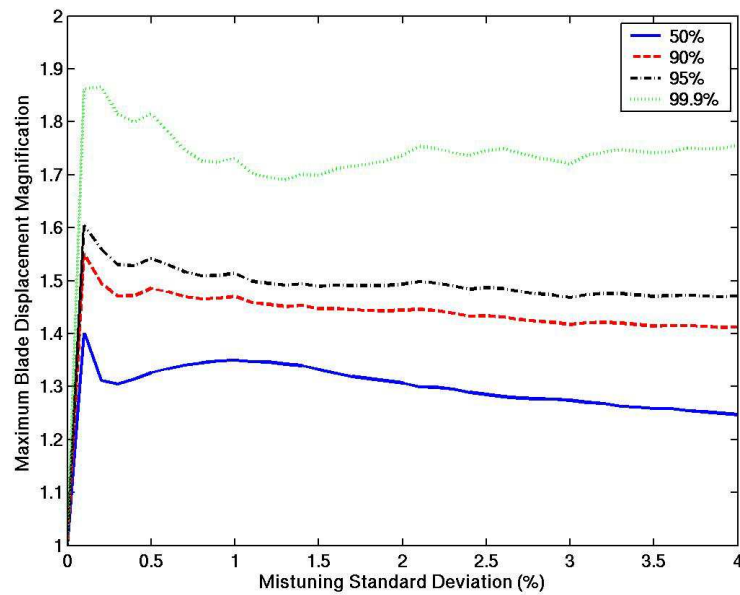


(b) EOE 9

Figure 3.4: Monte Carlo simulation of originally mistuned system by engine order excitation (EOE) 8 – 9, 1000 random mistuning.



(a) EOE 10



(b) EOE 11

Figure 3.5: Monte Carlo simulation of originally mistuned system by engine order excitation (EOE) 10 – 11, 1000 random mistuning.

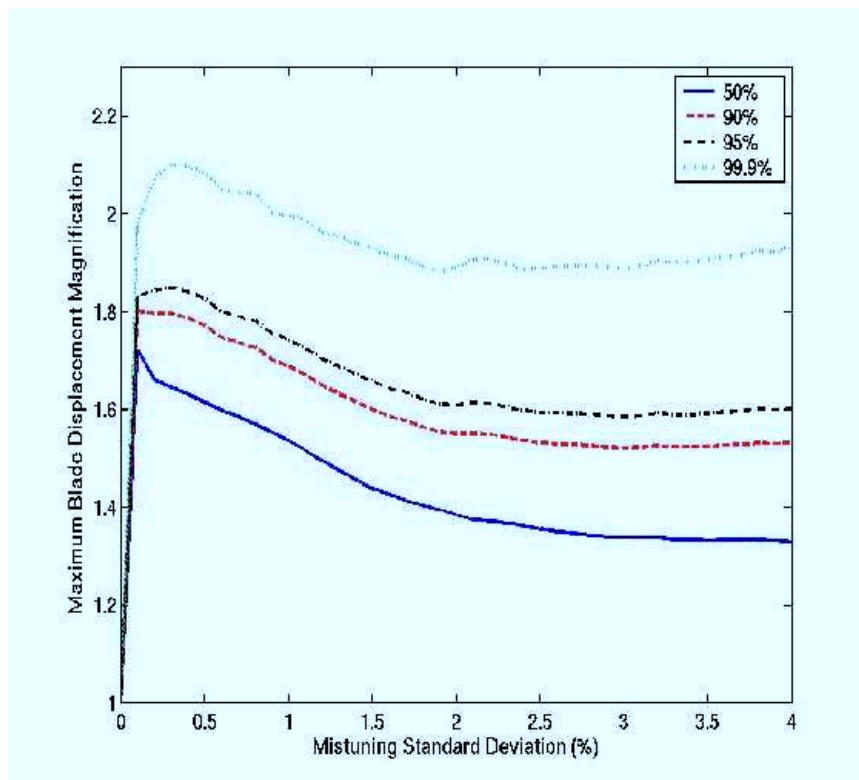


Figure 3.6: Monte Carlo simulation of originally mistuned system by engine order excitation (EOE) 12, 1000 random mistuning.

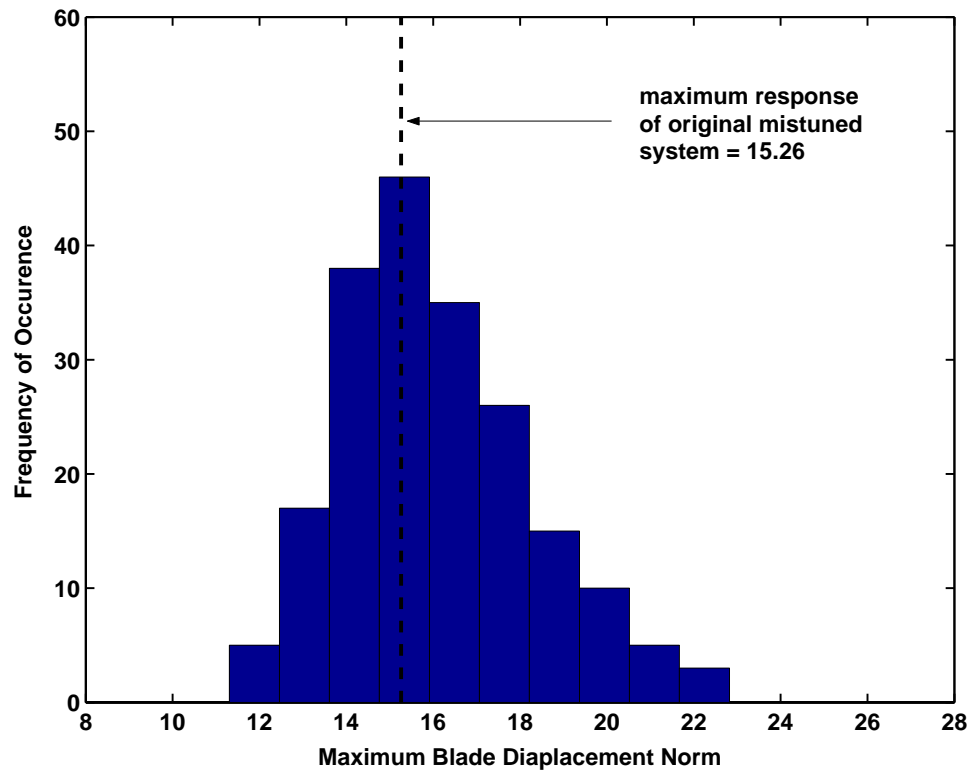


Figure 3.7: Histogram of the maximum blade response amplitude obtained by Monte Carlo simulation, based on 200 mistuning patterns generated from a uniform distribution with standard deviation = 0.1%.

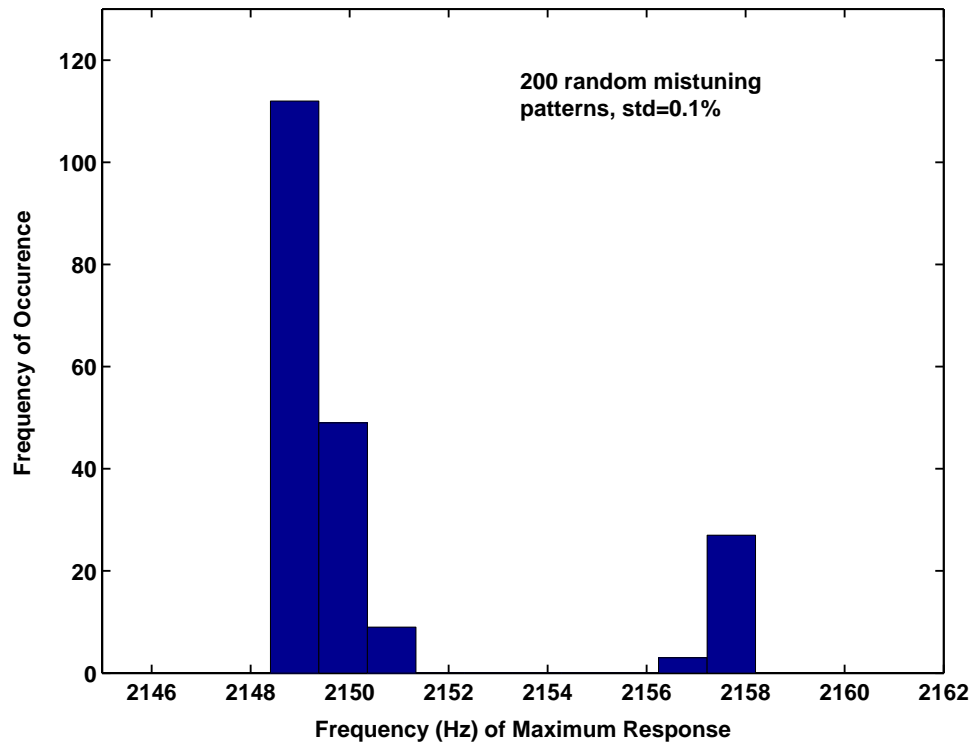


Figure 3.8: Histogram of the frequencies at which the maximum response amplitudes occurred, based on 200 mistuning patterns generated from a uniform distribution with standard deviation = 0.1%.

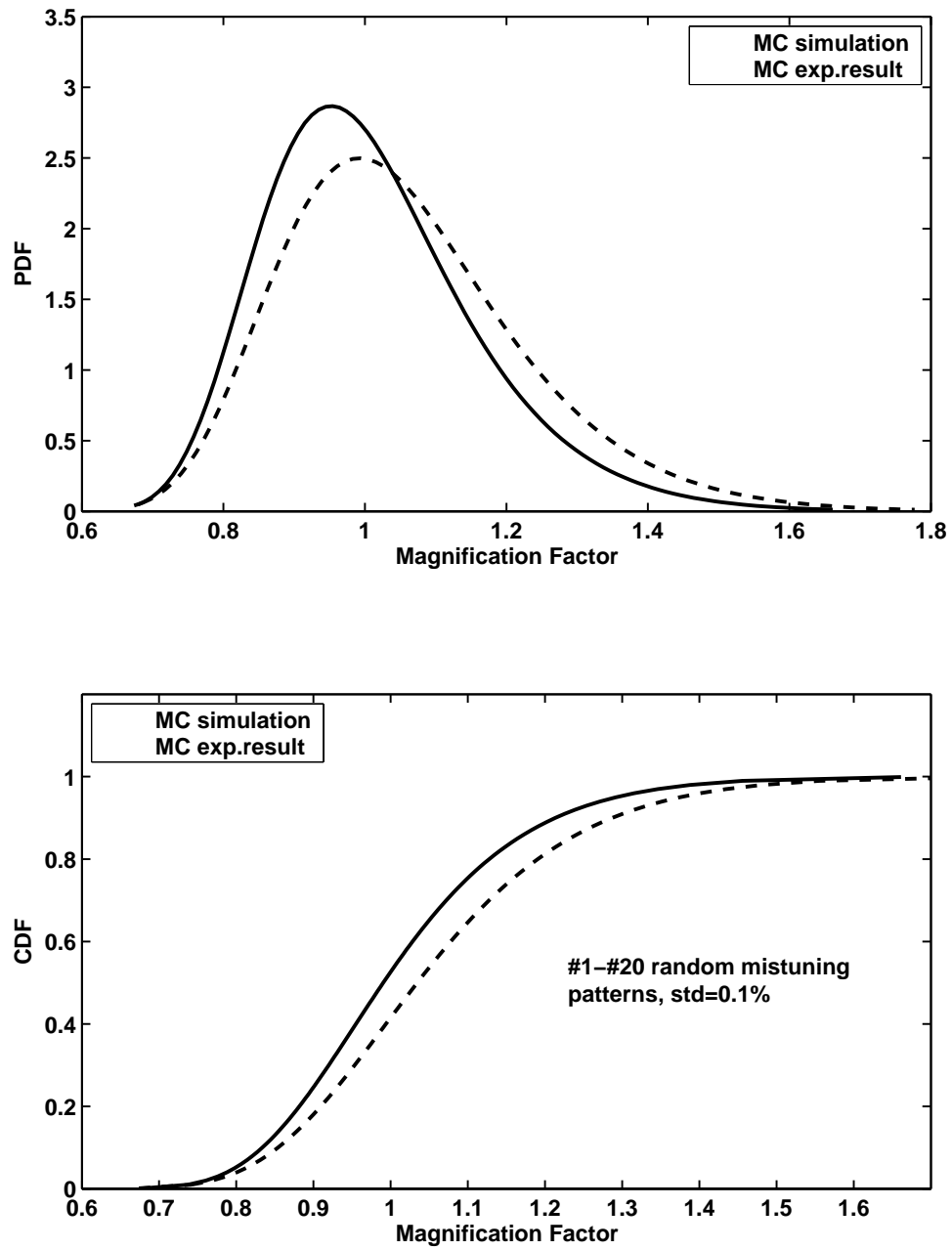


Figure 3.9: Trial 1, 20 mistuning patterns generated from a uniform distribution with standard deviation = 0.1%. Comparison of the probability density function (PDF) and cumulative distribution function (CDF) between the experimental results and the predictions based on the updated CMM model.

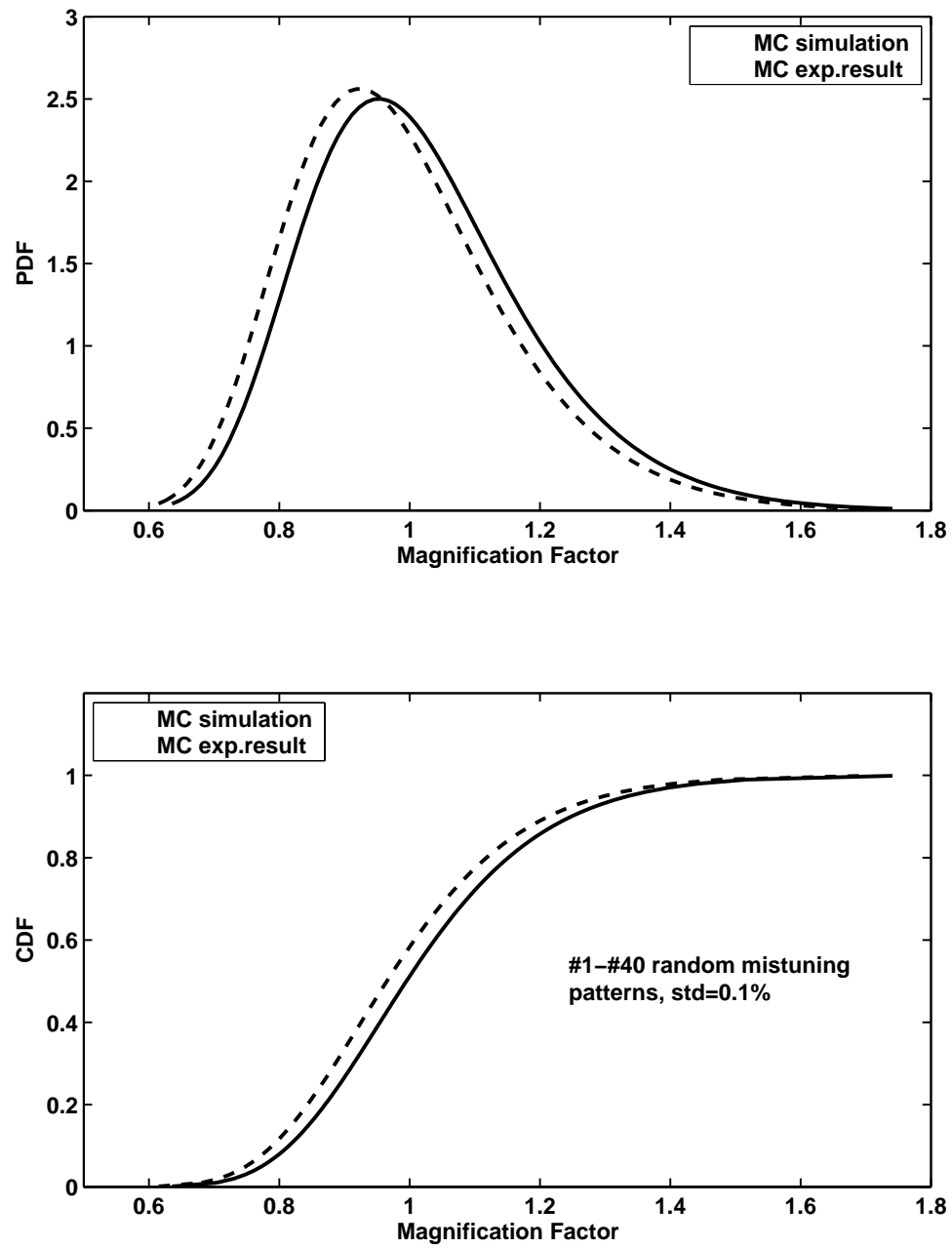


Figure 3.10: Trial 1, 40 mistuning patterns generated from a uniform distribution with standard deviation = 0.1%. Comparison of the probability density function (PDF) and cumulative distribution function (CDF) between the experimental results and the predictions based on the updated CMM model.

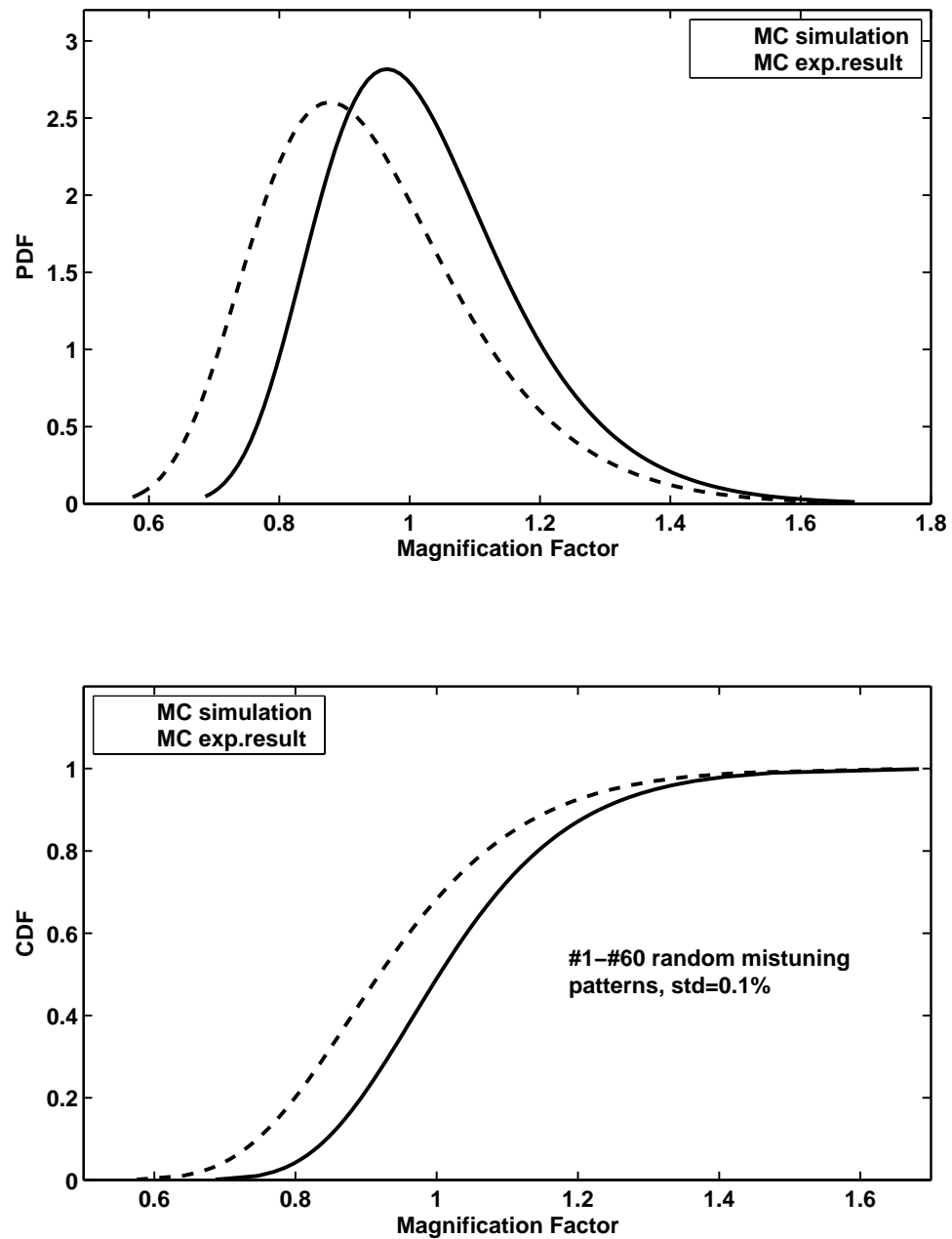


Figure 3.11: Trial 1, 60 mistuning patterns generated from a uniform distribution with standard deviation = 0.1%. Comparison of the probability density function (PDF) and cumulative distribution function (CDF) between the experimental results and the predictions based on the updated CMM model.

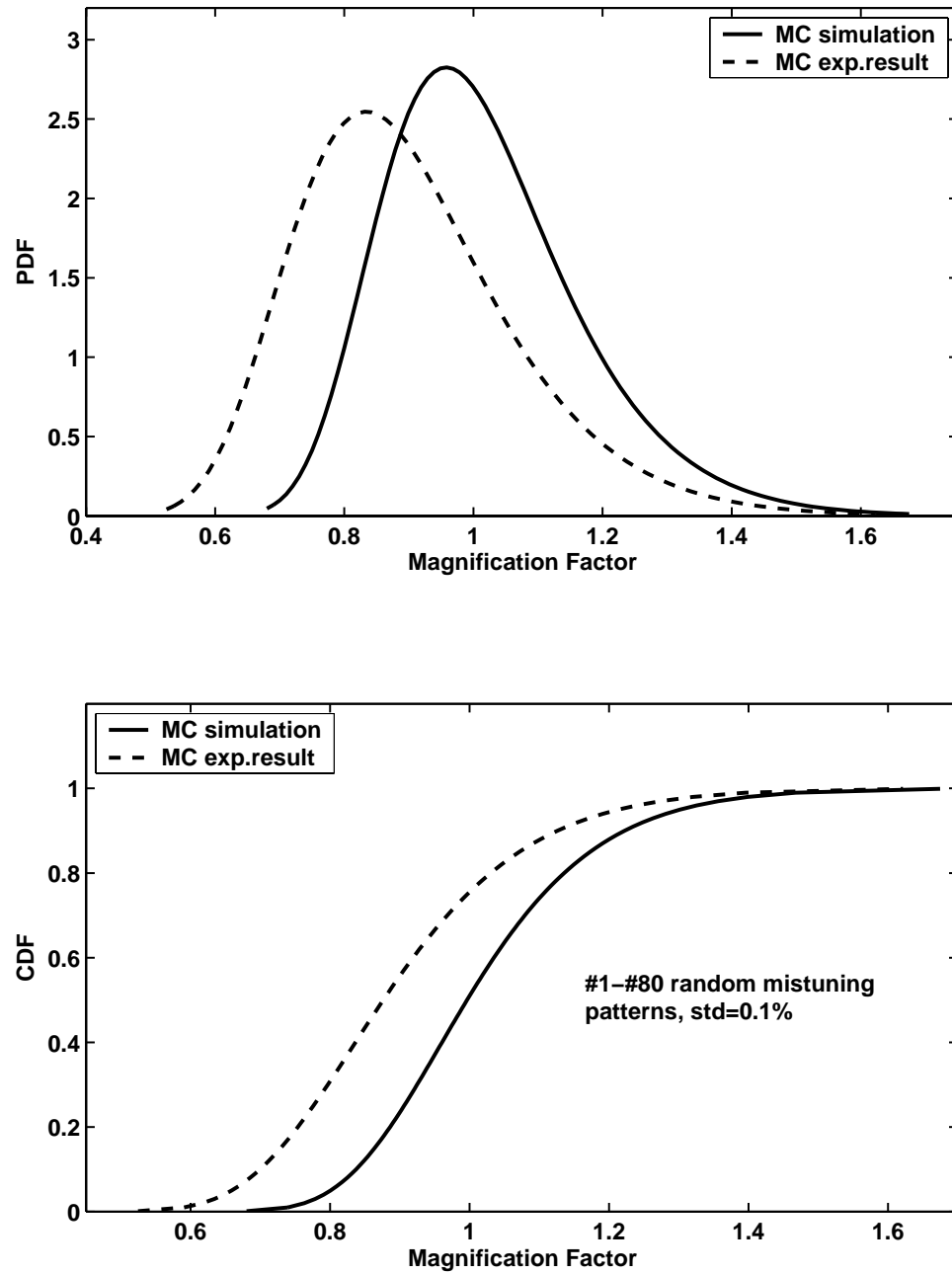


Figure 3.12: Trial 1, 80 mistuning patterns generated from a uniform distribution with standard deviation = 0.1%. Comparison of the probability density function (PDF) and cumulative distribution function (CDF) between the experimental results and the predictions based on the updated CMM model.

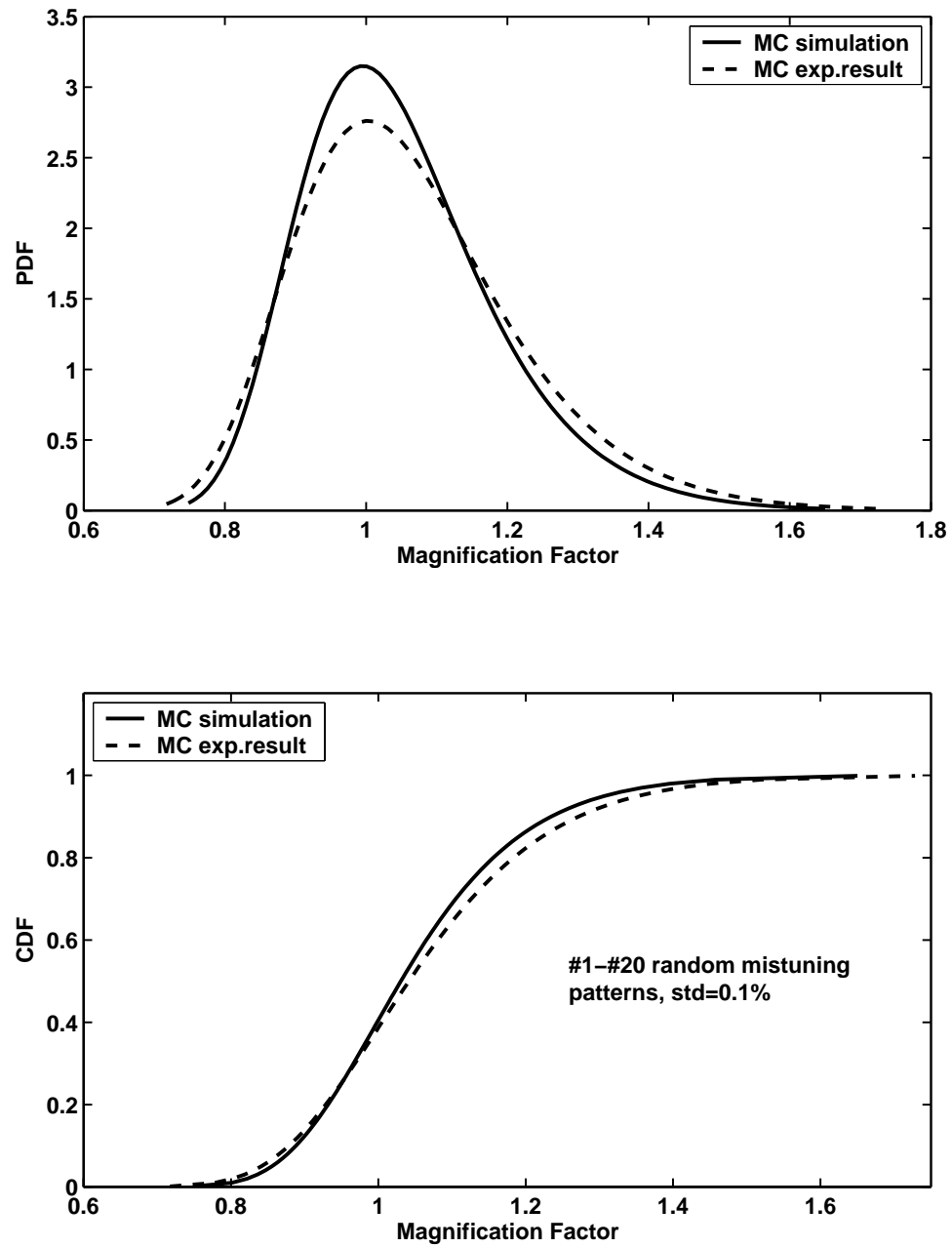


Figure 3.13: Trial 2, 20 mistuning patterns generated from a uniform distribution with standard deviation = 0.1%. Comparison of the probability density function (PDF) and cumulative distribution function (CDF) between the experimental results and the predictions based on the updated CMM model.

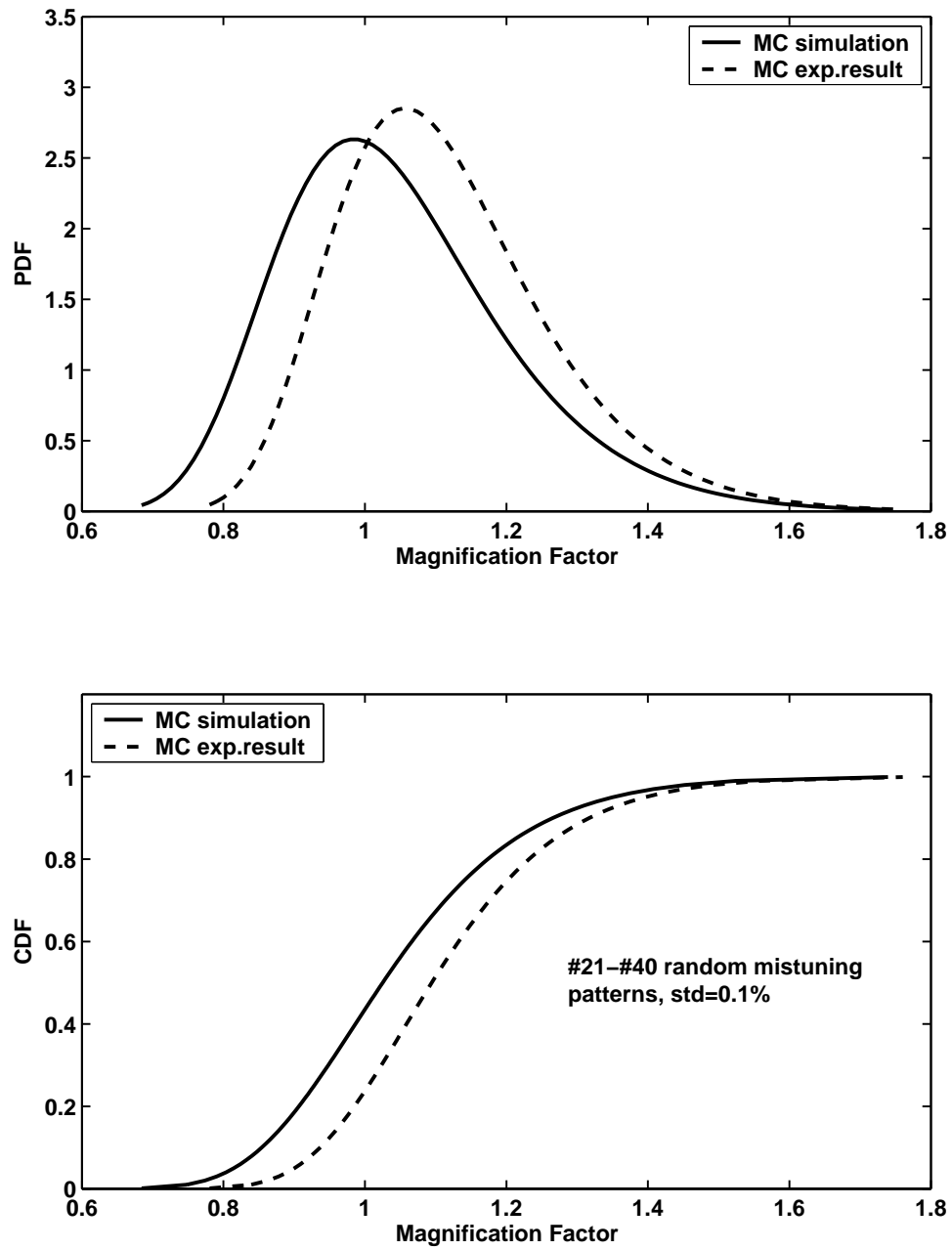


Figure 3.14: Trial 2, 40 mistuning patterns generated from a uniform distribution with standard deviation = 0.1%. Comparison of the probability density function (PDF) and cumulative distribution function (CDF) between the experimental results and the predictions based on the updated CMM model.

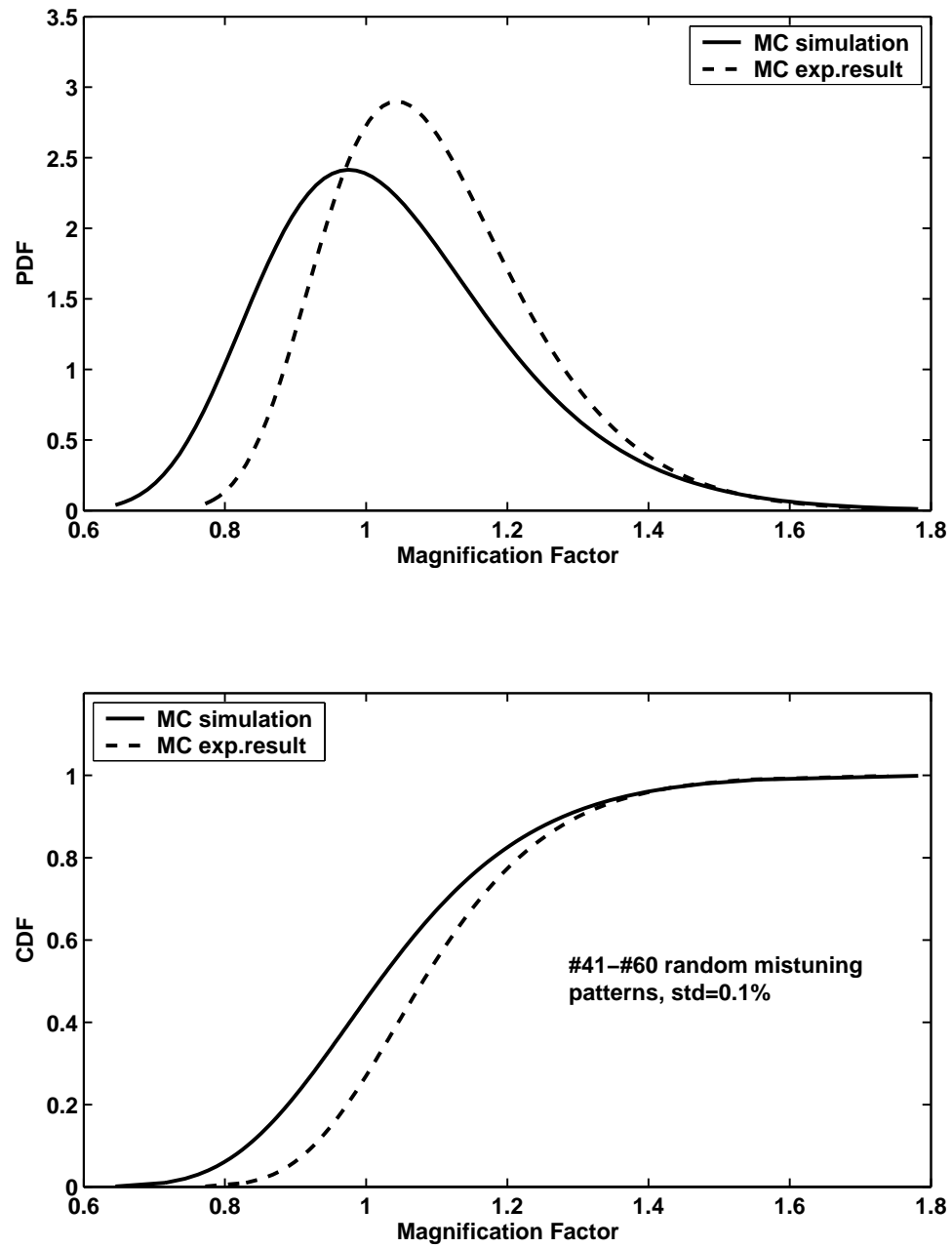


Figure 3.15: Trial 2, 60 mistuning patterns generated from a uniform distribution with standard deviation = 0.1%. Comparison of the probability density function (PDF) and cumulative distribution function (CDF) between the experimental results and the predictions based on the updated CMM model.

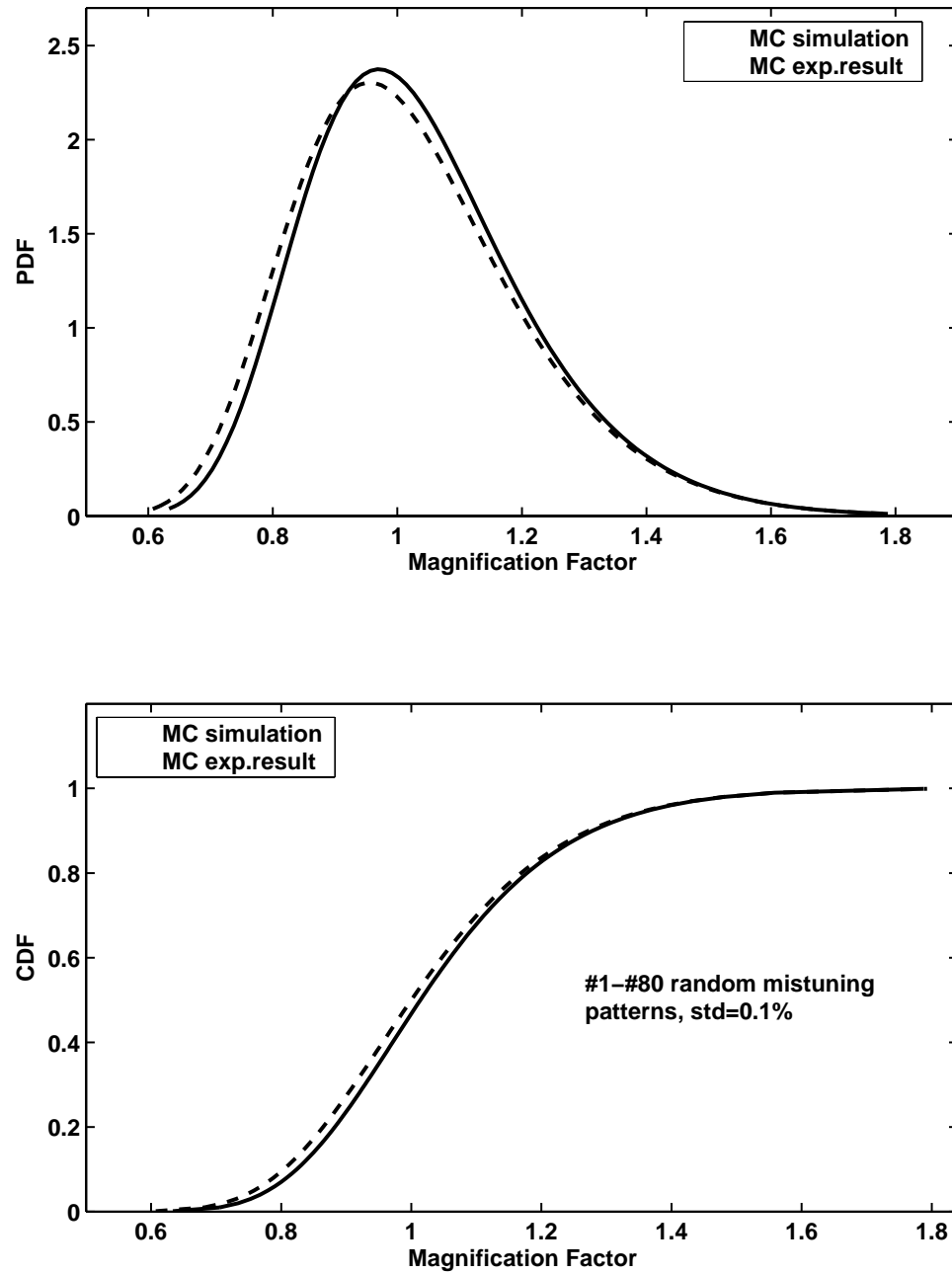


Figure 3.16: Trial 2, 80 mistuning patterns generated from a uniform distribution with standard deviation = 0.1%. Comparison of the probability density function (PDF) and cumulative distribution function (CDF) between the experimental results and the predictions based on the updated CMM model.

## CHAPTER IV

# Identification of Blade Excitation Parameters in Mistuned Blisk Vibration Tests

It is well known that the vibration response of bladed disks found in turbine engine rotors can be extremely sensitive to small, random blade-to-blade variations, or mistuning. In particular, mistuning can lead to the vibration energy becoming localized in a few blades, causing significant increases in maximum blade amplitude and stress levels. In order to predict the mistuned forced response in a computationally efficient manner, several reduced-order modeling techniques have been developed. Some of these methods have been used as a basis for developing an experimental mistuning identification method for one-piece bladed disks, or blisks. By running only a few forced response tests for the full blisk, the individual blade mistuning values can be extracted. However, the accuracy of a blisk vibration test often depends on the careful positioning and calibration of the external excitation system. For example, to generate engine order excitation in a bench test environment, a sinusoidal forcing must be delivered with the same amplitude at each blade, and the blade-to-blade phase lag must also be consistent throughout the system. In very recent work by the investigators, it has been found that variations in the actual forcing pattern from perfect engine order excitation can have a similar effect as structural blade mistuning on the system response. Thus, accounting for the uncertainties in the forcing

may be crucial to improving the calibration and accuracy of blisk vibration tests. In this paper, a mistuning identification method is extended to also identify the forcing amplitude and phase parameters for the excited blades. It is shown that blade mistuning and excitation parameters can be identified either simultaneously or sequentially using data obtained from a small set of prescribed forced response tests. This new technique is validated using both numerical simulations and experiments for a blisk with 24 blades. It is seen that this approach shows promise as a powerful tool for controlling excitation levels and accelerating calibration procedures.

## 4.1 Introduction

Bladed disks such as those in turbine engines are ideally assumed to be an assembly of identical substructures (or sectors) that are dynamically coupled in an identical manner. However, there are always small, random deviations in the sector properties due to manufacturing tolerances, material defects, operational wear, *etc.* It has long been known that these small, random blade-to-blade discrepancies, known as mistuning, can have a drastic effect on the vibration response of a bladed disk [2–4]. In particular, mistuning can lead to the vibration energy becoming localized in a few blades, causing significant increases in maximum blade vibration amplitudes and stress levels. In order to predict the mistuned forced response in a computationally efficient manner, several reduced-order modeling techniques have been developed using component-modes-based methods [13, 14, 72, 73] or system-mode-based methods [15–18, 64].

The development of these reduced-order modeling techniques has led to increased research activity in vibration testing of bladed disks. Many of these efforts have focused on one-piece bladed disks, or blisks, in part because their vibration response can be examined in a stationary bench test environment, which is simpler than having to test the system in

a spin rig. Nevertheless, the accuracy of blisk vibration tests still depends on the careful positioning of the test specimen as well as the calibration of the external excitation system. This is especially true for the case of engine order excitation. To generate true engine order excitation in a bench test environment, a sinusoidal forcing must be delivered with the same amplitude at each blade, and the blade-to-blade phase lag must also be consistent throughout the system. Such engine order or traveling wave excitation systems have employed speakers, horn drivers with vinyl tubing, electromagnets, or a specifically designed flywheel to excite the blades [22, 31, 33, 34]. Regardless of the excitation method, time-consuming calibration procedures are required in order to obtain the specific relations between any two of the three key elements—frequency, amplitude and phase—so that the desired output signals are guaranteed. Moreover, for those excitation systems without precisely controlled positioning, it may be necessary to account for another factor in the calibration process, which is the distance between the excitation system and the blade.

Even when meticulous calibrations of the speakers or other excitation devices are performed beforehand, uncertainties in forcing are inevitable during vibration tests. For example, in a traveling wave excitation system employing speakers [23, 30, 53, 74], uncertainties in forcing could be caused by random noise in the signal conditioning circuits, gradual wear of the speakers, positioning variance due to rearranging the speaker configuration, etc. Moreover, it has been found that variations in the actual forcing pattern from perfect engine order excitation can have a similar effect as structural blade mistuning on the system response [74]. Shah *et al.* [75] conducted a numerical probabilistic analysis on a mistuned turbine rotor and reported significant effect of uncertainties in the excitation frequency to mistuning leading to larger magnification factors. Thus, accounting for the uncertainties in the forcing may be crucial to improve the calibration and accuracy of bladed disk vibration tests, which is especially true in realistic engine operation en-

vironment considering the complexity of controlling the forcing in the engine exactly as designed.

In this chapter, the identification and impact of uncertainties in the external excitation are investigated in detail. The primary contribution is that a mistuning identification method is extended to also identify the amplitude and phase of the forcing applied to each excited blade. It is shown that blade mistuning and forcing parameters can be identified simultaneously or sequentially by carrying out a small set of prescribed forced response experiments. This new technique is validated using both numerical simulations and experiments. It is shown that this approach shows promise as a powerful tool for accelerating the calibration process.

This chapter is organized as follows. The simultaneous and sequential methods for mistuning and external forcing identification are derived in section 4.2. In section 4.3, several different examples are employed to numerically validate the proposed algorithm. In section 4.4, experimental results for a 24-blade blisk are presented. Conclusions from this study are given in section 4.5.

## **4.2 External Forcing Identification**

### **4.2.1 Background—CMM Modeling for Mistuned Bladed Disks**

In this section, the component mode mistuning (CMM) method for reduced-order modeling of mistuned bladed disks, and a CMM-based mistuning identification technique, are briefly reviewed. These methods were originally presented in refereces [18, 21, 52]. In the case of small mistuning, the author suggested that the blade-alone mistuning in the ROM can be projected from cantilevered blade normal mode coordinates to the tuned system modal coordinates, by representing the blade motion with its modal participation factors. Here, it is assumed that the blade mass matrix is tuned and that mistuning only occurs in

the stiffness matrix. In addition, for convenience, it is assumed that only one mode or mode pair per harmonic (nodal diameter) is kept in the reduced-order model, and that these are mostly blade-dominated modes corresponding to a single cantilevered blade mode. These assumptions are not required, but they simplify the derivation. In particular, only one mistuning parameter must be identified for each blade, and the number of reduced-order model degrees of freedom (DOF) is equal to the number of blades.

Following the above ideas and assumptions, the equations of motion can be expressed in tuned system modal coordinates as:

$$\left[ -\omega^2 \mathbf{I} + (1 + j\gamma) \left( \mathbf{\Lambda}^S + \delta \mathbf{\Lambda}^S + \mathbf{Q}^{CBT} \delta \mathbf{\Lambda}^{CB} \mathbf{Q}^{CB} \right) \right] \mathbf{p} = \mathbf{f}^S \quad (4.1)$$

where  $\omega$  is the excitation frequency,  $\gamma$  is the structural damping factor, and  $\mathbf{p}$  and  $\mathbf{f}^S$  are both vectors in tuned-system modal coordinates containing blade displacement and applied force respectively. In addition,  $\mathbf{\Lambda}^S$  is the diagonal matrix of eigenvalues for the selected set of system modes used as a modeling basis. Individual blade mistuning is modeled as the deviation of mistuned cantilevered blade eigenvalues from the tuned values. The diagonal matrix containing the mistuning values for all of the blades in cantilevered blade modal coordinates is  $\delta \mathbf{\Lambda}^{CB}$ . The off-diagonal terms which representing the coupling between cantilevered blade modes due to mistuning are neglected. This individual blade mistuning is then projected to the reduced-order model of the system by relating the cantilevered-blade (component) mode shapes to the blade part of the system mode shapes. In particular, a matrix of modal participation factors,  $\mathbf{Q}^{CB}$ , is generated, which defines the transformation of blade mistuning from cantilevered-blade modal coordinates to the generalized coordinates of the reduced-order model. Moreover, the ‘‘cyclic modeling error’’ terms,  $\delta \mathbf{\Lambda}^S$ , are defined as the difference between the tuned system eigenvalues of an actual bladed disk and the eigenvalues predicted from the tuned finite element model [21].

Because there is no tuned system in reality, the tuned eigenvalues of the actual system are deduced from the test data by assuming the mistuning has a mean value of zero. The concept of cyclic modeling error was originally motivated by a sensitivity study that was performed to consider the influence of errors in modeling parameters and measured data on the mistuning identification results [18]. It was observed that the identification results were most sensitive to errors in the tuned system eigenvalues.

While an inverse process for identifying the blade mistuning cyclic modeling error is pursued, the forcing is eliminated by subtracting the equations at two different resonant frequencies,  $\omega_i$  and  $\omega_j$ , assuming the same external forcing at each excitation frequency. Applying this approach to Eq. 4.1 leads to the following expression:

$$-(\omega_i^2 \mathbf{p}_i - \omega_j^2 \mathbf{p}_j) + (1 + j\gamma) \left[ \mathbf{\Lambda}^S + \delta \mathbf{\Lambda}^S + \mathbf{Q}^{CBT} \delta \mathbf{\Lambda}^{CB} \mathbf{Q}^{CB} \right] (\mathbf{p}_i - \mathbf{p}_j) = \mathbf{0} \quad (4.2)$$

Otherwise, if the structural damping is small and individual system modes can be excited near their natural frequencies, the forcing in Eq. 4.1 can be ignored by assuming a free response case:

$$\left[ -\omega^2 \mathbf{I} + (1 + j\gamma) \left( \mathbf{\Lambda}^S + \delta \mathbf{\Lambda}^S + \mathbf{Q}^{CBT} \delta \mathbf{\Lambda}^{CB} \mathbf{Q}^{CB} \right) \right] \mathbf{p} = \mathbf{0} \quad (4.3)$$

Although  $\delta \mathbf{\Lambda}^S$  and  $\delta \mathbf{\Lambda}^{CB}$  are the unknowns introduced in the Eq. 4.1, the actual variables identified from the algorithm,  $\mathbf{D}^S$  and  $\mathbf{D}^{CB}$ , are slightly different yet related to them based on the following expressions:

$$\delta \mathbf{\Lambda}^S = \mathbf{\Lambda}^S \cdot \mathbf{D}^S \quad (4.4a)$$

$$\delta \mathbf{\Lambda}^{CB} = \lambda^{CB} \cdot \mathbf{D}^{CB} \quad (4.4b)$$

where  $\lambda^{CB}$  is the tuned cantilevered blade eigenvalue for this investigated family,  $\mathbf{D}^S$  and  $\mathbf{D}^{CB}$  are diagonal matrix respectively in the same format as  $\delta\Lambda^S$  and  $\delta\Lambda^{CB}$ . Therefore the Eq. 4.3 can be re-written as follows:

$$\left[ -\omega^2 \mathbf{I} + (1 + j\gamma) \left( \Lambda^S (\mathbf{I} + \mathbf{D}^S) + \mathbf{Q}^{CBT} (\lambda^{CB} \cdot \mathbf{D}^{CB}) \mathbf{Q}^{CB} \right) \right] \mathbf{p} = \mathbf{0} \quad (4.5)$$

Since the unknowns in this case are only the diagonal terms of  $\mathbf{D}^S$  and  $\mathbf{D}^{CB}$ , which can be represented respectively by two vectors notated as  $\mathbf{d}^S$  and  $\mathbf{d}^{CB}$ , the algorithm for mistuning identification and model updating can be cast into the following form:

$$\begin{bmatrix} \mathbf{A}_S & \mathbf{A}_{CB} \end{bmatrix} \begin{Bmatrix} \mathbf{d}^S \\ \mathbf{d}^{CB} \end{Bmatrix} = \mathbf{B} \quad (4.6)$$

where  $\mathbf{A}_S$  and  $\mathbf{A}_{CB}$  are the reframed coefficient matrices in order to arrange unknowns from  $\delta\Lambda^S$  and  $\delta\Lambda^{CB}$  into  $\mathbf{d}^S$  and  $\mathbf{d}^{CB}$ . All of them are fully known once the blade responses  $\mathbf{p}$  are obtained at desired excitation frequencies  $\omega$ . A more detailed formulation of the mistuning identification and model updating equations, including the matrix reformatting process, is provided in Appendix A.

#### 4.2.2 Simultaneous System and Forcing Identification

As discussed above, in previous research on mistuning identification, the external forcing was either ignored (free response) or eliminated by subtracting equations at different frequencies based on the assumption of consistent forcing within the investigated frequency range. However, the recent investigation covered in the preceding chapter has shown that variations in the actual forcing pattern from perfect engine order excitation can have a similar effect as structural blade mistuning on the system response. Such “mistuned forcing” cases will inevitably occur in vibration tests, due to calibration errors, sig-

nal conditioning errors in amplifier circuits, *etc.* Moreover, it is highly time-consuming and cumbersome to delicately calibrate the external forcing in order to keep it consistent. Therefore, it is of practical importance to assess the mistuning of external forces—that is, to identify the actual forcing that the blades receive.

For forcing identification, the suggested approach is straightforward. It is assumed that an external force is applied at a certain point on each blade. A node in the blade finite element model is selected to approximately match to the position of the actual forcing given in the vibration testing. According to Eq. 4.1, assuming the external forcing vector is expressed in physical coordinates and has one DOF per blade, the equations of motion can be reframed as:

$$\left[ -\omega^2 \mathbf{I} + (1 + j\gamma) (\boldsymbol{\Lambda}^S + \delta \boldsymbol{\Lambda}^S + \mathbf{Q}^{CBT} \delta \boldsymbol{\Lambda}^{CB} \mathbf{Q}^{CB}) \right] \mathbf{p} = \boldsymbol{\Phi}_{CB}^{ST} \mathbf{f}^{CB} \quad (4.7)$$

Compared to Eq. 4.3, there is one more unknown variable introduced into the equation, external forcing  $\mathbf{f}^{CB}$ . And  $\boldsymbol{\Phi}_{CB}^S$  is the matrix of the blade part of tuned-system mode shapes, which defines the transformation of physical forcing on each blade to the forcing in modal coordinates. It is convenient to expand the brief format of Eq. 4.6 as:

$$\begin{bmatrix} \mathbf{A}_S & \mathbf{A}_{CB} & \mathbf{A}_f \end{bmatrix} \left\{ \begin{array}{c} \mathbf{d}^S \\ \mathbf{d}^{CB} \\ \mathbf{f}^{CB} \end{array} \right\} = \mathbf{B} \quad (4.8a)$$

$$\mathbf{A}_f = -\boldsymbol{\Phi}_{CB}^{ST} \quad (4.8b)$$

where  $\mathbf{A}_S$  and  $\mathbf{A}_{CB}$  are the same as described in the section above, and  $\mathbf{A}_f$  is the coefficient matrix of the new unknown, external forcing  $\mathbf{f}^{CB}$ . In the algorithm of mistun-

ing identification and model updating shown as Eq. 4.6, the least squares method is employed to optimize the solution results (minimize the residual) for the typical case in which the coefficient matrix is non-square, *i.e.*, there are more equations than unknowns due to the amount of collected test data. Nevertheless, in forcing identification, the coefficient matrix associated with unknown forcing implicates no relation with the measurements  $\mathbf{x}(\mathbf{p} = \Phi_{CB}^S \mathbf{x})$ , the least squares method will not provide more accurate results. It is apparent that the size of matrices  $\mathbf{A}_S$  and  $\mathbf{A}_{CB}$  grow with the increasing number of measurements because of the involvement of  $\mathbf{x}$ , however, the  $\mathbf{A}_f$  is simply expanded by repeating  $\Phi_{CB}^{ST}$ . It is the redundancy of matrix  $\mathbf{A}_f$  that introduces variations from the expected values of forcing.

### 4.2.3 Sequential System and Forcing Identification

Considering the random testing error and the advantage of the least squares method, an alternative approach is presented as sequential system and forcing identification which consists of two steps. At first the blade mistuning and cyclic modeling error are identified while the external forcing is neglected as shown in Eq. 4.6. After using the identification results to construct a reduced-order model of the mistuned bladed disk, the external forcing can be calculated according to Eq. 4.1. By this mean, it is a repeat use of the same group of information without demanding additional measurements. And more important, the sequential process can benefit from the least squares method when the testing error is inevitable.

$$\mathbf{f}^{CB} = \Phi_{CB}^{ST^{-1}} \left[ -\omega^2 \mathbf{I} + (1 + j\gamma) \mathbf{K}^U \right] \mathbf{p} \quad (4.9a)$$

$$\mathbf{K}^U = \mathbf{\Lambda}^S + \delta \mathbf{\Lambda}^S + \mathbf{Q}^{CBT} \delta \mathbf{\Lambda}^{CB} \mathbf{Q}^{CB} \quad (4.9b)$$

For example, a frequency sweep is performed within the interested frequency range of  $50Hz$  while the step size is set as  $0.1Hz$ . There are 20 mistuned system modes involved so that the blade responses  $\mathbf{p} = [\mathbf{p}_1 \quad \mathbf{p}_2 \quad \cdots \quad \mathbf{p}_{20}]$  are selected at those 20 resonant peaks since they meet the two particular assumptions for applying Eq. 4.6. Then the CMM model of the mistuned bladed disk is updated to provide a known base for calculating the 500 different external forcing at each measured frequencies ( $50Hz/0.1Hz= 500$ ). One application is to document these 500 forces as a calibration file for excitation in the  $50Hz$  range.

### 4.3 Numerical Validation

#### 4.3.1 Simultaneous Identification Method — Industrial Blisk

A 29-blade compressor stage from an industrial gas turbine was first used to numerically validate the simultaneous system and forcing identification approach. Figure 4.1 shows the finite element model (FEM) of this industrial blisk and Fig. 4.2 shows the system natural frequencies versus nodal diameters. The abbreviations on the plot identify the corresponding blade mode family. For example, 1F stands for the first flexural (F) bending mode family. The other mode types are torsion (T), stripe (S) or chordwise bending, and edgewise (E) bending.

The general procedure for numerical validation is described as follows. First, a tuned CMM model of this industrial blisk was generated from using model data and results from the parent FEM, e.g., tuned-system eigenvalues  $\Lambda^S$ . Then it was mistuned by a given blade stiffness mistuning pattern,  $\delta\Lambda^{CB}$ , and a given set of cyclic modeling error values,  $\delta\Lambda^S$ . Next, either single-blade excitation (SBE) or multi-blade excitation (MBE), with forcing vector  $\mathbf{f}^{CB}$ , was applied to the mistuned CMM model, and the mistuned response  $\mathbf{x}$  was obtained at all resonant frequencies. Finally, the response vectors  $\mathbf{x}$  and resonant

frequencies  $\omega$  were used as “test” data for the identification algorithm Eq. 4.8 to calculate both mistuning and external forcing parameters.

### **First Flexural (1F) Bending Mode Family**

For the first flexural bending mode family around 2300 Hz, there were three different cases investigated: SBE(3), MBE(3,17), and MBE(3,17,20). The numbers in parentheses denote the blades on which forcing is applied, and the forcing values used for all three cases are listed in Table 4.1. For example, for SBE(3), all the elements of the forcing vector were zero except the one corresponding to blade 3:

$$\mathbf{f}^{CB} = [f_1 \quad f_2 \quad f_3 \cdots f_{28} \quad f_{29}] \quad (4.10a)$$

$$f_3 = 8.665 - j4.237; \quad f_i = 0, i \neq 3 \quad (4.10b)$$

The real and imaginary parts of  $f_3$  were selected arbitrarily. Note that the identification process was performed using a compact CMM model with the number of DOF equal to the number of blades.

Figure 4.4 presents the identification results for SBE(3). The horizontal axis, labeled “System Mode Used”, represents the mode number (corresponding to one specific resonant frequency) for which the measurement is taken. Note that all the identification results were obtained by only including one measurement in Eq. 4.8, which means that  $\mathbf{x}$  is a single column vector. More specifically, for Eq. 4.8, there were 29 unknown blade mistuning values, 15 unknown cyclic modeling errors (one each for nodal diameters 0–14), plus 2 more unknown forcing terms (the real and imaginary parts of  $f_3$ ). However, one  $\mathbf{x}$  yields 58 equations, counting both the real and imaginary parts. Therefore, only one measurement is sufficient to identify the force as well as the mistuning. It can be seen in the left

column of Fig. 4.4 that fairly good agreement is observed between most of the predictions (circles) and identification results (stars). In the right column, the errors of simultaneous forcing identification for amplitude and phase are depicted. Most of the errors are less than 3% except those identification results obtained by using measurements at mode 28 and 29, which probably drift apart from the expected value line due to the redundancy of the coefficient matrix  $\mathbf{A}_f$ .

Figures 4.5 and 4.7 show the errors of the identification results for MBE(3,17) and MBE(3,17,20), respectively. The match is generally good, with errors less than 3%. Figure 4.3 compares the simultaneous results of mistuning identification to the known mistuning patterns for all three forcing cases. For these examples, the accuracy of mistuning identification was not adversely affected by identifying external forcing at the same time. The maximum errors appear when the assigned mistuning values are close to zero, such that any small deviation leads to high relative error values.

### **Mixed 2F/2T Mode Family**

A higher frequency range around 15  $kHz$ , which is the mixed second flexural bending and second torsion mode family, was also considered to examine the capability of the simultaneous identification algorithm. The SBE(3) case was used for the forcing, and only one measurement at one resonant frequency was substituted into Eq. 4.8 for the simultaneous identification process. The identification results are displayed in Fig. 4.9. These results consistently match with the assigned forcing values, indicating that the approach works well for this higher frequency range for the industrial blisk. However, it is noted that, because the validation is numerical, no errors exist in the input data to the identification equations.

### 4.3.2 Simultaneous Identification Method — NASA Blisk

For an additional example system for numerical validation, the identification algorithm was applied to a 26-blade NASA compressor rotor. Figure 4.10 shows the finite element model of this NASA blisk. Note that this system features a more complex blade geometry than the other examples. The basic procedure was repeated as described in section of Industrial Blisk above. Since the FEM of the NASA blisk is much larger in terms of DOF than the previous example, and the finite element analysis runs required for validation purposes are computationally expensive, only single-blade excitation (applied to blade 4) was considered in this study.

Figures 4.12 and 4.13 present the identification results for the external forcing and mistuning, respectively. Each result was obtained using only a single resonant response measurement vector, with the system mode corresponding to the resonance shown as the  $x$  axis. In general, these identification results match well with the known values. For a few modes, however, there is significant error in the results, especially for mode 12. One approach to making the results more robust would be to discard the outliers and average the remaining values. A more rigorous strategy would be to use the model and/or test data to determine which resonant response measurements will work best for accurate identification. However, this is beyond the scope of the present study and is left for future work.

### 4.3.3 Comparison of Simultaneous and Sequential Identification Methods — Validation Blisk

Figure 4.14 shows the finite element model of a 24-blade blisk that was designed at the University of Michigan specifically for validation purposes. This is referred to as the validation blisk, and it has a structural damping factor of 0.00015.

First, the simultaneous identification method was examined with this example system.

The MBE(2,9,17) case was applied to the validation blisk around 2100  $Hz$ , the first flexural bending (1F) family, and the blade responses were collected to identify the external forcing as suggested in the section above. Figure 4.16 shows very scattered identification results with generally poor agreement with the known values. This inaccuracy might be caused the low levels of both structural damping and mistuning for this blisk, which lead to the mode shapes and forced response shapes being almost identical. According to Eq. 4.1, if  $\mathbf{p}$  is substituted by mode shape then the  $\mathbf{f}$  on the right side should be set as 0. However, in forcing identification, the same equation is used assuming there is nonzero external forcing, which causes the deviation.

An alternative approach, sequential system and forcing identification, is applied to assess the performance of the sequential method in this challenging case. The unknown system properties (blade stiffness mistuning and cyclic modeling error parameters) were obtained first using the previously developed identification process. Then, based on the updated reduced-order model and test results (numerically generated or experimentally measured) for blade response, the external forcing can be calculated directly from the equations of motion.

This sequential approach has some clear advantages over the simultaneous approach. First, because the system identification process remains unchanged, its accuracy cannot be adversely affected by performing forcing identification. Second, because the forcing identification is treated as a separate, optional process, it is simpler to implement in analysis software and experimental procedures. Third, because the least squares optimization is applied sequentially to two smaller problems, this may improve the accuracy of the forcing identification process.

The numerical results for the sequential identification method are presented in Fig. 4.17. Note that there is excellent agreement with the known values, in stark contrast to the poor

results from the simultaneous method. This illustrates the advantages of the sequential approach described above. Figure 4.18 shows the errors of sequential forcing identification for blade 2 compared to simultaneous forcing identification. Clearly, the sequential method is much more accurate for this case, with the maximum error less than 3% compared to an error of more than 140% for the simultaneous approach.

Moreover, in vibration tests, it is sufficiently difficult to identify the modal parameters considering testing errors, environment noise, *etc.*, without enlarging the scope of the problem to identify more parameters. Therefore, the sequential approach is recommended for identifying the external forcing.

## **4.4 Experimental Validation**

### **4.4.1 Experimental Specimen and Excitation System**

The 24-blade validation blisk introduced in previous section was also employed for the purpose of experimental validation. The actual blisk, which was manufactured to extremely tight tolerances[30], is shown in Fig. 4.21. This blisk has previously been used to experimentally validate the CMM approach and the reduced-order model updating method discussed above [53].

Acoustic excitation was provided to the blades by an array of speakers[22, 23], as seen in Fig. 4.21. Behind each blade, a round speaker was mounted parallel to the surface of the blade in order to apply an acoustic force. These speakers were driven by a series of Hewlett-Packard 8904 Multifunction Synthesizers, each with two independent but phase-synchronized channels. The speakers were carefully calibrated using white noise excitation first. Then, the speakers were mounted on the plastic fixtures, and a sinusoidal signal was sent to each speaker, one at a time. A calibrated microphone was used to record the sound pressure level at a fixed distance from the speaker, similar to the distance to

the individual blade when it is mounted on the fixture. The amplitude and phase of the excitation signal were both documented as reference.

#### 4.4.2 Single-Blade Excitation

Because it was so carefully designed and manufactured, the original validation blisk was nearly tuned. Therefore, mistuning was added intentionally by attaching a group of small lead masses (details in table 4.2) to the tips of selected blades. By this means, a new baseline system was created, as shown in figure 4.22, in order to observe localized responses that are more typical of an actual blisk. Therefore, the contribution of external forcing to the blade responses can be more readily evidenced. The resonant frequencies for part of the first flexural bending (1F) family of the intentionally mistuned rotor, including only blade-dominated system modes, was found within the range of 2100.0—2160.0  $Hz$  as predicted.

As for the benchmark test, the external forcing of SBE was set as  $f_i = 1 \times \sin(\omega t + 45)$ , where  $i$  can be any one of the 24 speakers. The forcing was later changed into  $f_i = 0.5 \times \sin(\omega t + 225)$ . Thus, the difference between the two applied forcing cases should appear as a 180-degree increase in phase and a 50% decrease in magnitude. First, SBE(17) was applied, followed by SBE(24). In both cases, the blade responses  $x$  at resonant frequencies within 2100–2160  $Hz$  were measured and then placed into Eq. 4.6, while the forcing terms were neglected. Figure 4.22 shows the mistuning pattern identified from experimental measurements for SBE(17). Note the excellent agreement between known and identified mistuning patterns. The results for SBE(24) were nearly identical, so they are not shown. Using these results, the CMM model was updated to represent the mistuned system. Figure 4.23 and 4.24 show the results of forcing identification based on the updated CMM model according to Eq. 4.7, using the same group of measurements. It is

seen that the shifts in magnitude and phase are captured accurately. This approach is very efficient because the whole system, not only the reduced-order model of the rotor itself but also the external excitation system, is identified and updated consecutively using same group of measurements, and no previous calibration is required.

#### 4.4.3 Multi-Blade Excitation

For the MBE(17,24) case, blades 17 and 24 were excited simultaneously in the exact same manner as described above for the SBE(17) and SBE(24) cases. The identified forcing parameters for blades 17 and 24 are depicted in Fig. 4.25. The shifts in phase and magnitude are well captured for the MBE(17,24) case. The errors in identified magnitude and phase values are displayed in Fig. 4.26. For the phase, there was a system error of about 8 degrees due to the phase delay between input signal and speaker response. It is encouraging that the accuracy of forcing identification was robust with respect to this experimental error. These results again suggest that the sequential approach for forcing identification shows great promise for implementation as a practical calibration tool in the laboratory.

#### 4.4.4 Perturbed Engine Order Excitation

To achieve engine order excitation, all the speakers were driven simultaneously to deliver forces of the same amplitude, but with a specified phase lag between adjacent speakers:

$$\phi = \frac{2\pi C}{N} \quad (4.11)$$

where  $C$  is the engine order of the excitation. Thus, the force for blade number  $n$  can be written as:

$$f_n = f_0 \cos(\omega t + (n - 1) \phi) \quad (4.12)$$

where  $f_0$  is the force amplitude. Thus any engine order excitation can be obtained by simply changing the phase lag. The traveling-wave excitation system not only simulates the forcing experienced by a rotating bladed disk in an engine, but it also provides non-contacting excitation [23, 30].

In order to further validate the sequential method, a random perturbation was added to the pure engine order excitation. Figure 4.27 compares the pure engine order 8 excitation generated by calibrating all the speakers carefully and the perturbed engine order 8 excitation that results from introducing errors into the phase lags between adjacent speakers. All the forcing terms were calculated as follows: 1) a frequency sweep was conducted within 2110–2160 Hz; 2) mistuning identification and model updating were performed using selected blade responses at resonant frequencies by neglecting the forcing according to Eq. 4.6; 3) external forcing was identified based on the same set of blade responses as showed in Eq. 4.9, with no extra tests performed; 4) finally, the identified forcing term was substituted into Eq. 4.1 to calculate the expected blisk response to the actual forcing.

In Fig. 4.28 and 4.29, the experimental results of frequency sweep on blade 2 and blade 9 are compared to the predictions for the pure and perturbed engine order 8 excitation cases. Apparently, the identified forcing captures the small perturbations added to the pure engine excitation, and therefore it yields great agreement between expected and measured response values. Therefore, this sequential approach is useful not only for initial calibration purposes, but also for flagging and quantifying the deviations from intended excitation patterns in subsequent forced response tests.

## 4.5 Conclusions

In this chapter, the identification and impact of uncertainties in the external excitation for blisk vibration tests were investigated in detail. The mistuning identification method

was extended to also identify the forcing applied to the blades. It was shown that blade mistuning and forcing parameters can be identified either simultaneously or sequentially by carrying out a small set of prescribed forced response experiments. A numerical validation study was carried out with several example models of blisks to examine the accuracy and robustness of the new methods. It was seen that the simultaneous method generally yielded good results, but also led to poor results for some cases. When applied to the same case, the sequential method was much more robust and accurate. The sequential method was also validated experimentally with a 24-blade blisk. This approach shows great promise as a powerful tool for accelerating the calibration process, and also for supporting subsequent forced response tests.

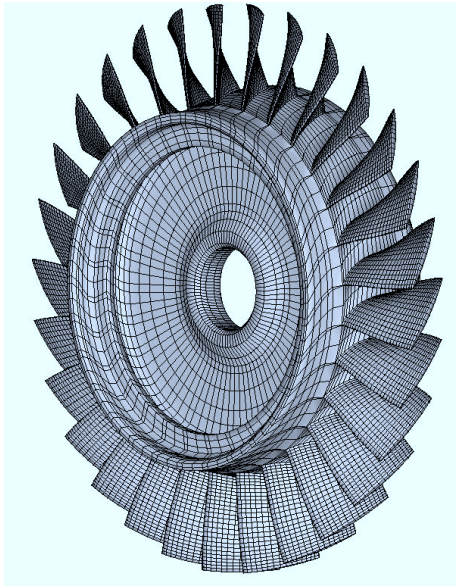


Figure 4.1: Finite element model of the industrial blisk.

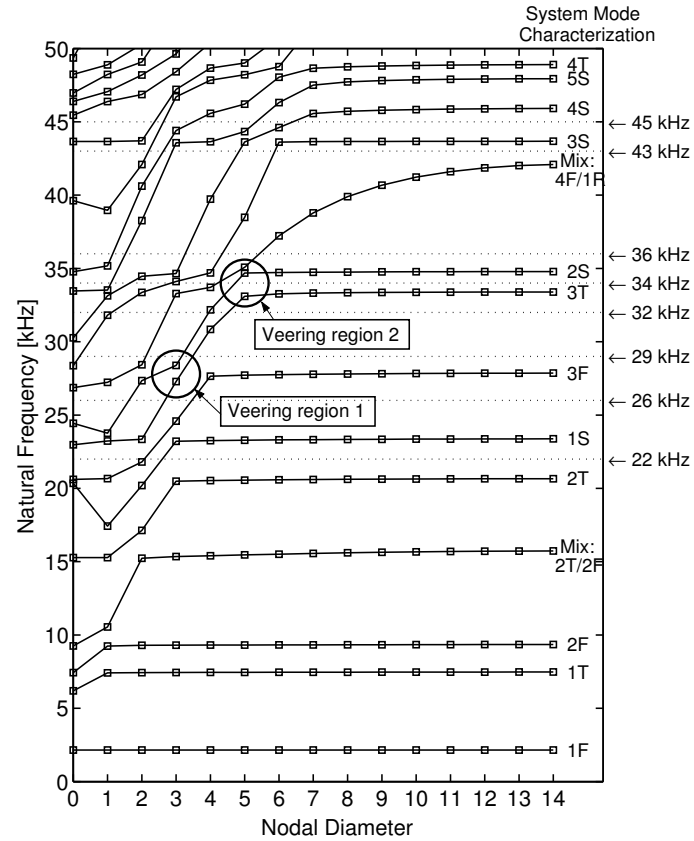


Figure 4.2: Natural frequencies versus the number of nodal diameters from the the tuned FEM of the industrial blisk.

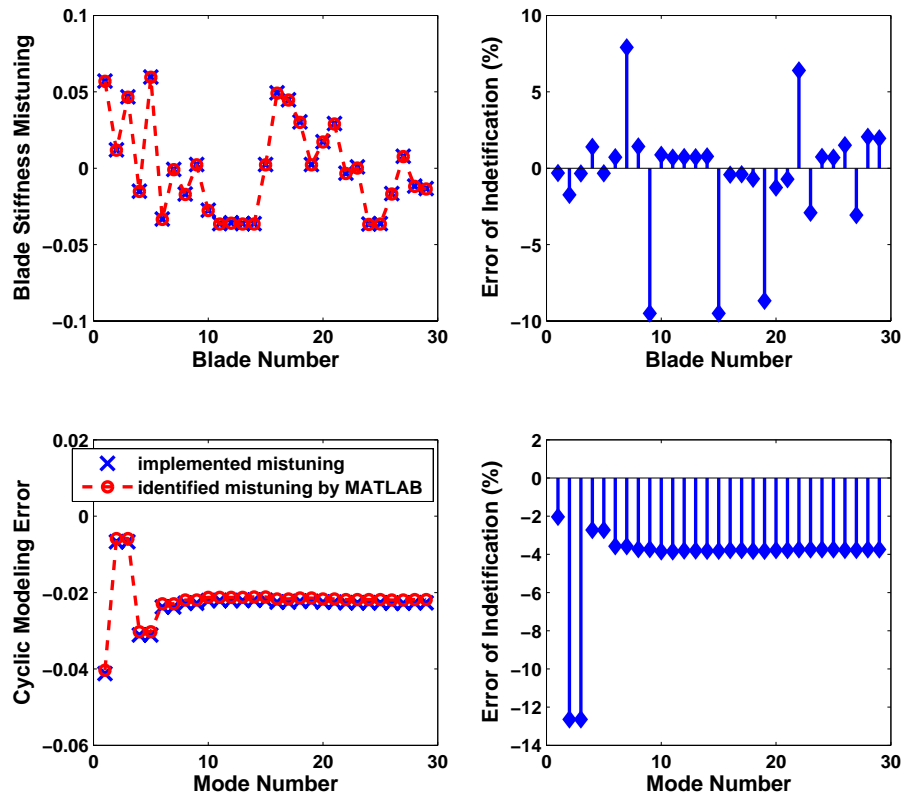


Figure 4.3: Mistuning identification of the industrial blisk with forcing identification simultaneously (all forcing cases), 1F mode family.

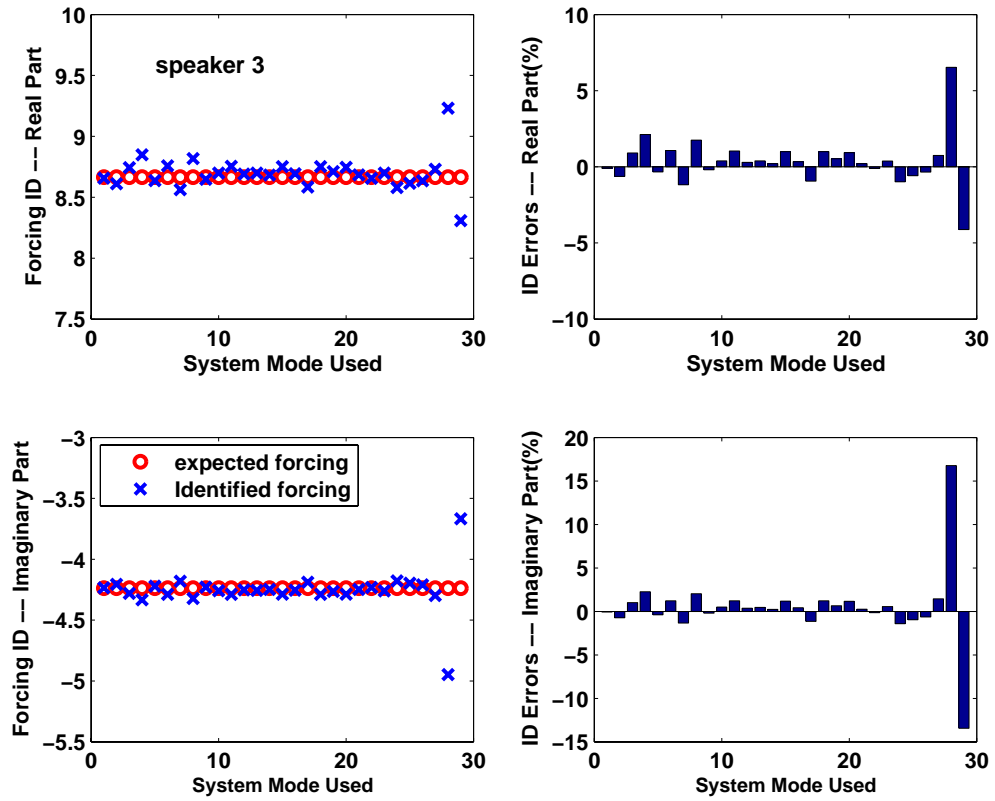


Figure 4.4: Forcing identification results and errors for the SBE(3) case for the industrial blisk, 1F mode family.

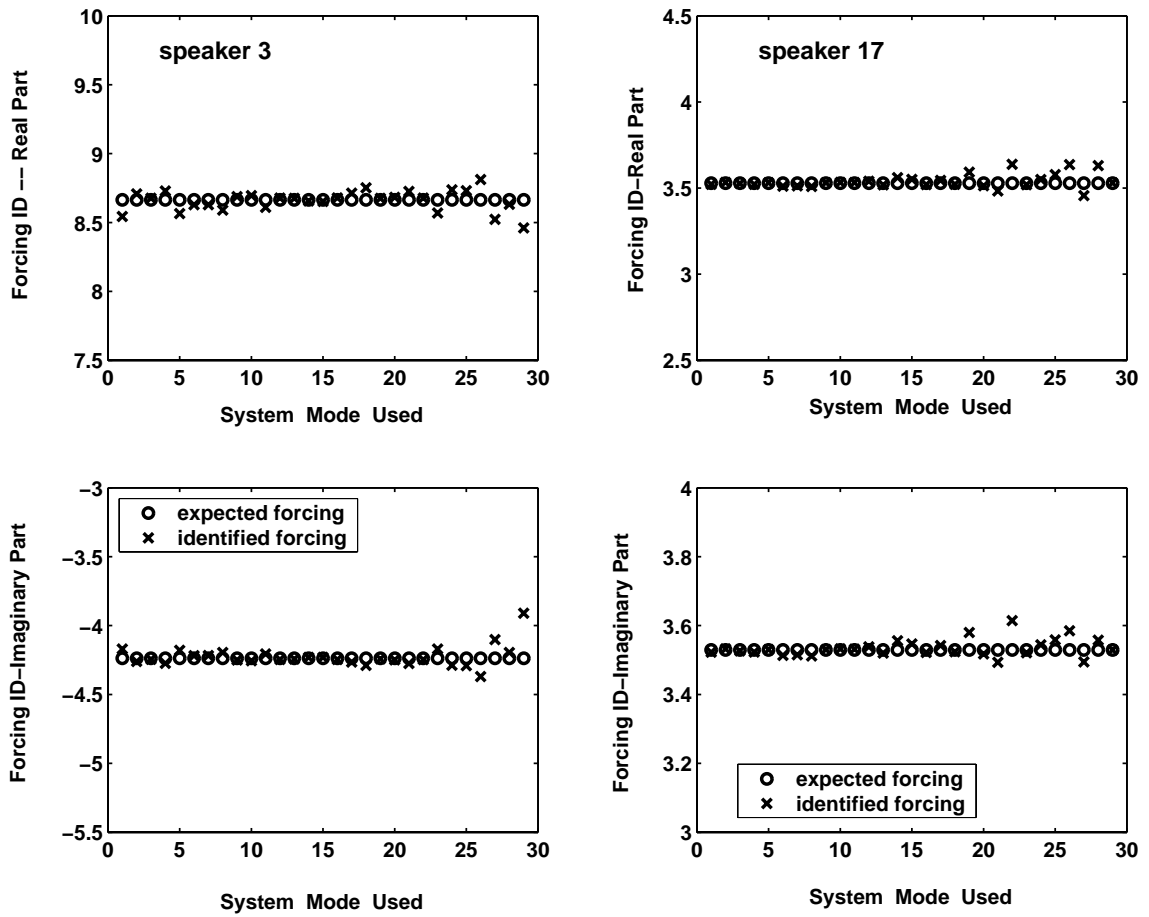


Figure 4.5: Forcing identification for the MBE(3,17) case for the industrial blisk, 1F mode family.

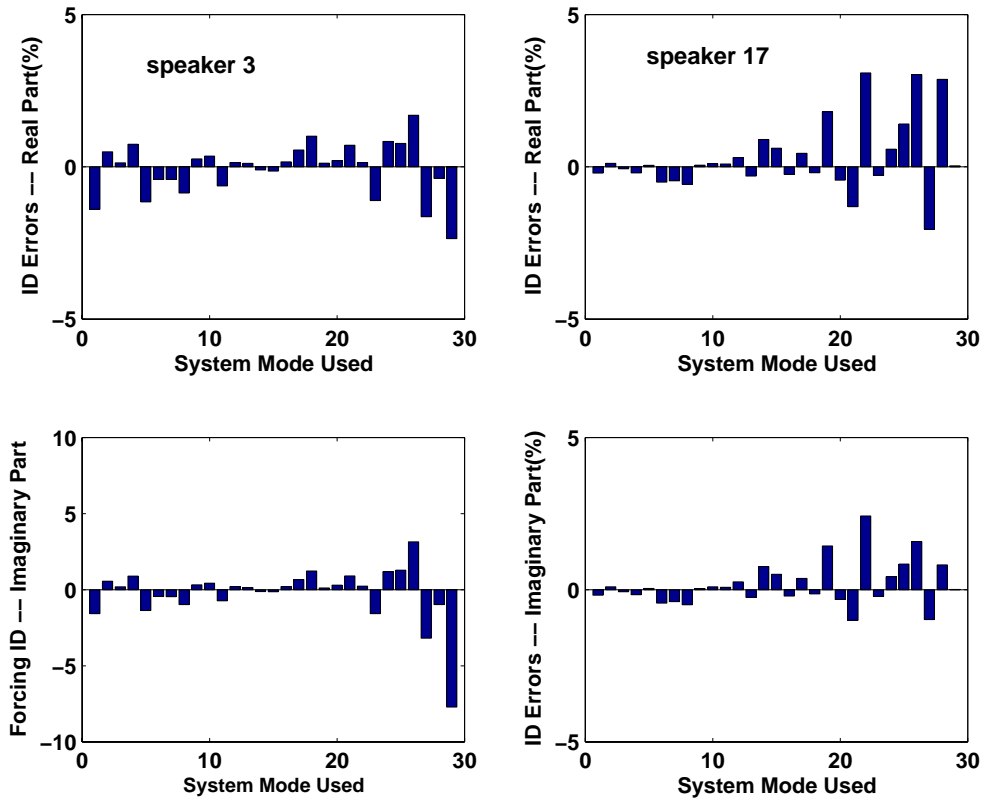


Figure 4.6: Errors in forcing identification for the MBE(3,17) case for the industrial blisk, 1F mode family.

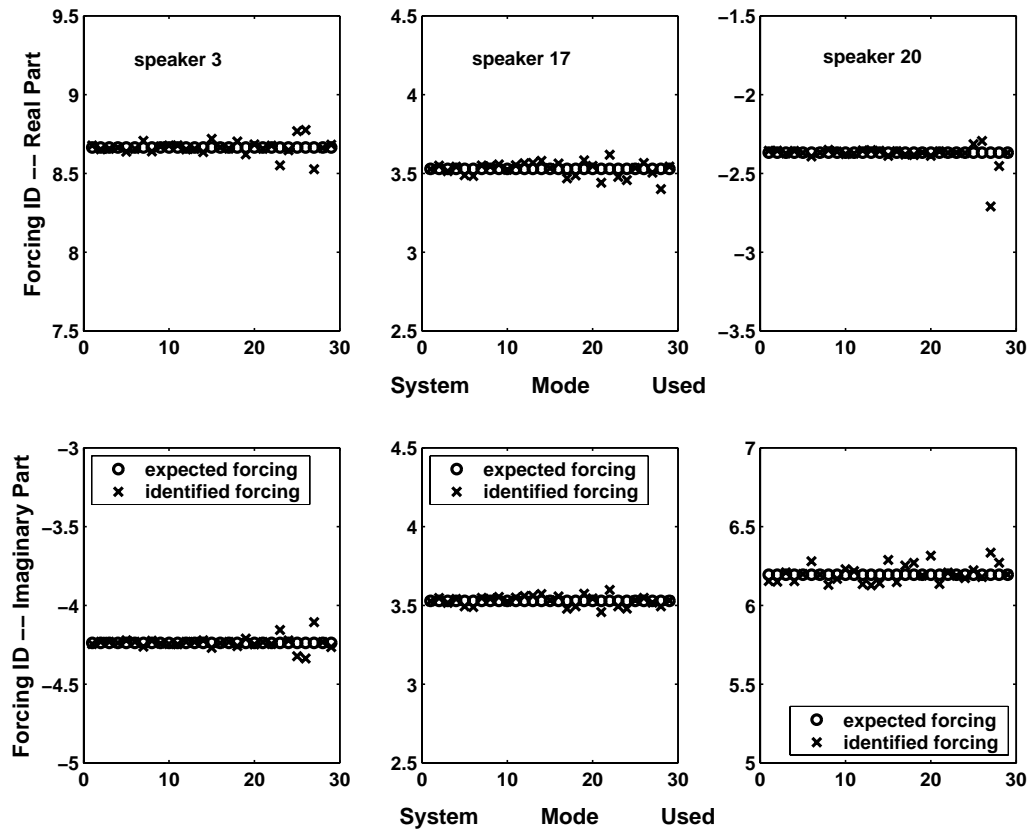


Figure 4.7: Forcing identification for the MBE(3,17,20) case for the industrial blisk, 1F mode family.

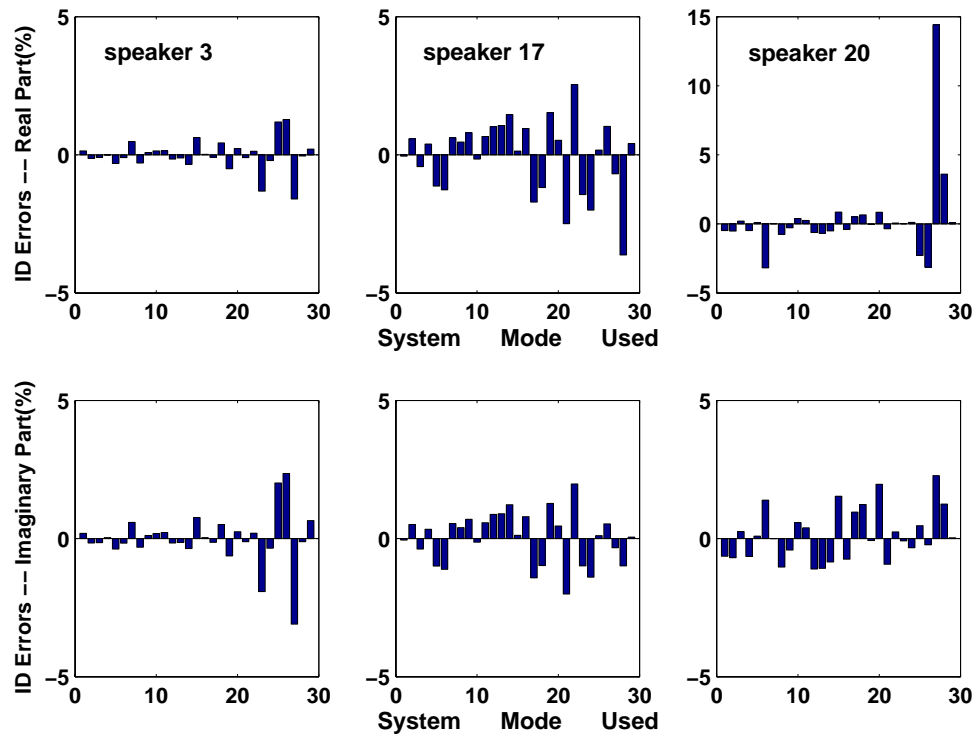


Figure 4.8: Errors in forcing identification for the MBE(3,17,20) case for the industrial blisk, 1F mode family.

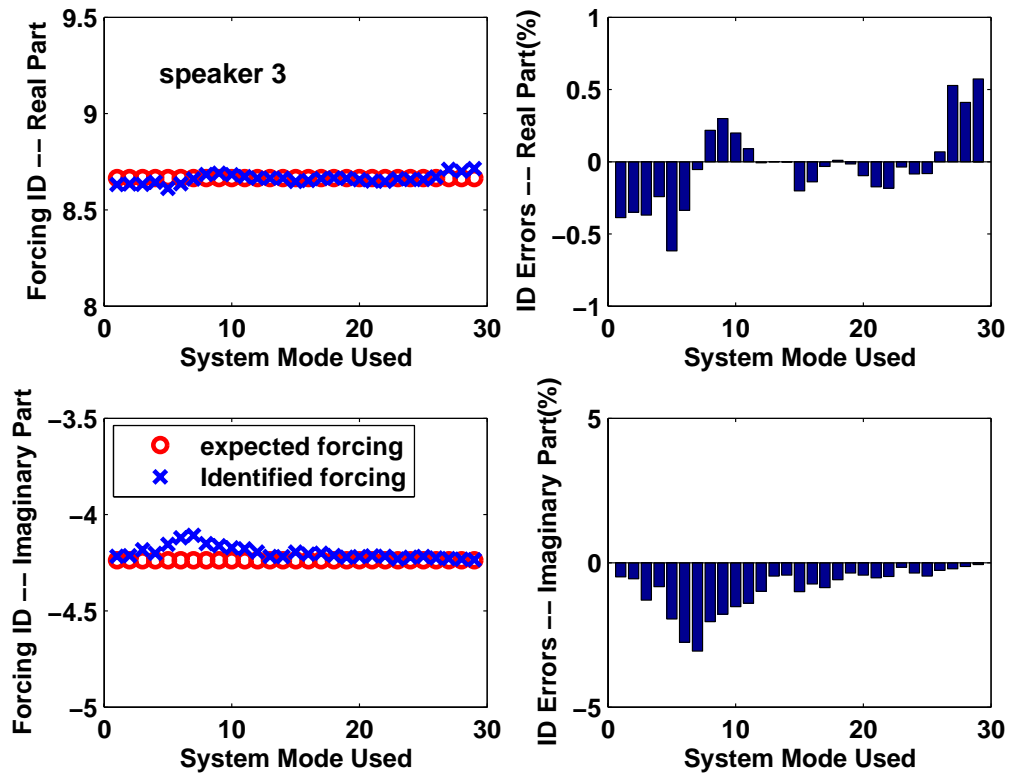


Figure 4.9: Forcing identification results and errors for the SBE(3) case for the industrial blisk, 2T/2F mode family.

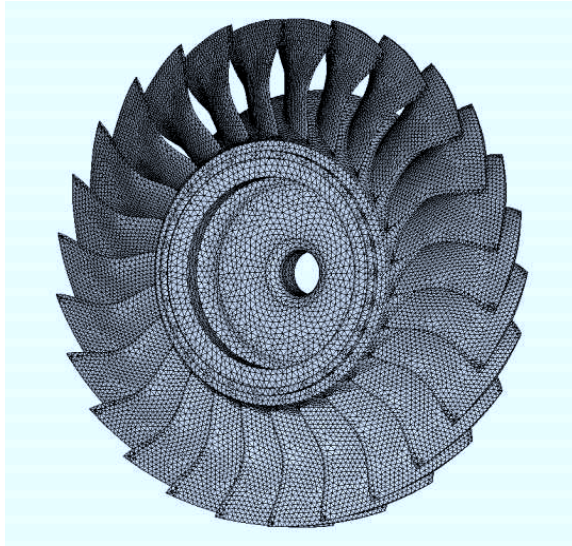


Figure 4.10: Finite element model of the NASA blisk.

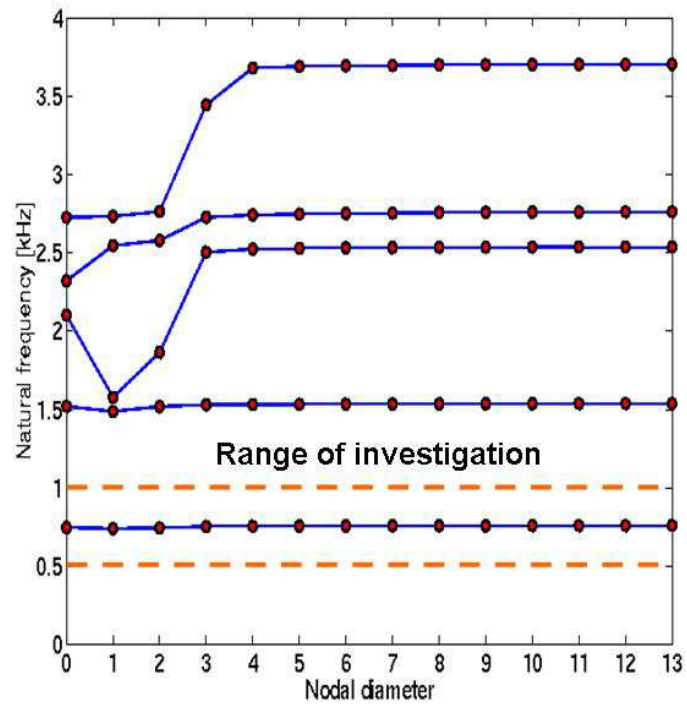


Figure 4.11: Natural frequencies versus the number of nodal diameters for the tuned FEM of the NASA blisk.

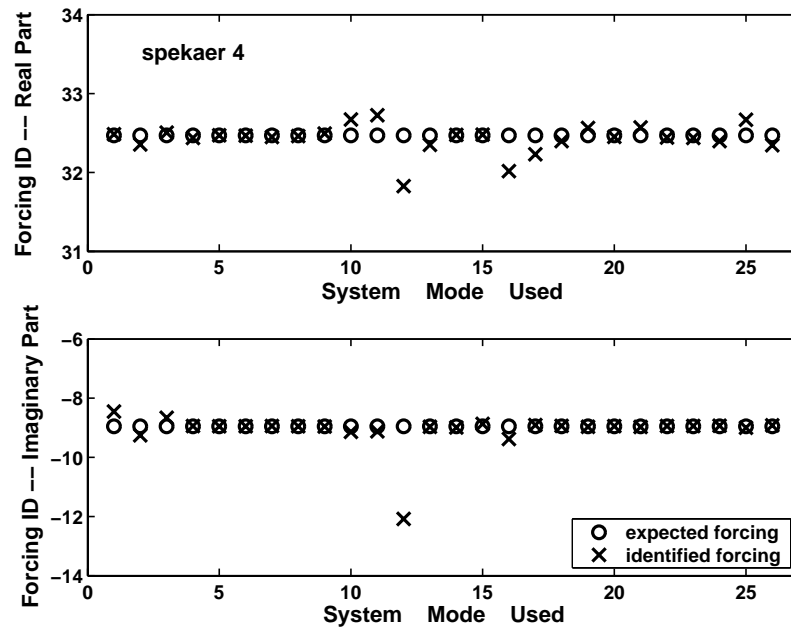


Figure 4.12: Forcing identification results for the SBE(4) case for the NASA blisk.

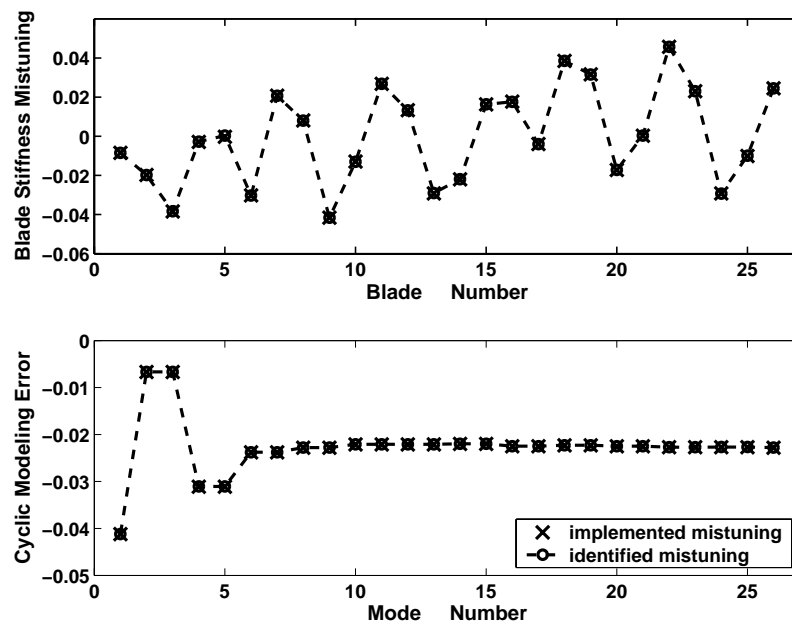


Figure 4.13: Simultaneous mistuning and forcing identification results for the NASA blisk.

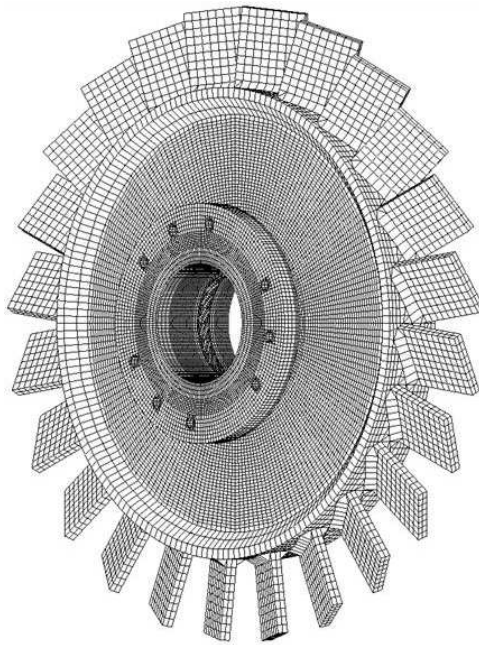


Figure 4.14: Finite element model of the validation blisk.

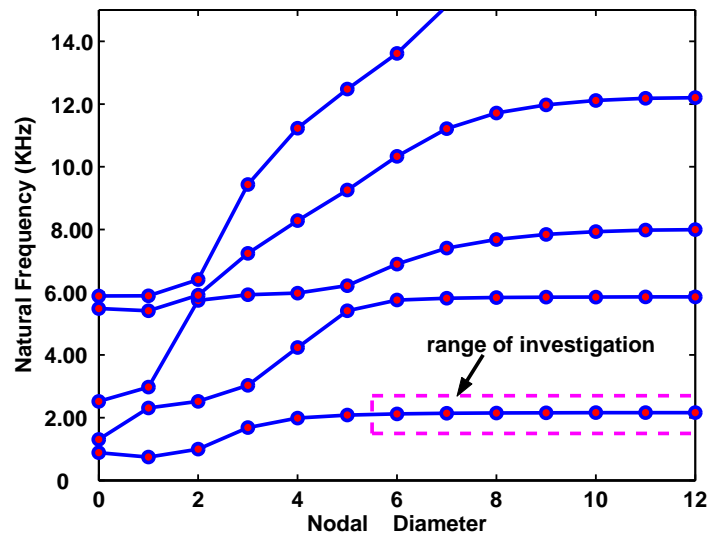


Figure 4.15: Natural frequencies versus the number of nodal diameters for the tuned FEM of the validation blisk.

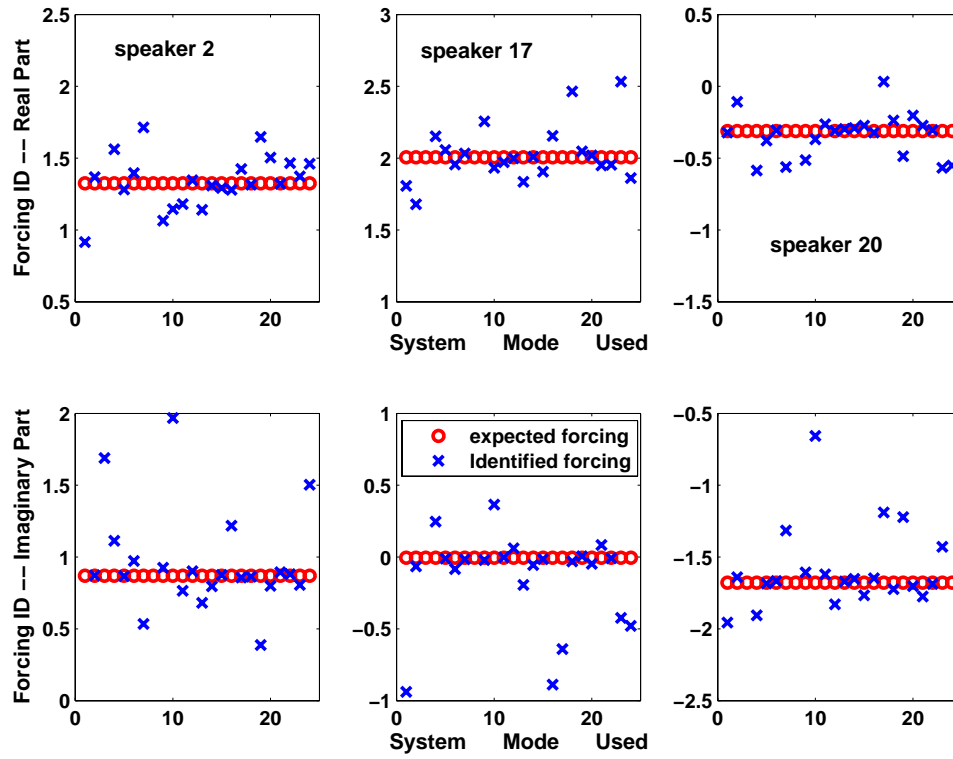


Figure 4.16: Simultaneous forcing identification results for the MBE(2,9,17) case for the validation blisk.

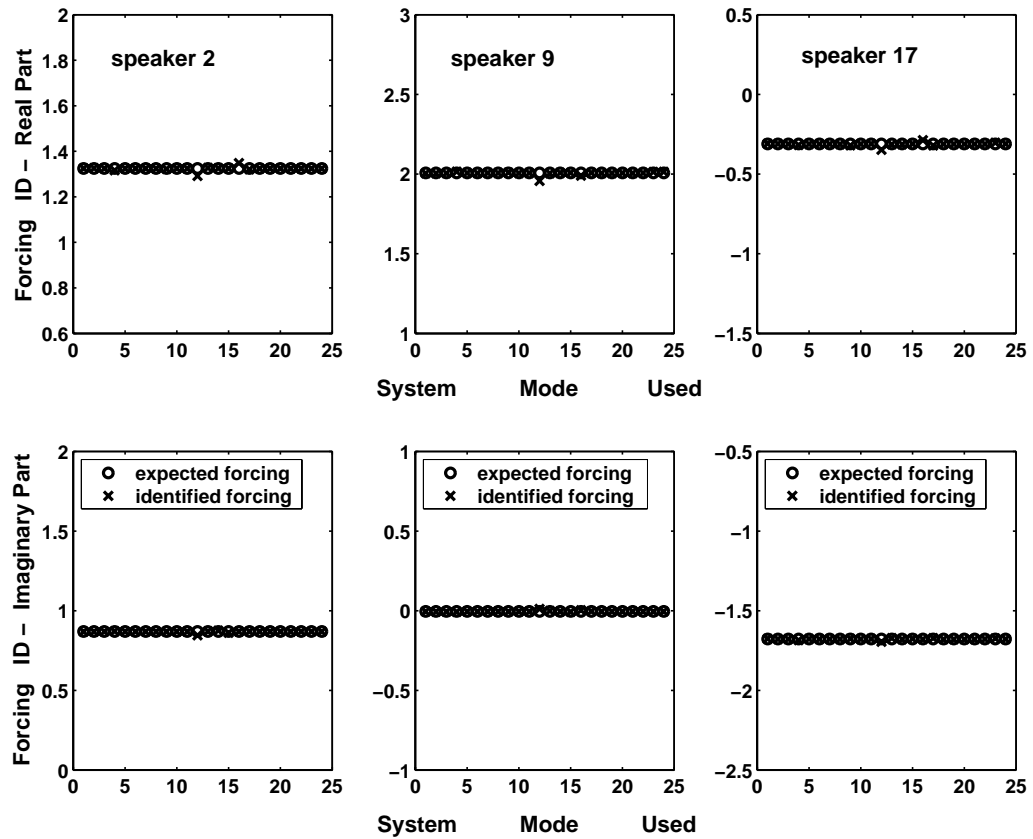


Figure 4.17: Sequential forcing identification results for the MBE(2,9,17) case for the validation blisk.

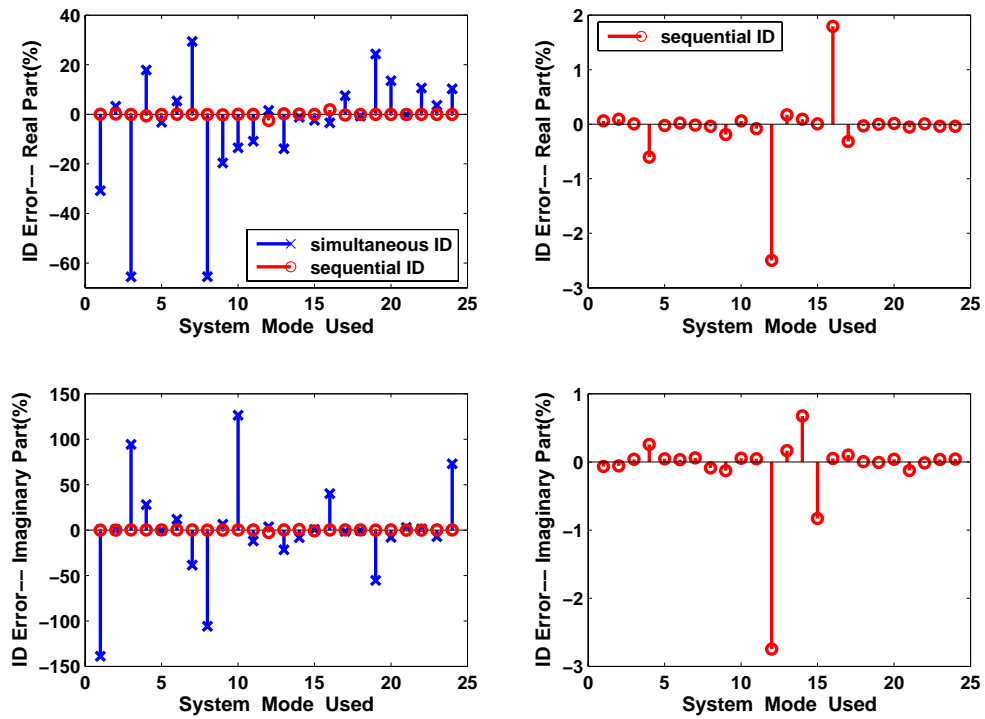


Figure 4.18: Forcing identification errors for blade 2 of the validation blisk for the MBE(2,9,17) case.



Figure 4.19: Actual 24-blade validation blisk used in the experiment.



Figure 4.20: Validation blisk shown with the acoustic excitation system.

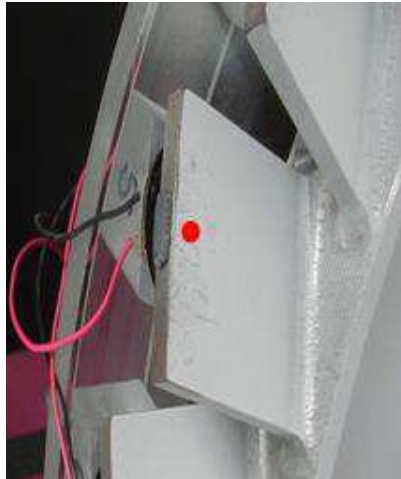


Figure 4.21: Detail of a blade with an attached mistuning mass. The selected measurement location is marked by a dot.

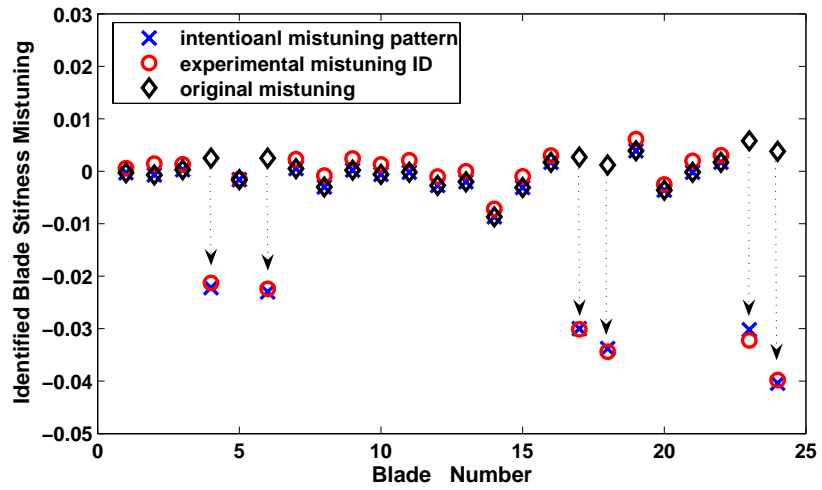


Figure 4.22: Comparison of intentional and identified blade stiffness mistuning values for the validation blisk, assuming consistent cyclic modeling errors before and after adding masses.

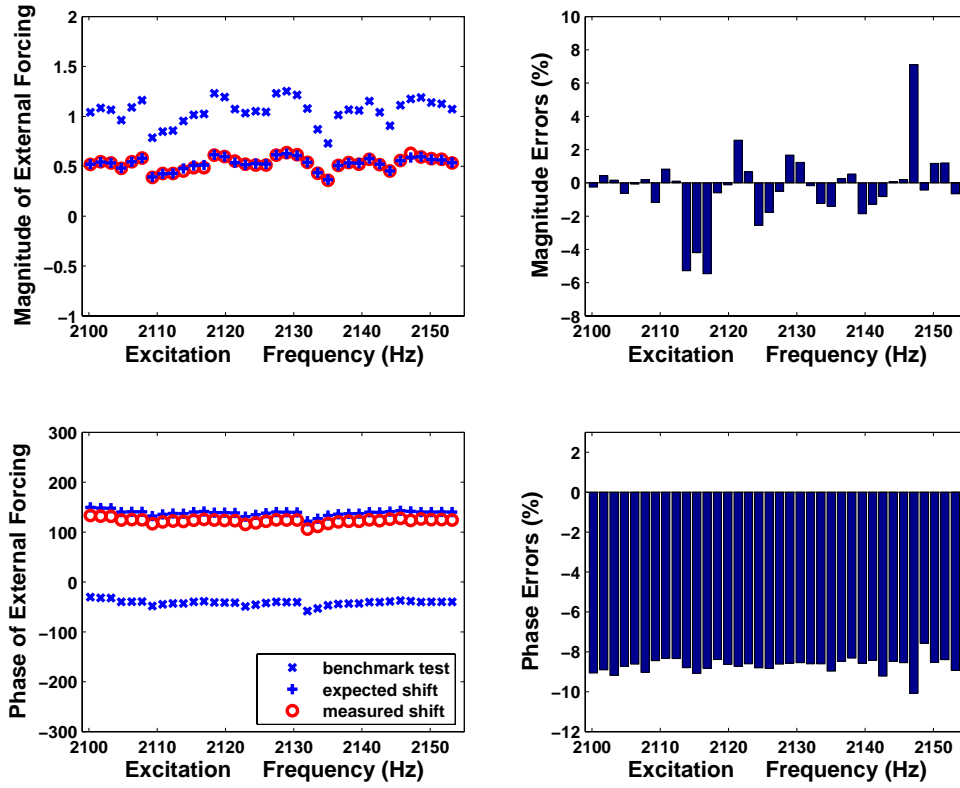


Figure 4.23: Forcing identification results and errors for the SBE(17) case for the validation blisk.

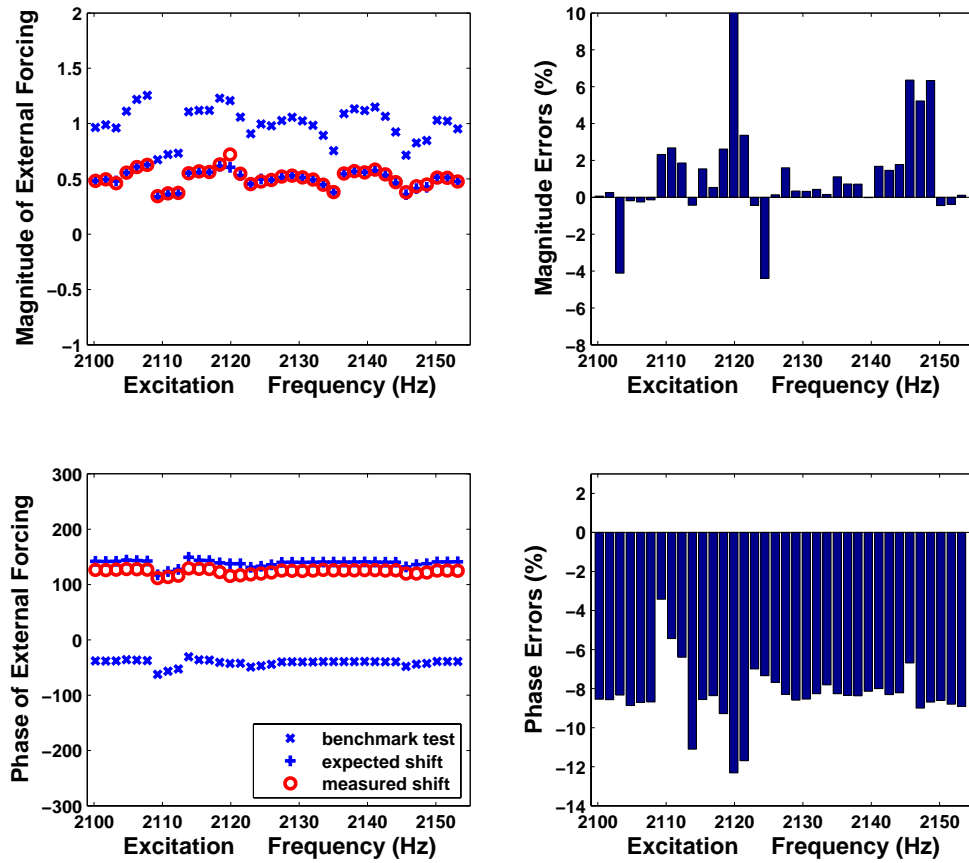


Figure 4.24: Forcing identification results and errors for the SBE(24) case for the validation blisk.

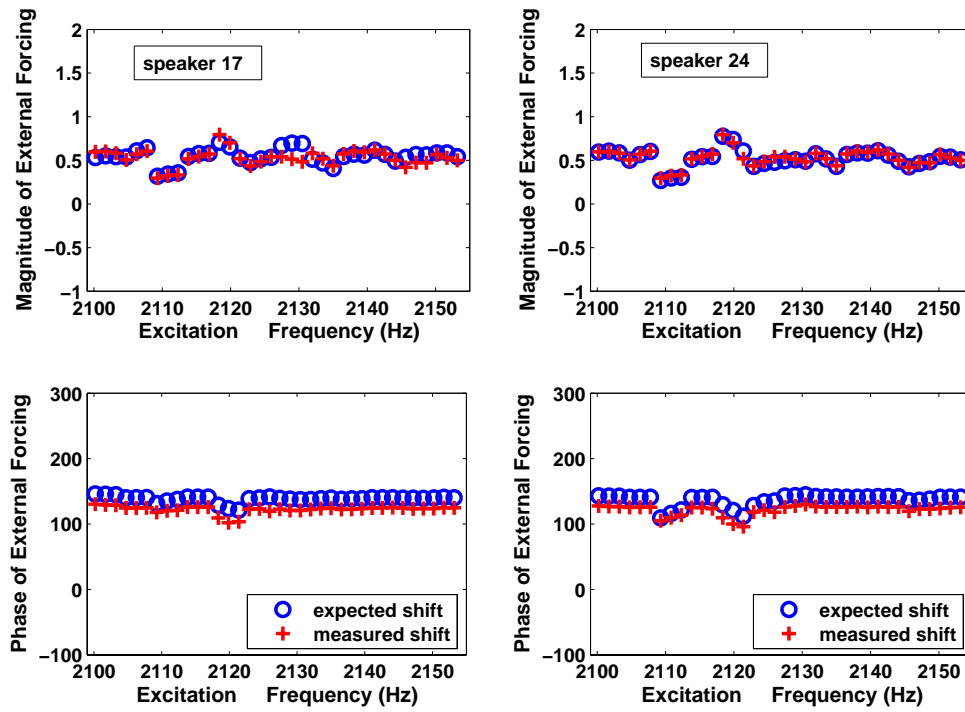


Figure 4.25: Forcing identification results for the MBE(17,24) case for the validation blisk.

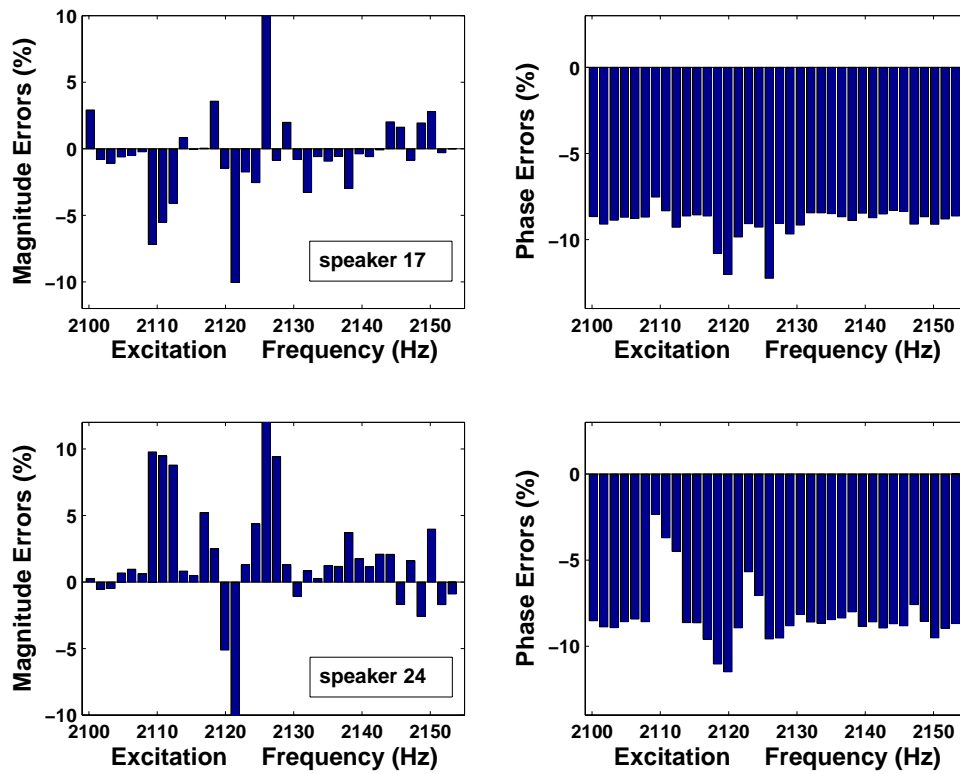


Figure 4.26: Forcing identification errors for the MBE(17,24) case for the validation blisk.

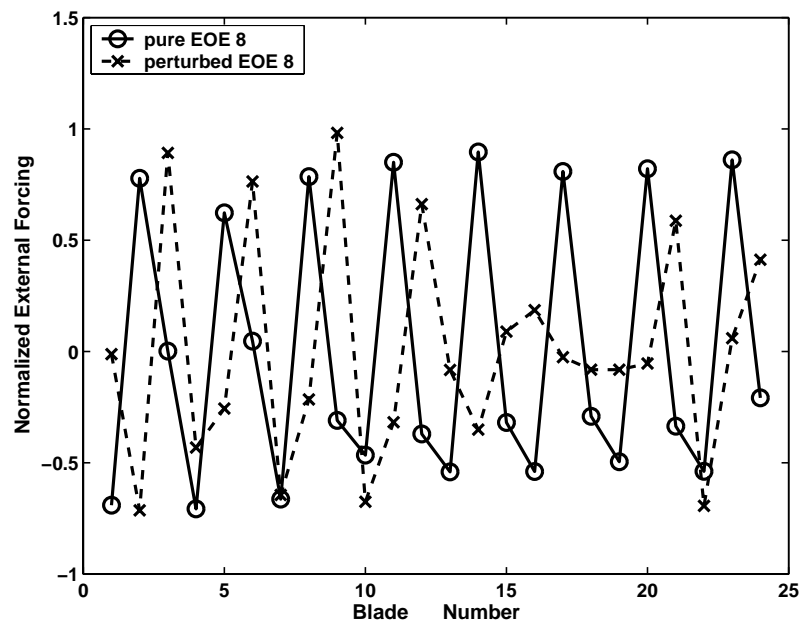


Figure 4.27: Comparison of pure and perturbed engine order 8 excitation, both calculated based on the experimental responses of the validation blisk.

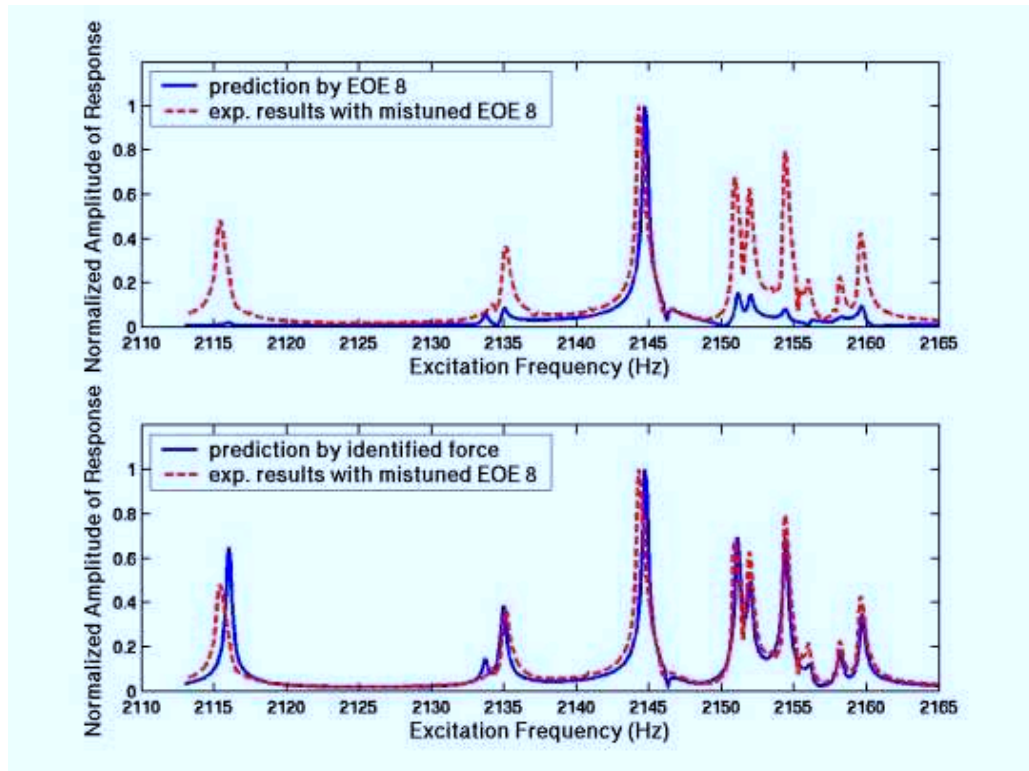


Figure 4.28: Comparison of frequency response results for blade 2 of the validation blisk subject to pure and perturbed engine order 8 excitation.

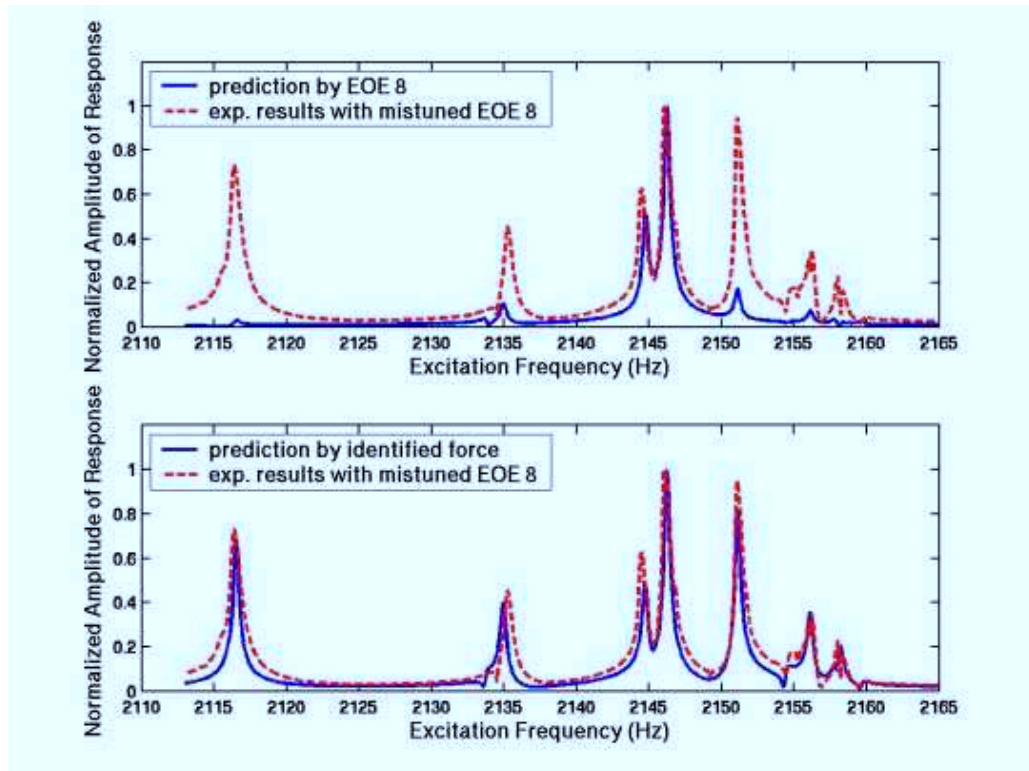


Figure 4.29: Comparison of frequency response results for blade 9 of the validation blisk subject to pure and perturbed engine order 8 excitation.

Table 4.1: External forcing values for the single-blade and multi-blade excitation cases.

<b>External</b>	<b>Blade Number</b>		
<b>Forcing</b>	3	17	20
SBE(3)	8.665-j4.237		
MBE(3,17)	8.665-j4.237	3.529+j3.529	
MBE(3,17,20)	8.665-j4.237	3.529+j3.529	-2.368+j6.194

Table 4.2: Mass of the leads added to the tip of blade of validation blisk and corresponding intentional blade stiffness mistuning.

blade number	lead mass (with estimated glue weight 0.005g)	intentional mistuning
4	0.575	-0.0247
6	0.595	-0.0255
17	0.783	-0.0327
19	0.843	-0.0350
23	0.869	-0.0360
24	1.089	-0.0442

## CHAPTER V

### Conclusions

#### 5.1 Dissertation Contributions

The main contributions of this dissertation are summarized as follows:

- In chapter II, a systematic experimental approach was presented to validate a new reduced-order modeling technique for mistuned bladed disks, as well as a new mistuning identification and model updating algorithm for blisks. It was shown that only a few system response measurements taken at resonant frequencies were required to identify the blade stiffness mistuning parameters and, if needed, the model updating parameters referred as “cyclic modeling error.” By identifying both cyclic modeling error and blade mistuning, the accuracy of the identification results were significantly improved. That is, by incorporating a model updating procedure, the identification method was made more robust with respect to errors in the tuned finite element model.
- In chapter III, an alternative approach for vibration testing of many mistuning patterns was developed and demonstrated. In particular, varying the external forcing function provided to the blades was used to mimic the influence of structural blade property mistuning on the vibration response. This innovative approach was re-

ferred to as experimental Monte Carlo mistuning assessment. The feasibility of this method was validated by repeatable experiments. Since it is much easier and more efficient to vary the external excitation than to physically alter the blades, this work has opened the possibility of running an experimental analog of a Monte Carlo simulation.

- In chapter IV, the mistuning identification method described in chapter II was extended to account for the effects of uncertainties in the forcing applied to the blades. It is shown that blade mistuning and forcing uncertainties can be identified simultaneously by carrying out a small set of prescribed forced response experiments. This approach shows promise as a powerful tool for accelerating the calibration process. Furthermore, this work demonstrated that the impact of forcing uncertainties on the application of system identification and reduced-order modeling techniques to actual bladed disks should not be neglected.

## 5.2 Future Research

Based on the work reported in this dissertation, some ideas for future research may be considered:

- The new technique of mistuning identification and model updating presented in Chapter II was validated both numerically and experimentally for only a single blade-dominated mode family. However, there is no assumption made to exclude a general case where more than one family mode can interact due to mistuning. The algorithm can be expanded to more general applications. For example:
  1. If only mistuning identification is required, this approach can be used for either blade-dominant or disk-dominant modes, since the results are optimized with

a least squares method. However, the accuracy of “cyclic modeling error” is only ensured while blade-dominant modes are considered. Developing mode selection criteria would improve not only the CMM modeling process but also the updating results.

2. For those cases in which more than one mode family is excited, the approach itself could be improved by allowing the identification of mistuning parameters for multiple blade modes. This would require introducing the Kronecker product into the algorithm. In this way, the mistuning identification and model updating procedure would have more general applicability.
  3. This approach can be accelerated and systemized by adopting an efficient test procedure. In the previous research work, more test results than was necessary were obtained without consideration for the time that the experiments required. In future work, a method should be developed for determining the minimum set of data that is required for obtaining system identification results within a specified accuracy or convergence tolerance.
- The experimental Monte Carlo assessment described in Chapter III is limited by the current test facilities. A new signal conditioning system is needed to realize the entirely independent control over amplitude and phase of the external forcing. With this improvement, more mistuning patterns with a wider range of standard deviations could be applied to the blisk by manipulating the excitation system. Other kinds of mistuning besides the traditional blade stiffness mistuning could be taken into consideration. Also, an advanced uncertainty study could be conducted based on the new test system. Another suggestion is to build a separate controlling station with GPIB (General Purpose Interface Bus), DAQ (Data Acquisition) board, address

selection chip, *etc.* Furthermore, thinking beyond the laboratory environment, it is important to note that perfect engine order excitation will never occur in an engine. Therefore, future research should address the level of “forcing mistuning” present in an engine, the effective increase in blade mistuning level due to this forcing mistuning, and the implications for durability and reliability of rotors.

- In Chapter IV, a forcing identification technique was presented, but the amount of time required to perform the necessary tests in order to develop a standard calibration procedure was not addressed. Basic experimental strategies and specific test procedures still need to be developed for performing the forcing identification and calibration in an efficient manner. In addition, it is noted that identifying the excitation parameters is only the first step towards calibration. More information is required, such as the relationship between the amplitude of input signal and phase of output signal within the frequency range of interest. The forcing identification method could be combined with an experimental investigation of other uncertainties to develop a more sophisticated testing and analysis framework.

## **APPENDICES**

## APPENDIX A

### Equation Reformatting in Computational Process for Mistuning Identification and Model Updating

The component mode mistuning (CMM) method for reduced-order modeling of mistuned bladed disks, and a CMM-based mistuning identification technique were originally presented in Refs. [18, 21, 52]. In this research work, it is always assumed that the mistuning only occurs in the blade stiffness matrix and the mass matrix is invariant(tuned); besides, for each harmonic (i.e., per nodal diameter), there is only one mode, or one pair of modes selected as CMM model basis. Thus the equation of motion can be expressed in tuned system modal coordinates as:

$$\left[ -\omega^2 \mathbf{I} + (1 + j\gamma) \left( \mathbf{\Lambda}^S + \delta \mathbf{\Lambda}^S + \mathbf{Q}^{CBT} \delta \mathbf{\Lambda}^{CB} \mathbf{Q}^{CB} \right) \right] \mathbf{p} = \mathbf{f}^S \quad (\text{A.1a})$$

$$\mathbf{x} = \mathbf{\Phi}_{CB}^S \mathbf{p} \quad (\text{A.1b})$$

$$\mathbf{f} = \mathbf{\Phi}_{CB}^{ST} \mathbf{f}^{CB} \quad (\text{A.1c})$$

All the variables listed in Eq. A.1 are explained as follows:

- $\omega$ : excitation frequency
- $\gamma$ : structural damping factor

- $\mathbf{p}$  and  $\mathbf{x}$ : modal and physical displacement vector
- $\mathbf{f}^S$  and  $\mathbf{f}^{CB}$ : modal and physical force vector
- $\Lambda^S$ : tuned-system eigenvalues
- $\delta\Lambda^S$ : cyclic modeling error
- $\mathbf{Q}^{CB}$ : modal participation factors
- $\delta\Lambda^{CB}$ : cantilevered-blade stiffness mistuning
- $\Phi_{CB}^S$ : blade portion of tuned-system mode shape

To identify both blade stiffness mistuning and cyclic modeling error correctly, only blade-dominant system modes are selected to create the modeling basis of CMM. For example, in case of an  $N$ -bladed disk is being examined, there are generally  $M$  modes,  $M \leq N$ , are blade-dominant and therefore kept. In the vibration test, assume that the steady state vibration is measured for only one degree of freedom (DOF) on each blade, at approximately the same location for each blade. Consequently, for any measured frequency, the dimensions of the matrices and vectors in Eq. A.1 are summarized as follows:

- $\Lambda^S$  and  $\delta\Lambda^S$ :  $M \times M$  diagonal matrices
- $\delta\Lambda^{CB}$ :  $N \times N$  diagonal matrix
- $\mathbf{Q}^{CB}$  and  $\Phi_{CB}^S$ :  $N \times M$  full matrix
- $\mathbf{x}$  and  $\mathbf{f}^{CB}$ :  $N \times 1$  vector
- $\mathbf{p}$  and  $\mathbf{f}^S$ :  $M \times 1$  vector

Ideally, a measurement taken at one resonant frequency, a single  $M \times 1$  vector  $\mathbf{x}$ , would be sufficient to solve the identification problem. The reason is that this measurement  $\mathbf{x}$ , including vibration amplitude and phase at one DOF for each blade, yields  $2 \times N$  equations when listing real and imaginary part separately which exceeds the number of unknowns  $N + M$ . In the identification process, it is assumed that the cyclic modeling error is the same for the 2 modes at the same harmonic which reduces the number of unknowns further to  $N + M/2$  (if  $M$  is odd, the number of unknowns is  $N + (M + 1)/2$ ). However, more than one measurement are always required for experimental validation because of random testing errors.

Although  $\delta\Lambda^S$  and  $\delta\Lambda^{CB}$  are the unknowns introduced in the Eq. A.1, the actual variables identified from the algorithm,  $\mathbf{D}^S$  and  $\mathbf{D}^{CB}$ , are slightly different yet related to them based on the following expressions:

$$\delta\Lambda^S = \Lambda^S \cdot \mathbf{D}^S \quad (\text{A.2a})$$

$$\delta\Lambda^{CB} = \lambda^{CB} \cdot \mathbf{D}^{CB} \quad (\text{A.2b})$$

where  $\lambda^{CB}$  is the tuned cantilevered blade eigenvalue for this investigated family,  $\mathbf{D}^S$  and  $\mathbf{D}^{CB}$  are  $M \times M$  and  $N \times N$  diagonal matrix respectively as same format as  $\delta\Lambda^S$  and  $\delta\Lambda^{CB}$ :

$$\mathbf{D}^S = \begin{bmatrix} d_1^S & 0 & \cdots & 0 \\ 0 & d_2^S & \cdots & 0 \\ \vdots & \vdots & \ddots & \vdots \\ 0 & 0 & \cdots & d_M^S \end{bmatrix}, \quad \mathbf{D}^{CB} = \begin{bmatrix} d_1^{CB} & 0 & \cdots & 0 \\ 0 & d_2^{CB} & \cdots & 0 \\ \vdots & \vdots & \ddots & \vdots \\ 0 & 0 & \cdots & d_N^{CB} \end{bmatrix} \quad (\text{A.3})$$

Then the Eq. A.1 can be re-written if  $\mathbf{p}$  is treated as free-response:

$$\left[ -\omega^2 \mathbf{I} + (1 + j\gamma) \left( \Lambda^S (\mathbf{I} + \mathbf{D}^S) + \mathbf{Q}^{CBT} (\lambda^{CB} \cdot \mathbf{D}^{CB}) \mathbf{Q}^{CB} \right) \right] \mathbf{p} = \mathbf{0} \quad (\text{A.4a})$$

$$(1 + j\gamma) \Lambda^S \mathbf{D}^S \mathbf{p} + \lambda^{CB} \mathbf{Q}^{CBT} \mathbf{D}^{CB} \mathbf{Q}^{CB} \mathbf{p} = \left[ \omega^2 \mathbf{I} - (1 + j\gamma) \Lambda^S \right] \mathbf{p} \quad (\text{A.4b})$$

Since the unknowns in this case is only the diagonal terms of  $\mathbf{D}^S$  and  $\mathbf{D}^{CB}$  which can be represented respectively by two vectors notated as  $\mathbf{d}^S$  and  $\mathbf{d}^{CB}$ , where

$$\mathbf{d}^S = \begin{Bmatrix} d_1^S \\ d_2^S \\ \dots \\ d_M^S \end{Bmatrix}, \quad \mathbf{d}^{CB} = \begin{Bmatrix} d_1^{CB} \\ d_2^{CB} \\ \dots \\ d_N^{CB} \end{Bmatrix} \quad (\text{A.5})$$

And the abbreviation of Eq. A.4 can be written as:

$$\begin{bmatrix} \tilde{\mathbf{A}}_S & \tilde{\mathbf{A}}_{CB} \end{bmatrix} \cdot \begin{bmatrix} \mathbf{d}^S \\ \mathbf{d}^{CB} \end{bmatrix} = \tilde{\mathbf{B}} \quad (\text{A.6})$$

where  $\tilde{\mathbf{A}}_S$  and  $\tilde{\mathbf{A}}_{CB}$  are the reframed coefficient matrices in order to arrange unknowns from  $\mathbf{D}^S$  and  $\mathbf{D}^{CB}$  into  $\mathbf{d}^S$  and  $\mathbf{d}^{CB}$ , and  $\tilde{\mathbf{B}} = \left[ \omega^2 \mathbf{I} - (1 + j\gamma) \Lambda^S \right] \mathbf{p}$ . All of them are fully known once the blade responses in modal coordinates  $\mathbf{p}$  are obtained at desired excitation frequencies  $\omega$ . Here  $\mathbf{p}$  is one measurement ( $M \times 1$  vector) at one frequency  $\omega$ .

$$\tilde{\mathbf{A}}_S(:, i) = \mathbf{U}_i \cdot \mathbf{p}, \quad \mathbf{U}_i = (\mathbf{1} + \mathbf{j}\gamma) \cdot \Lambda^S(\mathbf{i}, \mathbf{i}) \cdot \tilde{\mathbf{I}} \quad (\text{A.7a})$$

$$\tilde{\mathbf{A}}_{CB}(:, k) = \mathbf{T}_k \cdot \mathbf{p}, \quad \mathbf{T}_k = (\mathbf{1} + \mathbf{j}\gamma) \cdot \mathbf{Q}^{CB}(\mathbf{k}, :)^T \cdot \mathbf{Q}^{CB}(\mathbf{k}, :) \quad (\text{A.7b})$$

$$\tilde{\mathbf{B}} = \mathbf{V} \cdot \mathbf{p}, \quad \mathbf{V} = \omega^2 \mathbf{I} - (\mathbf{1} + \mathbf{j}\gamma) \Lambda^S \quad (\text{A.7c})$$

$$i = 1, 2, \dots, M; \quad k = 1, 2, \dots, N$$

The dimensions of the matrices and vectors in Eq. A.7 are summarized as follows:

- $\tilde{\mathbf{A}}_S$ :  $M \times M$  full matrices
- $\tilde{\mathbf{A}}_{CB}$ :  $M \times N$  full matrix
- $\tilde{\mathbf{B}}$ :  $M \times 1$  vector
- $\mathbf{d}^S$ :  $M \times 1$  vector
- $\mathbf{d}^{CB}$ :  $N \times 1$  vector

Generally more than one measurement are substituted into Eq. A.7, for example, a group of measurements  $\tilde{\mathbf{p}} = [\mathbf{p}_1 \quad \mathbf{p}_2 \quad \dots \quad \mathbf{p}_L]$  which are taken at the resonant frequencies  $\tilde{\omega} = [\omega_1 \quad \omega_2 \quad \dots \quad \omega_L]$  correspondingly, where  $L$  is the number of measurements. For each  $\mathbf{p}_\alpha$  and  $\omega_\alpha$  ( $\alpha = 1, 2, \dots, L$ ), the coefficient generating process described in Eq. A.7 is repeated for each  $\tilde{\mathbf{A}}_S^\alpha$ ,  $\tilde{\mathbf{A}}_{CB}^\alpha$  and  $\tilde{\mathbf{B}}^\alpha$  and larger coefficient matrices (with more rows) can be obtained as follow:

$$\mathbf{A}_S(:, \mathbf{i}) = \begin{bmatrix} \mathbf{U}_i \cdot \mathbf{p}_1 \\ \mathbf{U}_i \cdot \mathbf{p}_2 \\ \dots \\ \mathbf{U}_i \cdot \mathbf{p}_L \end{bmatrix}, \quad \mathbf{A}_{CB}(:, \mathbf{k}) = \begin{bmatrix} \mathbf{T}_k \cdot \mathbf{p}_1 \\ \mathbf{T}_k \cdot \mathbf{p}_2 \\ \dots \\ \mathbf{T}_k \cdot \mathbf{p}_L \end{bmatrix} \quad (\text{A.8a})$$

$$\mathbf{B} = \begin{bmatrix} \mathbf{V}_1 \cdot \mathbf{p}_1 \\ \mathbf{V}_2 \cdot \mathbf{p}_2 \\ \dots \\ \mathbf{V}_L \cdot \mathbf{p}_L \end{bmatrix}, \quad \mathbf{V}_\alpha = \omega_\alpha^2 \mathbf{I} - (\mathbf{1} + \mathbf{j}\gamma) \boldsymbol{\Lambda}^S \quad (\text{A.8b})$$

As  $L$  increasing, there are more than necessary rows added to the coefficient matrices  $\mathbf{A}_S$  and  $\mathbf{A}_{CB}$ . In other word, there are more equations than unknowns so that least squares method is adopted by applying pseudo inverse on the entire coefficient matrix in the purpose of minimizing the fitting errors.

$$\begin{bmatrix} \mathbf{d}^S \\ \mathbf{d}^{CB} \end{bmatrix} = \text{pinv} \left( \begin{bmatrix} \mathbf{A}_S & \mathbf{A}_{CB} \end{bmatrix} \right) \cdot \mathbf{B} \quad (\text{A.9})$$

## APPENDIX B

### Optimization of Identification – Least Squares Method

In chapter II, section 2.2.3, the abbreviated expression of the algorithm for mistuning identification and model updating is derived as follows:

$$\begin{bmatrix} \mathbf{A}_S & \mathbf{A}_{CB} \end{bmatrix} \cdot \begin{bmatrix} \mathbf{d}^S \\ \mathbf{d}^{CB} \end{bmatrix} = \mathbf{B} \quad (\text{B.1})$$

where  $\mathbf{A}_S$  and  $\mathbf{A}_{CB}$  are the reframed coefficient matrices in order to arrange unknowns from  $\delta\Lambda^S$  (cyclic modeling error) and  $\delta\Lambda^{CB}$  (blade stiffness mistuning) into  $\mathbf{d}^S$  and  $\mathbf{d}^{CB}$ , and  $\mathbf{B}$  is a vector. All of them are fully known once the blade responses  $\mathbf{p}$  are obtained at desired excitation frequencies  $\omega$ .

For a mistuned bladed disk system with  $N$  blades, in case of only one family of modes being investigated (one pair per harmonic), there are  $N$  mistuned system modes involved in the CMM model. Thus  $2N$  unknowns are introduced into the Eq. B.1, which are  $N$  blade stiffness mistuning and  $N$  “cyclic modeling error”. Therefore, only one measurement featuring 1 DOF per blade is sufficient in theory to yield an accurate solution since the each system response is treated as a complex vector which leads to  $2N$  equations. However, in the vibration test, no single one measurement is perfect enough for acceptable identification and more data than necessary are used as input information to the identification algorithm. At this point, the least squares method is employed to optimize the test results.

Eq. B.1 can be written in a more general format as:

$$\mathbf{K}\mathbf{x} = \mathbf{B} \quad (\text{B.2})$$

where  $\mathbf{K} = [\mathbf{A}_S \quad \mathbf{A}_{CB}]$  is the coefficient matrix and  $\mathbf{x} = [\mathbf{d}^S \quad \mathbf{d}^{CB}]^T$  is the vector of unknowns. When the number of equations exceeds the number of unknowns, Eq. B.2 is reformatted as follows:

$$\mathbf{K}\mathbf{x} - \mathbf{B} = \boldsymbol{\lambda} \quad (\text{B.3})$$

where  $\boldsymbol{\lambda}$  is the discrepancy between actual and exact solution for equation. The purpose of optimization is to minimize the discrepancy  $\boldsymbol{\lambda}$ , which is expressed as:

$$\mathbf{G} = \boldsymbol{\lambda}^T \cdot \boldsymbol{\lambda} \quad (\text{B.4a})$$

$$\min(\mathbf{G}) \Rightarrow \frac{\partial \mathbf{G}}{\partial \mathbf{x}} = \mathbf{0} \Rightarrow \mathbf{K}^T \cdot \mathbf{K} \cdot \mathbf{x} - \mathbf{K}^T \cdot \mathbf{B} = \mathbf{0} \quad (\text{B.4b})$$

$$\Rightarrow \mathbf{x} = (\mathbf{K}^T \cdot \mathbf{K})^{-1} \cdot \mathbf{K}^T \cdot \mathbf{B} \quad (\text{B.4c})$$

Thus the solution of  $\mathbf{x}$  provided by the calculation above is the optimized results in case the imperfect experiment data is used to apply the identification algorithm.

In Matlab, a embedded function referred as pseudo-inverse “*pinv*” is programmed to deal with the inverse solution for a non-square matrix denoted as  $\mathbf{K}$  to match with the previous coefficient matrix mention in Eq. B.2– B.4.

$$\mathbf{K} \cdot \text{pinv}(\mathbf{K}) = \mathbf{I} \quad (\text{B.5a})$$

$$\Rightarrow \mathbf{K}^T \cdot \mathbf{K} \cdot \text{pinv}(\mathbf{K}) = \mathbf{K}^T \cdot \mathbf{I} = \mathbf{K}^T \quad (\text{B.5b})$$

$$\Rightarrow \text{pinv}(\mathbf{K}) = (\mathbf{K}^T \cdot \mathbf{K})^{-1} \cdot \mathbf{K}^T \quad (\text{B.5c})$$

Considering the advantage of this pseudo-inverse function “*pinv*” in Matlab, the identification algorithm is optimized by adopting it then the actual solution of  $\mathbf{x}$  is written as:

$$\mathbf{x} = \text{pinv}(\mathbf{K}) \cdot \mathbf{B} \quad (\text{B.6})$$

Similarly the solution of Eq. B.1 is derived as follows:

$$\begin{bmatrix} \mathbf{d}^S \\ \mathbf{d}^{CB} \end{bmatrix} = \text{pinv} \left( \begin{bmatrix} \mathbf{A}_S & \mathbf{A}_{CB} \end{bmatrix} \right) \cdot \mathbf{B} \quad (\text{B.7})$$

## APPENDIX C

### **CMM Modeling Assumptions and Applying Limitations**

As presented in Chapter II, this new technique of mistuning identification and model updating relies on certain assumptions such as which modes should be associated with CMM in order to obtain the most accurate modeling. Creating a CMM model with majority of blade-dominant modes is one of these assumptions to ensure a successful identification. Figure C.2 shows the frequency map verses nodal diameter for the validation rotor, whose FEM model is depicted in fig. C.1. In a single mode family, there are two types of modes: blade-dominant and disk dominant. As can be seen in figure C.2, the 17 modes circled within a green box are blade-dominant modes and the other 7 modes added into the mauve box are disk-dominant. This criteria is a qualitative judgement based on previous frequency analysis of substructure such as cantilevered blade and disk part alone. Note that there is no strict dividing line between blade-dominant and disk-dominant modes according to this criteria. However, it can be improved by adopting strain energy factor to distinguish those two kinds of modes quantitatively.

Because of the assumptions made in CMM modeling process, there are different limitations in case of applying the algorithm of mistuning identification and model updating to a single mode family. All the results followed were obtained from numerical simulation for the validation rotor.

## C.1 Blade Stiffness Mistuning Identification Only

In case of only blade stiffness mistuning is required to be identified, any mode including disk-dominant mode within the single mode family can be involved while creating a CMM model for the bladed disk. Nevertheless, it is mandatory to keep blade-dominant modes as majority otherwise the identification results is unacceptable.

- The CMM model associated with either 17 blade-dominant modes or 24, including 7 additional disk-dominant modes, could provide satisfied identification as shown in figure C.4 and C.5. However, the results with different modes involved varies case by case considering the specific model of bladed disk. For the validation rotor, the accuracy keeps untacked. More information feeded in to the optimization of least squares method might be one main reason.
- A possible cause of wrong identification is more measured data at resonant frequencies than system modes involved in the CMM model. As depicted in figure C.6, 24 measurements are substituted into a CMM model created with 17 system modes which provide wrong identification for blade stiffness mistuning. On the contrary, if the CMM model is associated with 24 system modes, an incomplete set of measurements at 17 resonant frequencies could yield accurate identification.
- There is an example of failed mode selection where the disk-dominant modes are majority as indicated in figure C.3. Figure C.7 compares the identified blade stiffness mistuning when this collection is in use to the expected values. It is clearly a disagreement.

Therefore the conclusion is that when identifying the blade stiffness mistuning only, minority disk-dominant modes can be included in the CMM model and there is no need

to distinct them from blade-dominant modes. The identified results might still keep the accuracy or be disturbed slightly.

## **C.2 Mistuning identification and model updating**

In case of both blade stiffness mistuning and cyclic modeling error are required to be identified, all previous observations for blade stiffness mistuning are expectable with any CMM modeling process. However, only cyclic modeling error with respect to the modes which are blade-dominant can be identified correctly even if the CMM modeling only involves minority disk-dominant modes.

While creating a CMM model for the mistuned bladed disk system, the blade mistuning is projected into the tuned system modal coordinates based on the assumption that only blade-dominant modes are qualified. Figure C.2 compare the identification results of blade stiffness mistuning and cyclic modeling error to the expected values and the agreement is fairly well. In this case a CMM model with 17 blade-dominant modes only (as shown in green box in fig. C.2) was created.

By definition, the cyclic modeling errors are identified as the difference between the eigenvalues of tuned system and actual ones therefore they are directly related to each system modes. While disk-dominant modes is involved the identification is incorrect since the reduced order model itself lose accuracy when these modes are involved. For blade stiffness mistuning, the error of including disk-dominant modes can be compelled to the minimum by least squares method since the mistuning is assigned to each blade, not each system mode. More information related to non-qualified modes may attack the identification slightly.

An example is shown in figure C.9 and it is clear that the identified results are wrong related to the disk dominant modes while the others related to the blade-dominant modes

are accurate. These wrong identification results should be excluded when updating the CMM model. It is suggested as follows:

- Exclude disk-dominant modes while creating the CMM model.
- Skip the mode selection step and exclude the identification results for cyclic modeling error related to the disk-dominant modes. No model updating is allowed for those modes as well.

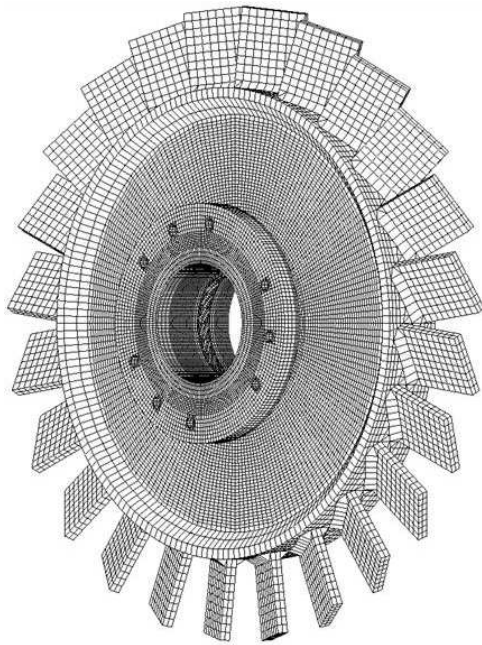


Figure C.1: Finite element model of the validation bladed disk.

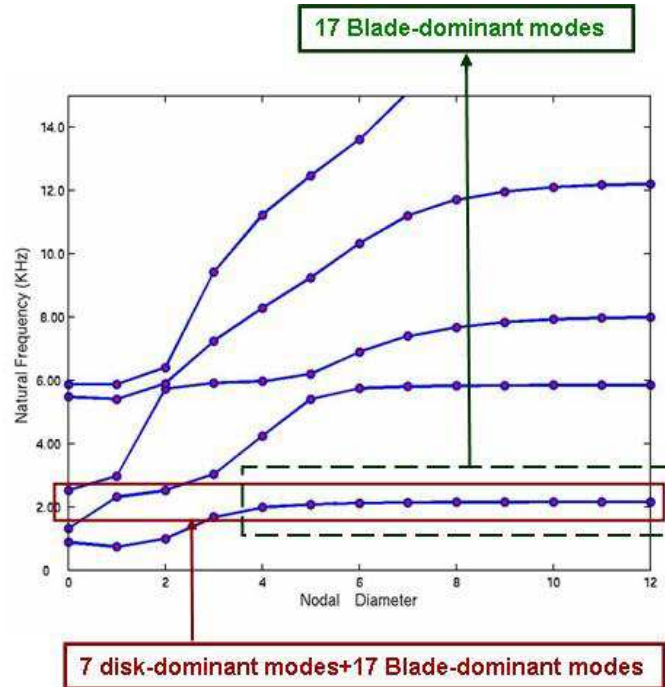


Figure C.2: Modes Selection for CMM modeling of the validation rotor, blade-dominant mode is majority.

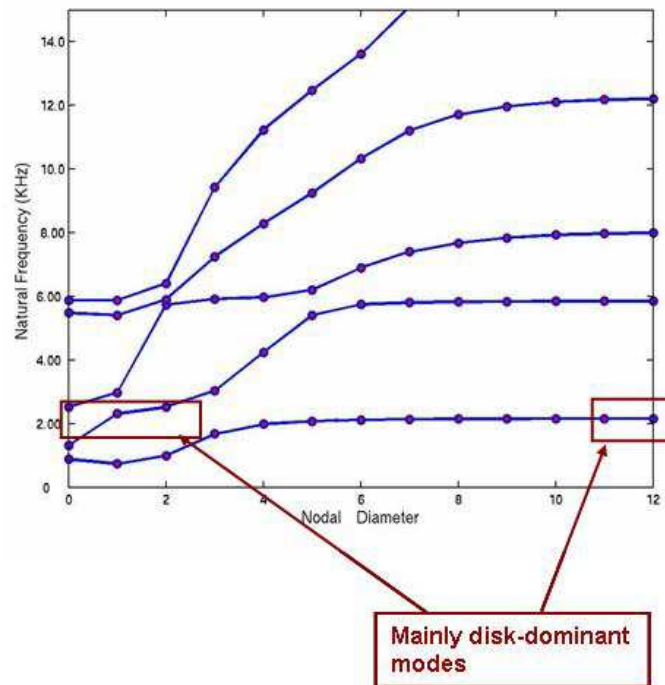


Figure C.3: Modes Selection for CMM modeling of the validation rotor, disk-dominant mode is majority.

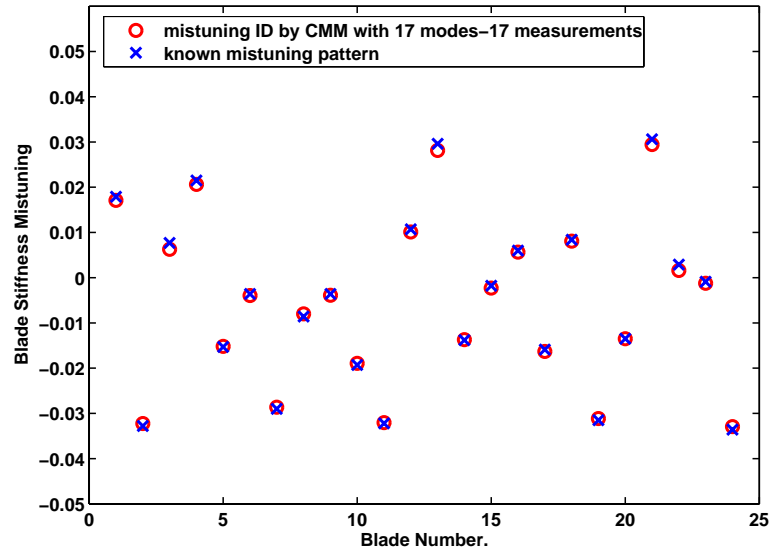


Figure C.4: Identification results of blade stiffness mistuning based on a CMM model with 17 blade-dominant modes.

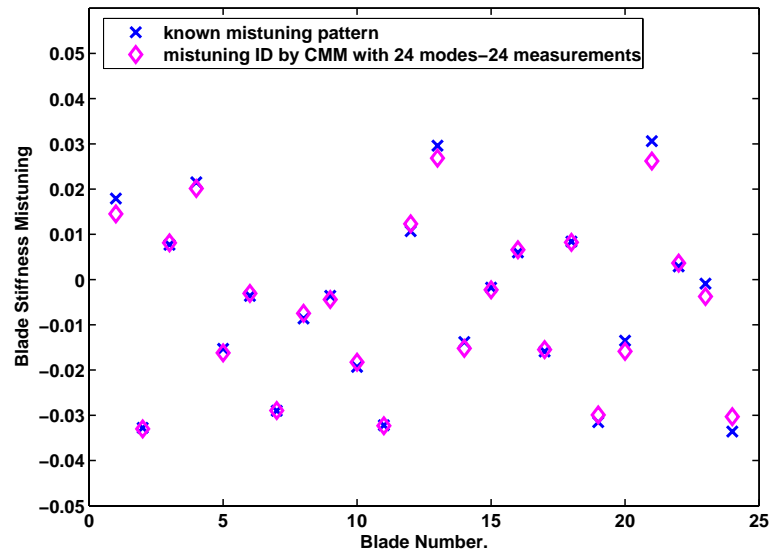


Figure C.5: Identification results of blade stiffness mistuning based on a CMM model with 17 blade-dominant modes and 7 disk-dominant modes.

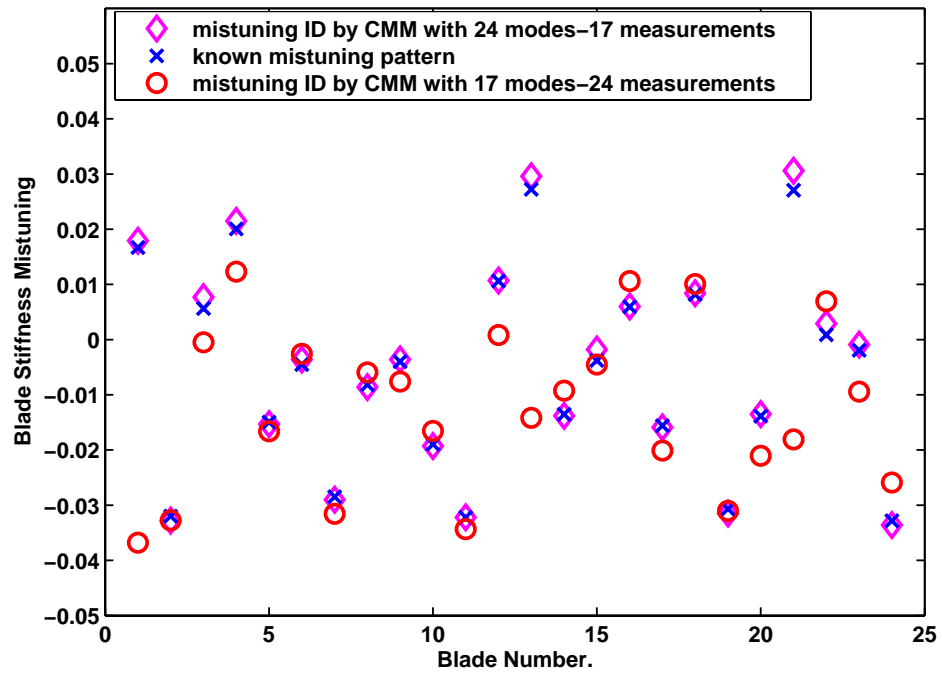


Figure C.6: Wrong identification results of blade stiffness mistuning based on a CMM model with 17 blade-dominant modes, using 24 measured data at resonant frequencies.

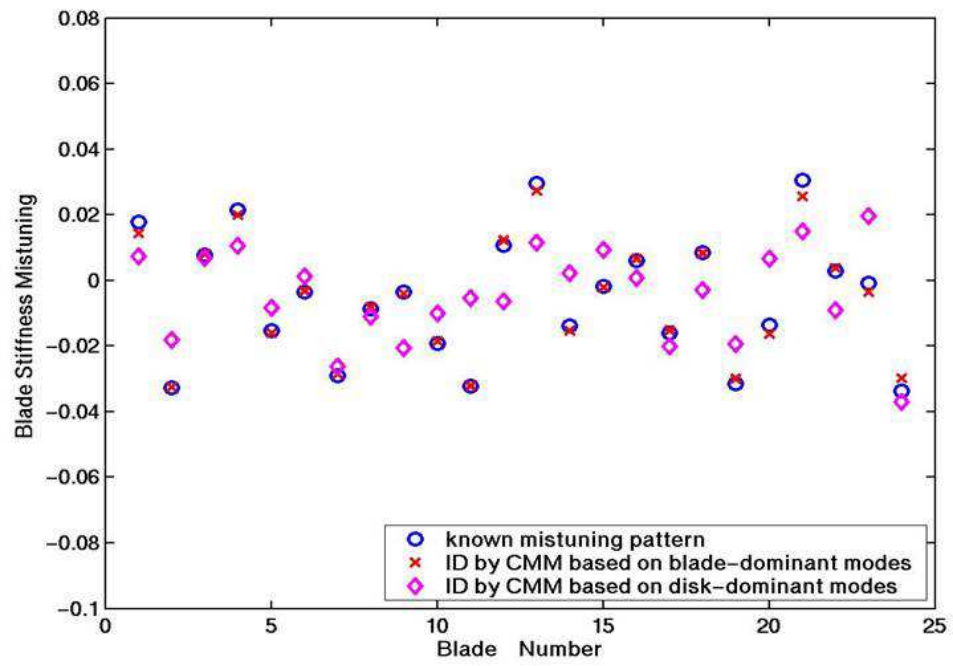


Figure C.7: Identification results of blade stiffness mistuning based on different CMM models.

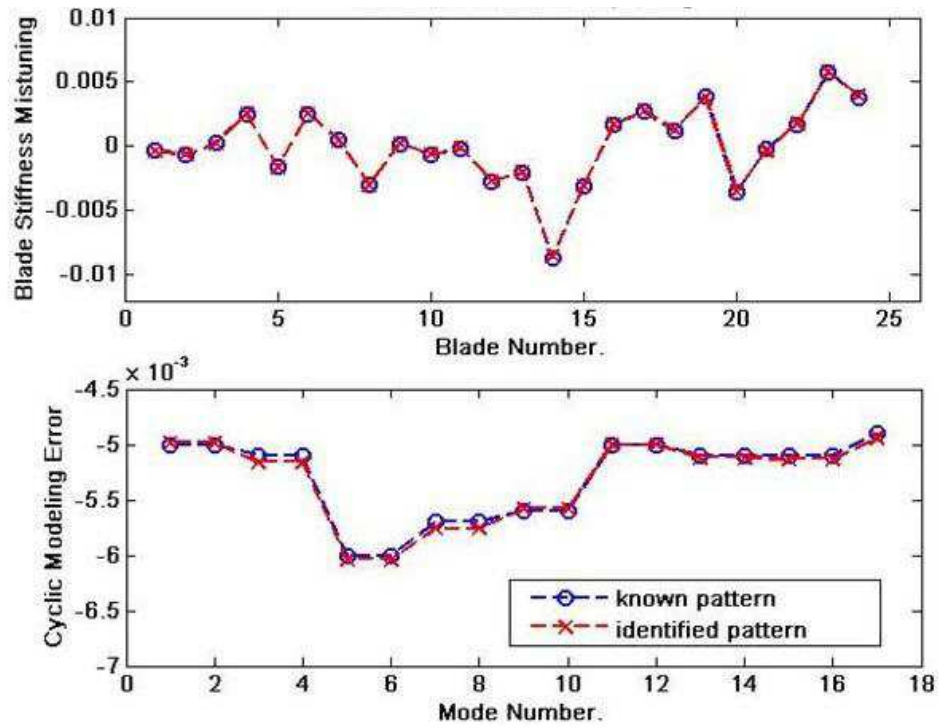


Figure C.8: Identification results of blade stiffness mistuning and cyclic modeling error based on a CMM model with 17 blade-dominant modes.

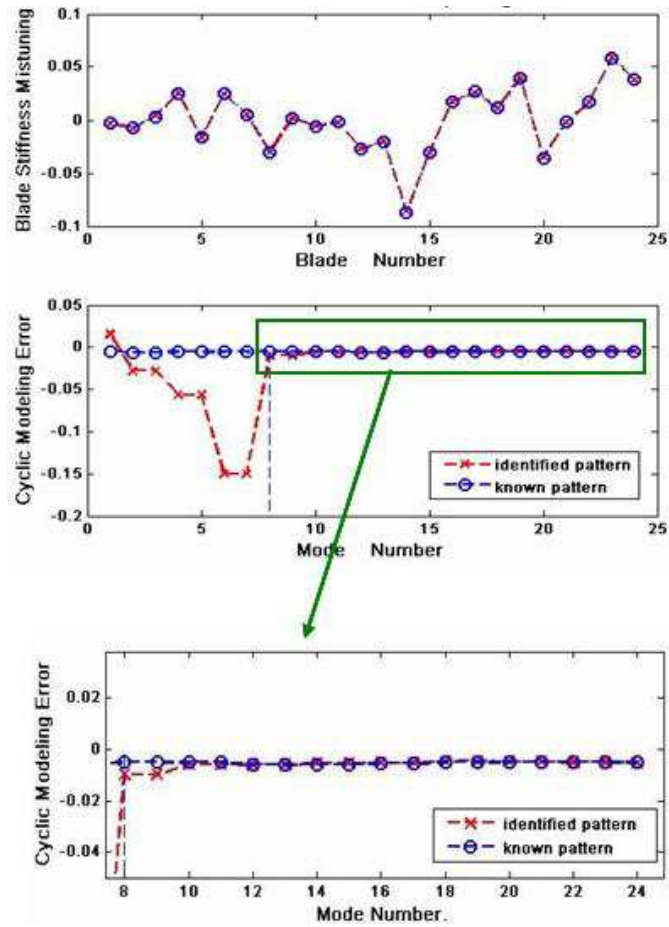


Figure C.9: Identification results of blade stiffness mistuning and cyclic modeling error based on a CMM model with 17 blade-dominant modes and 7 disk-dominant modes.

## **APPENDIX D**

### **Automatic Vibration Test System**

The experimental facility used to examine the effect of mistuning in a controlled environment, shown in Figure D.1, includes a non-contacting, traveling-wave excitation system, as well as a non-contacting measurement system featuring a Scanning Laser Doppler Vibrometer (SLDV). In an automatic vibration test, the excitation system, measurement system as well as the data analysis system are integrated together through software controlling to execute each command given by computer.

#### **D.1 Scanning Laser Vibrometer**

At the beginning stage of vibration test, for example, the experimental validation of the new developed mistuning identification technique discussed in chapter 2, the measurement system consisted of a single point laser vibrometer (SPLV) and a electronic speckle pattern interferometry (ESPI). The SPLV is used to take quantitative measurement including amplitude and phase information and these data can be used as input to the identification algorithm. And the ESPI captures qualitative system response and it visualizes the measurement. This non-contacting measurement system is updated later featuring a scanning laser doppler vibrometer (SLDV) which meets both quantitative and qualitative requirement.

### **D.1.1 PSV–Software Environment for SLDV**

The SLDV mentioned above is manufactured by Polytec and a well-functional integrated software named Polytec Scanning Vibrometer (PSV) serves as the interface. There are two basic modes, Acquisition and Presentation, designed and framed to take the measurement and display the results. Previously a single Labview code was used to control the SPLV automatically and it is challenging to inherit the set up directly for SLDV since there are more communication channel and knowledge necessary for sending command to the inside mirrors and video card, etc. However, the PSV software is equipped with Macro through “VBEng”, it provides a standard protocol for calling any other external softwares or codes, such as Labview and Matlab.

### **D.1.2 PSV Acquisition Set Up**

As can be seen in the Macro source code, a setup file (e.g., “24PointsSetting”) is first loaded before running the PSV to scan the bladed disk. In PSV, all setup-including acquisition setup, camera setup, and window layout-can be saved or loaded by clicking “Setting Manager” in the menu. A typical setup procedure is described as follows:

- ⇒ Set Up Camera (get a good picture of the bladed disk)
- ⇒ Set Up Acquisition Mode (such as channels, filters, triggers, etc)
- ⇒ Define Scanning Points
- ⇒ Choose Window Layout

In this section there is an example of acquisition mode setup for a 24-point scanning process used in vibration tests for the 24-blade validation rotor in the UM lab. After scanning the bladed disk with this setting, a file named FrequencySweep.svd is saved. There is another, similar setting file for only 1 scanning point. Except for the number of defined scanning points, the other settings-including acquisition setup, camera setup, and

window layout-are the same as above. After scanning the bladed disk with this particular setting, a file named ScanTestDump.svd is saved. This setup of 1 scanning point is used to run a dummy scanning to release the “FrequencySweep.svd” saved in the previous step, so that the Matlab code can access this file.

A typical step-by-step acquisition setup is shown as Fig. D.3– D.10.

## **D.2 Excitation System**

In the non-contacting excitation system for vibration test of bladed disks, there is a round speaker mounted behind each blade in a parallel position with the surface of the blade in order to apply an acoustic force. These speakers are driven by a series of Hewlett-Packard 8904 Multifunction Synthesizers, which is controlled and synchronized by Labview code through the General Purpose Interface Bus (GPIB) to generate sinusoidal wave for speakers. These signals are first conditioned by calibration factors and initial phases of each speaker respectively in order to achieve desired excitation manner, *i.e.* engine order excitation, single blade excitation or unique shape excitation. Nevertheless, the Labview code has to be re-designed specifically regarding to the calling requirement from PSV. In other word, for those Labview codes that can be called from the PSV Macro, for instance, the number of the inputs created on the connector panel shown in Fig. D.2 must match with the size of the variable named “paramVals” in PSV Macro. And the name of those inputs must match exactly with those assigned to another variable named “paramNames” in the PSV Macro literally. There is no certain order for these inputs. However, it is necessary to pair up the “paramNames” and “paramVals” in the PSV Macro. It is necessary to design a time delay in the Labview code for the excitation system to ensure that the bladed disk vibration can reach its steady state. The current Labview code included for PSV Macro, such as “SetSpeaker5.vi” and “Speaker Control For Macro.vi”, are all written with respect

to the current TWE system with speakers at the UM Turbomachinery Vibration Laboratory. If the hardware configuration changes, the corresponding Labview code has to be modified for the purpose of successful communication.

### **D.3 Data Process System**

As described in section D.1.1, the measurement can be display directly with PSV Presentation Mode. However, since the mistuning identification is written with Matlab, the measured data is expected to be exported from PSV and can be suited into Matlab code. The official format specifically for a scanning result taken by SLDV is “\*.svd” and can not be read into Matlab. Thus another Matlab code provided by Polytec is used to extract both the amplitude and phase information in order to create input files for mistuning identification algorithm. Thanks to the VBEng, it is possible for PSV Macro to call Matlab after performing measurement to export the data in a certain order. Note that the order is randomly made by PSV scanning function and might be different as the order when scanning point is defined. As it can be seen, an accompany Matlab code is employed to adjust the data order so that the displaying in PSV Presentation Mode agrees with any figure shown in Matlab.

### **D.4 Automatic Test Control Code**

A control code written with Visual Basic and ran as Macro in PSV is the connection between Labview and Matlab. Note that the mandatory requirements are listed as follows:

- Polytec File Access is available, which provides the communication channel between PSV and Matlab so that the Matlab code can be called to extract the measured data which are saved in PSV format.

- VBEng is in position so that Macro function in PSV can be used to call other software.
- In the current Macro code, the desired measurement frequencies are input manually and directly at the beginning of the Macro code. A possible automatic approach is to read in those frequencies from an Excel file (which could be the result of former test) and there is an example BAS code for I/O between PSV and Excel in the program folder of Polytec software -PSV.
- Make sure there is a setting up for another round of “dummy” scanning, otherwise the results for the “desired” scanning is held by PSV itself and it’s impossible for Matlab code to get access to those measured data.

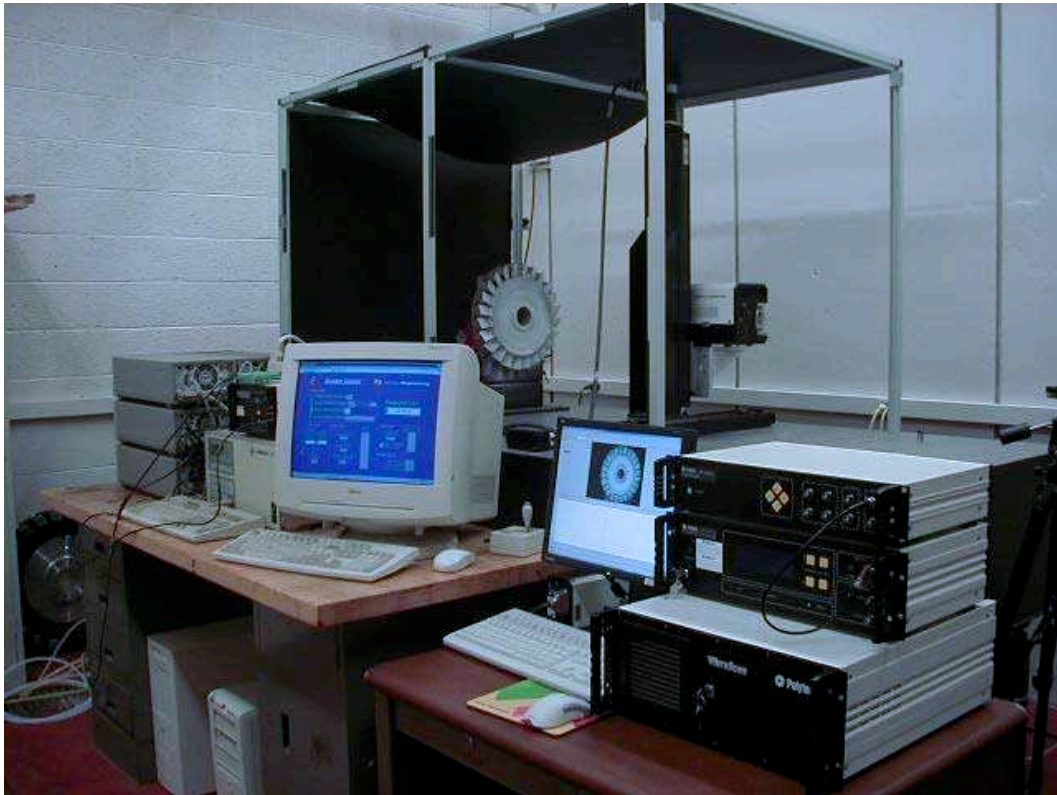


Figure D.1: Experimental set up of the non-contacting excitation and measurement system.

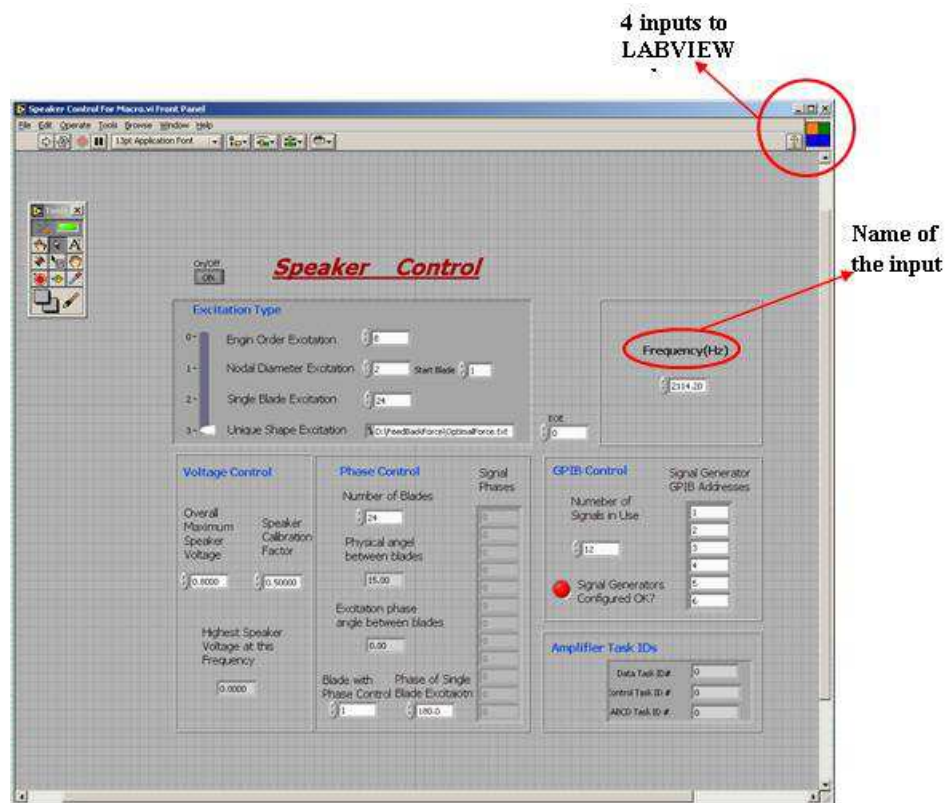


Figure D.2: Front panel of a Labview code with 4 inputs, "Speaker Control.vi".



Figure D.3: PSV acquisition modes set up: step 1 General.

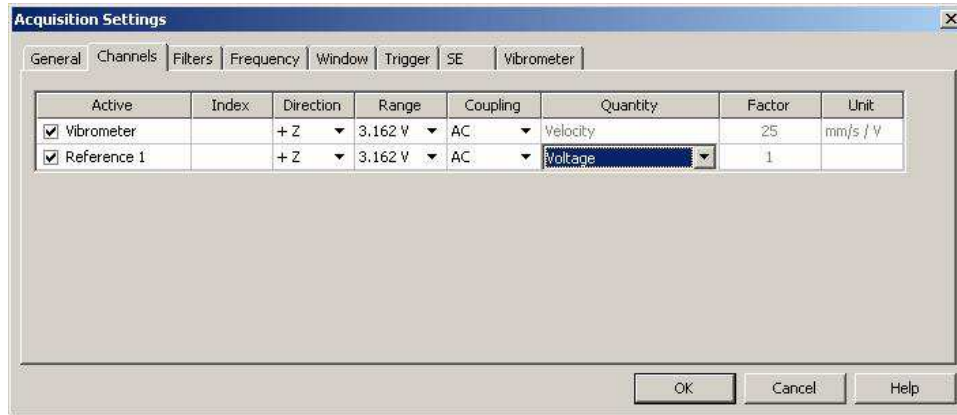


Figure D.4: PSV acquisition modes set up: step 2 Channel.

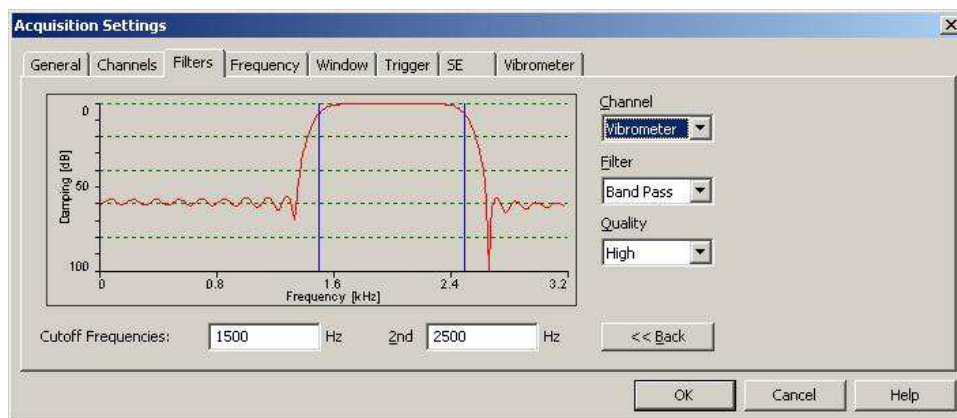


Figure D.5: PSV acquisition modes set up: step 3 Filters.

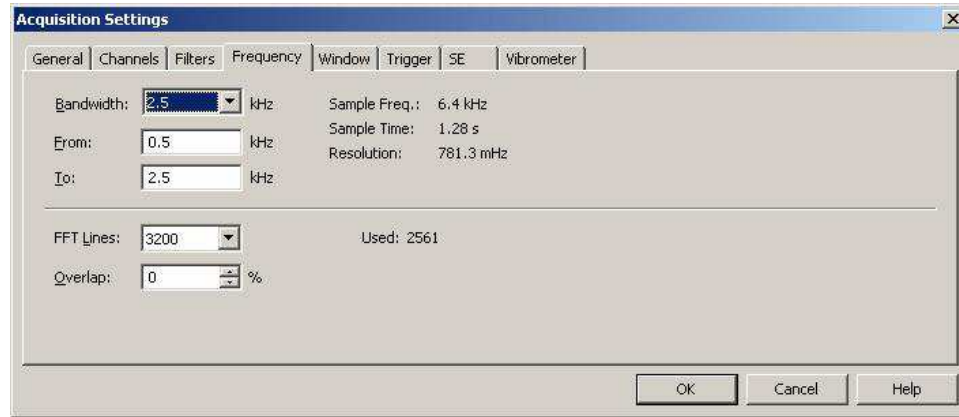


Figure D.6: PSV acquisition modes set up: step 4 Frequency.

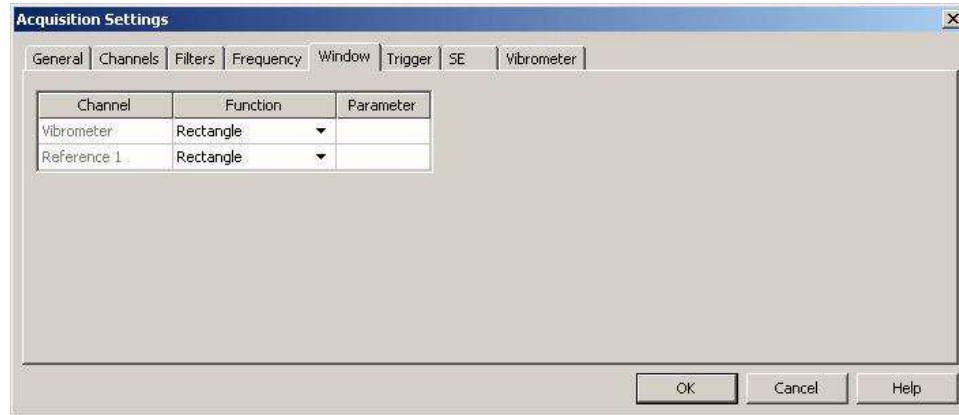


Figure D.7: PSV acquisition modes set up: step 5 Window.

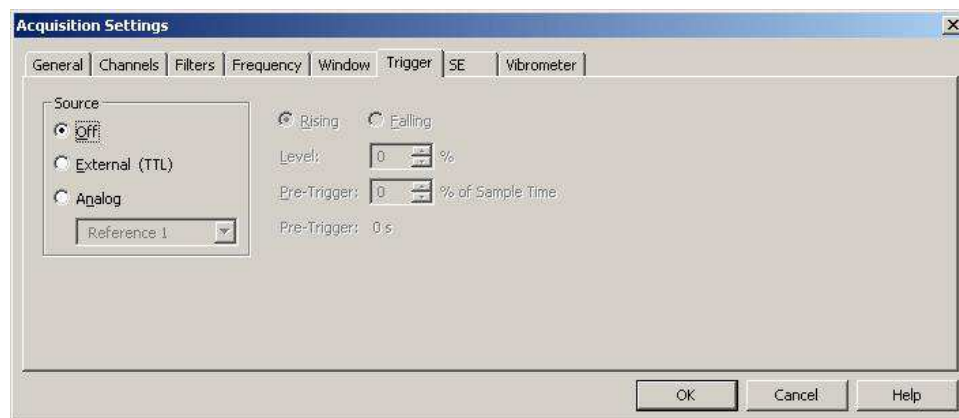


Figure D.8: PSV acquisition modes set up: step 6 Triggers.



Figure D.9: PSV acquisition modes set up: step 7 SE.

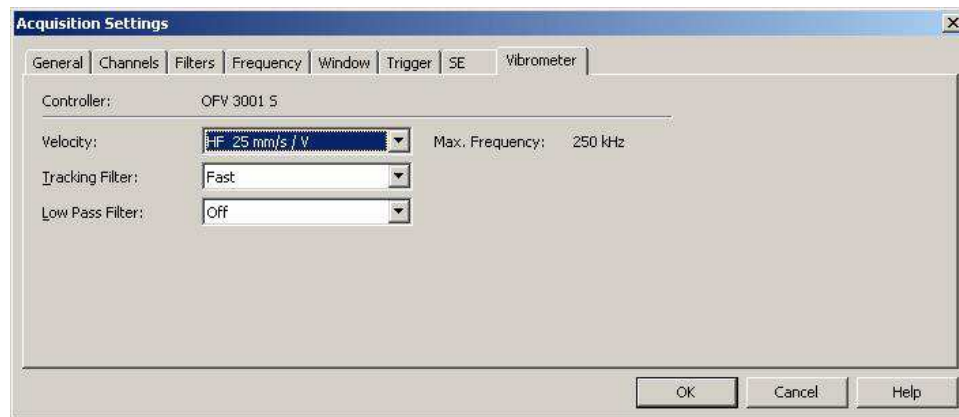


Figure D.10: PSV acquisition modes set up: step 8 Vibrometer.

## **BIBLIOGRAPHY**

## BIBLIOGRAPHY

- [1] S. A. Tobias and R. N. Arnold. The Influence of Dynamical Imperfection on the Vibration of Rotating Disks. *Proceedings of the Institution of Mechanical Engineers*, 171:669–690, 1957.
- [2] D. S. Whitehead. Effect of mistuning on the vibration of turbomachine blades induced by wakes. *Journal of Mechanical Engineering Science*, 8(1):15–21, 1966.
- [3] R. C. F. Dye and T. A. Henry. Vibration Amplitudes of Compressor Blades Resulting From Scatter in Blade Natural Frequencies. *Journal of Engineering for Power*, 91(3):182–188, 1969.
- [4] D. J. Ewins. The Effects of Detuning Upon the Forced Vibrations of Bladed Disks. *Journal of Sound and Vibration*, 9(1):65–79, 1969.
- [5] D. J. Ewins. A Study of Resonance Coincidence in Bladed Discs. *Journal Mechanical Engineering Science*, 12(5):305–312, 1970.
- [6] D. J. Ewins. Vibration Characteristics of Bladed Disc Assemblies. *Journal Mechanical Engineering Science*, 15(3):165–186, 1973.
- [7] D. J. Ewins. Vibration Modes of Mistuned Bladed Disks. *ASME Journal of Engineering for Power*, 98(3):349–355, 1976.
- [8] D. J. Ewins and Z. S. Han. Resonant Vibration Levels of a Mistuned Bladed Disk. *ASME Journal of Vibration, Acoustics, Stress, and Reliability in Design*, 106(2):211–217, 1984.
- [9] W. A. Strange and J. C. MacBain. An Investigation of Dual mode Phenomena in a Mistuned Bladed Disk. *ASME Journal of Vibration, Acoustics, Stress, and Reliability in Design*, 105:402–407, 1983.
- [10] R.L. Jay, J. C. MacBain, and D. W. Burns. Structural Response Due to Blade Vane Interaction. *ASME Journal of Engineering for Gas Turbines and Power*, 106:50–56, 1984.
- [11] J. C. MacBain and P. W. Whaley. Maximum Resonant Response of Mistuned Bladed Disk. *ASME Journal of Vibration, Acoustics, Stress, and Reliability in Design*, 106:218–223, 1984.

- [12] R.L. Jay and D. W. Burns. Characteristics of the Diametral Resonant Response of a Shrouded Fan under Prescribed Distortion. *ASME Journal of Vibration, Acoustics, Stress, and Reliability in Design*, 108:125–131, 1986.
- [13] M. P. Castanier, G. Ottarsson, and C. Pierre. A Reduced-Order Modeling Technique for Mistuned Bladed Disks. *Journal of Vibration and Acoustics*, 119(3):439–447, 1997.
- [14] R. Bladh, M. P. Castanier, and C. Pierre. Reduced Order Modeling and Vibration Analysis of Mistuned Bladed Disk Assemblies with Shrouds. *ASME Journal of Engineering for Gas Turbines and Power*, 121(3):515–522, 1999.
- [15] M.-T. Yang and J. H. Griffin. A Reduced Order Model of Mistuning Using a Subset of Nominal System Modes. *Journal of Engineering for Gas Turbines and Power*, 123:893–900, 2001.
- [16] D. M. Feiner and J. H. Griffin. Mistuning Identification of Bladed Disk Using a Fundamental Mistuning Model-Part I: Theory. *Journal of Turbomachinery*, 126:150–158, 2004.
- [17] D. M. Feiner and J. H. Griffin. Mistuning Identification of Bladed Disk Using a Fundamental Mistuning Model-Part II: Application. *Journal of Turbomachinery*, 126:159–165, 2004.
- [18] S. Lim, R. Bladh, M. P. Castanier, and C. Pierre. A Compact, Generalized Component Mode Mistuning Representation for Modeling Bladed Disk Vibrations. In *Proceedings of the 44th AIAA/ASME/ASCE/AMS Structures, Structural Dynamics and Material Conference*, volume 2, pages 1359–1380, Reston, VA, 2003. AIAA.
- [19] M. P. Castanier and C. Pierre. Modeling and Analysis of Mistuned Bladed Disk Vibration: Status and Emerging Directions. *Journal of Propulsion and Power*, 22(2):384–396, 2006.
- [20] M. P. Mignolet and C.-C. Lin. Identification of Structural Parameters in Mistuned Bladed Disks. *ASME Journal of Vibration and Acoustics*, 119(3):428–438, 1997.
- [21] S. Lim, C. Pierre, and M. P. Castanier. Mistuning identification and reduced-order model updating for bladed disk based on a component mode mistuning technique. In *Proceedings of the 9th National Turbine Engine High Cycle Fatigue Conference*, Pinehurst, North Carolina, 2004.
- [22] J. A. Judge, C. Pierre, and O. Mehmed. Experimental Investigation of Model Localization and Forced Response Amplitude Magnification for a Mistuned Bladed Disk. *ASME Journal of Engineering for Gas Turbines and Power*, 123:940–950, 2001.
- [23] J. A. Judge, S. L. Ceccio, and C. Pierre. Traveling-Wave Excitation and Optical Measurement Techniques for Non-Contacting Investigation of Bladed Disks Dynamics. *Shock and Vibration Digest*, 35(3):183–190, 2003.

- [24] R. R. Craig and M. C. C. Bampton. Coupling of Substructures for Dynamics Analyses. *AIAA Journal*, 6(7):1313–1319, 1968.
- [25] R. Bladh, M. P. Castanier, and C. Pierre. Component-Mode-Based Reduced Order Modeling Techniques for Mistuned Bladed Disks—Part I: Theoretical Models. *ASME Journal of Engineering for Gas Turbines and Power*, 123(1):89–99, 2001.
- [26] R. Bladh, M. P. Castanier, and C. Pierre. Component-Mode-Based Reduced Order Modeling Techniques for Mistuned Bladed Disks—Part II: Application. *ASME Journal of Engineering for Gas Turbines and Power*, 123(1):100–108, 2001.
- [27] J. A. Judge, C. Pierre, S. L. Ceccio, and M. P. Castanier. Experimental Investigation of the Effects of Random and Intentional Mistuning on the Vibration of Bladed Disks. In *Proceedings of the 7th National Turbine Engine High Cycle Fatigue Conference*, Palm Beach Garden, Florida, 2002.
- [28] M. P. Castanier and C. Pierre. Using Intentional Mistuning in the Design of Turbomachinery Rotors. *AIAA Journal*, 40(10):2077–2086, 2002.
- [29] R. Bladh, M. P. Castanier, C. Pierre, and M. J. Kruse. Dynamic Response Predictions for a Mistuned Industrial Turbomachinery Rotor Using Reduced Order Modeling. *ASME Journal of Engineering for Gas Turbines and Power*, 124(2):311–324, 2002.
- [30] J. A. Judge. *Experimental Investigation of the Effects of Mistuning on Bladed Disk Dynamics*. PhD thesis, The University of Michigan, Ann Arbor, MI, 2002.
- [31] K. W. Jones. Mistuning for Minimum Maximum Bladed Disk Forced Response. In *Proceedings of the 40th AIAA/ASME/SAE/ASEE Joint Propulsion Conference and Exhibit*, Fort Lauderdale, FL, 2004. AIAA.
- [32] M. R. Rossi, D. M. Feiner, and J. H. Griffin. Experimental Study of the Fundamental Mistuning Model (FMM) for Probabilistic Analysis. In *Proceedings of the 9th National Turbine Engine High Cycle Fatigue Conference*, Pinehurst, NC, 2004. HCF.
- [33] C. J. Duffield and G. S. Agnes. An Experimental Investigation on Periodic Forced Vibration of A Bladed Disk. In AIAA Paper 2004-3755, *Proceedings of the 40th AIAA/ASME/ASCE/AMS Structures, Structural Dynamics and Material Conference*, Seattle, WA, 2001.
- [34] J. Keith and C. Charles. A Traveling Wave Excitation System for Bladed Disk. In *Proceedings of the 43rd AIAA/ASME/ASCE/AMS Structures, Structural Dynamics and Material Conference*, Denver, CO, 2002. AIAA.
- [35] S. T. Wei and C. Pierre. Localization Phenomena in Mistuned Assemblies with Cyclic Symmetry, Part I: Free Vibrations. *ASME Journal of Vibration, Acoustics, Stress, and Reliability in Design*, 110(4):429–438, 1988.

- [36] S. T. Wei and C. Pierre. Localization Phenomena in Mistuned Assemblies with Cyclic Symmetry, Part II: Forced Vibrations. *ASME Journal of Vibration, Acoustics, Stress, and Reliability in Design*, 110(4):439–449, 1988.
- [37] M. J. Kruse and C. Pierre. An Experimental Investigation of Vibration Localization in Bladed Disks, Part I: Free Response. In *Proceedings of the 42nd ASME Gas Turbine and Aeroengine Technical Congress, Exposition and Users Symposium*, Orlando, Florida, 1997.
- [38] M. J. Kruse and C. Pierre. An Experimental Investigation of Vibration Localization in Bladed Disks, Part II: Forced Response. In *Proceedings of the 42nd ASME Gas Turbine and Aeroengine Technical Congress, Exposition and Users Symposium*, Orlando, Florida, 1997.
- [39] M. P. Mignolet, A. J. Rivas-Guerra, and J. P. Delor. Identification of Mistuning Characteristics of Bladed Disks From Free Response Data - Part I. *Journal of Engineering for Gas Turbine and Power*, 123(2):395–403, 2001.
- [40] A. J. Rivas-Guerra, M. P. Mignolet, and J. P. Delor. Identification of Mistuning Characteristics of Bladed Disks From Free Response Data - Part II. *Journal of Engineering for Gas Turbine and Power*, 123(2):404–411, 2001.
- [41] J. Judge, C. Pierre, and S. L. Ceccio. Experimental Identification of Mistuning in Blisks. In *Proceedings of the 6th National Turbine Engine High Cycle Fatigue Conference*, Jacksonville, Florida, 2001.
- [42] J. A. Judge, C. Pierre, and S. L. Ceccio. Experimental Validation of Mistuning Identification Techniques and Vibration Predictions in Bladed Disks. In *Proceedings of the 2001 CEAS/AAIA/AIAE International Forum on Aeroelasticity and Structural Dynamics*, Madrid, Spain, volume 2, pages 89–98, 2001.
- [43] J. A. Judge, C. Pierre, and S. L. Ceccio. Mistuning Identification in Bladed Disks. In *Proceedings of the International Conference on Structural Dynamics Modeling*, Madeira Island, Portugal, 2002.
- [44] N. E. Kim and J. H. Griffin. System Identification in High Modal Density Regions of Bladed Disks. In *Proceedings of the 8th National Turbine Engine High Cycle Fatigue Conference*, Monterey, CA, 2003.
- [45] D. M. Feiner and J. H. Griffin. A Completely Experimental Method of Mistuning Identification in Integrally Bladed Rotors. In *Proceedings of the 8th National Turbine Engine High Cycle Fatigue Conference*, Monterey, CA, 2003.
- [46] A. Berman and E.J. Nagy. Improvement of a Large Analytical Model Using Test Date. *AIAA Journal*, 21(8):1168–1173, 1983.
- [47] Farhat C. and Hemrz F. M. Updating Finite Element Dynamics Models Using an Element-by-Element Sensitivity Methodology. *AIAA Journal*, 31(9):1702–1711, 1993.

- [48] Kaouk M. and Zimmermann D. C. Structural Damage Assessment Using a Generalized Minimum Rank Perturbation Theory. *AIAA Journal*, 32(4):836–842, 1994.
- [49] Doebling S. W. Minimum-Rank Optimal Update of Elemental Stiffness Parameters for Structural Damage Identification. *AIAA Journal*, 34(12):2615–2621, 1996.
- [50] Friswell M. I., Inman D. J., and Pilkey D. F. Direct Updating of Damping and Stiffness Matrices. *AIAA Journal*, 36(3):491–493, 1998.
- [51] J. K. Sinha and M. I. Friswell. Model Updating: A Tool for Reliable Modeling, Design Modification and Diagnosis. *The Shock and Vibration Digest*, 34(1):27–35, 2002.
- [52] S. Lim. *Dynamic Analysis and Design Strategies for Mistuned Bladed Disks*. PhD thesis, The University of Michigan, Ann Arbor, 2005.
- [53] J. Li, C. Pierre, and S. L. Ceccio. Validation of a New Technique for Mistuning Identification and Model Updating Based on Experimental Results for an Advanced Bladed Disk Prototype. In *Proceedings of the NATO AVT-121 Symposium on Evaluation, Control and Prevention of High Cycle Fatigue in Gas Turbine Engines for Land, Sea and Air Vehicles*, Granada, Spain, 2005.
- [54] M. J. Kruse and C. Pierre. Dynamic Response of an Industrial Turbomachinery Rotor. In *Proceedings of the 32nd AIAA/ASME/SAE/ASEE Joint Propulsion Conference and Exhibit*, Lake Buena Vista, Florida, 1996.
- [55] J. A. Judge, S. L. Ceccio, and C. Pierre. Experimental Investigation of Mistuned Bladed Disk Vibration. In *Proceedings of the 5th National Turbine Engine High Cycle Fatigue Conference*, Chandler, Arizona, 2000.
- [56] J. H. Griffin and T. M. Hoosac. Model Development and Statistical Investigation of Turbine Blade Mistuning. *Journal of Vibration, Acoustics, Stress and Reliability in Design*, 106:204–210, 1984.
- [57] G. S. Ottarsson and C. Pierre. On the Effects of Interblade Coupling on the Statistics of Maximum Forced Response Amplitudes in Mistuned Bladed Disks. In AIAA Paper 95-1494, *Proceedings of the 36th AIAA/ASME/ASCE/AHS Structures, Structural Dynamics, and Materials Conference*, New Orleans, Louisiana, number 5, pages 3070–3078. AIAA, New York, NY, 1995.
- [58] D. S. Whitehead. The Maximum Factor by Which Forced Vibration of Blades Can Increase Due to Mistuning. *Journal of Engineering for Gas Turbines and Power*, 120(1):115–119, 1998.
- [59] A. Sinha. Calculating the Statistics of Forced Response of a Mistuned Bladed Disk Assembly. *AIAA Journal*, 24(11):1797–1801, 1986.

- [60] A. Sinha and S. Chen. A Higher Order Technique to Compute the Statistics of Forced Response of a Mistuned Bladed Disk. *Journal of Sound and Vibration*, 130(2):207–221, 1989.
- [61] M. P. Mignolet and Hu W. Direct Prediction of the Effects of Mistuning on the Forced Response of a Mistuned Bladed Disk Assembly. *Journal of Engineering for Gas Turbine and Power*, 120(3):626–634, 1998.
- [62] M. P. Mignolet, A. J. Rivas-Guerra, and B. LaBorde. Towards a Comprehensive Direct Prediction Strategy of the Effects of Mistuning on the Forced Response of Turbomachinery Blades. *Aircraft Engineering and Aerospace Technology*, 71(5):462–469, 1999.
- [63] M. P. Mignolet, C.-C. Lin, and B. LaBorde. A Novel Limit Distribution for the Analysis of Randomly Mistuned Bladed Disks. *Journal of Engineering for Gas Turbine and Power*, 123(2):388–394, 2001.
- [64] E. P. Petrov, K. Y. Sanliturk, and D. J Ewins. A New Method for Dynamic Analysis of Mistuned Bladed Disks Based on the Exact Relationship between Tuned and Mistuned Systems. *Journal of Engineering for Gas Turbines and Power*, 124(3):586–597, 2002.
- [65] D. M. Feiner and J. H. Griffin. A Fundamental Model of Mistuning for a Single Family of Modes. *Journal of Turbomachinery*, 124(4):597–605, 2002.
- [66] S. T. Wei and C. Pierre. Statistical Analysis of the Forced Response of Mistuned Cyclic Assemblies. *AIAA Journal*, 28(5):861–868, 1990.
- [67] M. P. Castanier and C. Pierre. Consideration on the benefits of intentional blade mistuning for the forced response of turbomachinery rotors for the forced response of turbomachinery rotors. In *Analysis and Design Issues for Modern Aerospace Vehicles*, volume AD-55, pages 419–425. American Society of Mechanical Engineers, New York, 1997.
- [68] B.-K. Choi, J. Lentz, A. J. Rivas-Guerra, and M. P. Mignolet. Optimization of Intentional Mistuning Patterns for the Reduction of the Forced Response Effects of Unintentional Mistuning: Formulation and Assessment. *ASME Journal of Engineering for Gas Turbines and Power*, 125(1):131–140, 2003.
- [69] E. J. Gumbel. *Statistics of Extremes*. Columbia University Press, New York, NY, 5 edition, 1958.
- [70] E. Castillo. *Extreme Value Theory in Engineering*. Academic Press, Boston, MA, 5 edition, 1988.
- [71] Shelley F. J. and Clark W. W. Experimental Application of Feedback Control to Localize Vibration. *Journal of Vibration and Acoustics*, 122:143–150, 2000.

- [72] G. Óttarsson. *Dynamic Modeling and Vibration Analysis of Mistuned Bladed Disks*. PhD thesis, The University of Michigan, Ann Arbor, 1994.
- [73] M.-T. Yang and J. H. Griffin. A Reduced Order Approach for the Vibration of Mistuned Bladed Disk Assemblies. *Journal of Engineering for Gas Turbines and Power*, 119:161–167, 1997.
- [74] J. Li, M. P. Castanier, C. Pierre, and S. L. Ceccio. Experimental Monte Carlo Mistuning Assessment of Bladed Disk Vibration Using Forcing Variations. In *Proceedings of the 47th AIAA/ASME/ASCE/AMS Structures, Structural Dynamics and Material Conference*, Newport, RI, 2006. AIAA.
- [75] Shah A., Nagpal V. K., and C. C. Chamis. Probabilistic Analysis of Bladed Turbine Disks and The Effect of Mistuning. In AIAA Paper 90-1097, *Proceedings of the 31st AIAA/ASME/ASCE/AHS/ASC Structures, Structural Dynamics and Materials Conference*, pages 1033–1038, Long Beach, CA, 2000.

## **ABSTRACT**

# **EXPERIMENTAL INVESTIGATION ON MISTUNED BLADED DISK SYSTEM VIBRATION**

by

Jia Li

Co-Chairs: Christophe Pierre and Steven L. Ceccio

Bladed disks are critical structural components in jet engines and other turbomachinery. The nominal design for a bladed disk is typically assumed to have identical blades. However, there are always small, random variations in the blade properties due to manufacturing tolerances, material defects, and operational wear. These blade-to-blade discrepancies, called mistuning, can have a dramatic effect on bladed disk vibration. In particular, mistuning can cause localization of the response in a small region of the bladed disk, leading to higher blade stress and high-cycle fatigue concerns. While comprehensive analytical and computational studies of mistuning have been performed, relatively few experimental investigations have been conducted. The primary objective of this research is to experimentally investigate the fundamental structural dynamics of mistuned bladed disks, and to achieve a physical understanding of mistuning effects by accounting for the influence of important phenomena that have been largely neglected in previous mistuning models and system identification algorithms.

First, a systematic experimental approach is presented to validate a new mistuning identification and model updating algorithm for single-piece bladed disks, or blisks. It is shown that only a few system response measurements taken at resonant frequencies are required to identify the blade stiffness mistuning parameters and the model updating parameters referred to as cyclic modeling error. By incorporating a model updating procedure, the accuracy of the mistuning identification results are significantly improved. Second, an alternative approach for vibration testing of many mistuning patterns is proposed and validated. In particular, varying the external forcing function provided to the blades is used to mimic the influence of structural blade property mistuning on the vibration response. Since it is much easier and more efficient to vary the external excitation than to physically alter the blades, this work opens the possibility of running an experimental analog of a Monte Carlo simulation. Finally, the mistuning identification method is extended to also identify the forcing amplitude and phase applied to each blade. This approach shows promise as a powerful tool for accelerating calibration procedures, as well as for improving the accuracy and capability of experimental methods for bladed disks.